Dissertation

Faculty of Biosciences

Ruprecht - Karls - University Heidelberg

Communication between tumour cells and fibroblasts in the tumour microenvironment during melanoma progression

Saskia Tauch, M.Sc.

February 2023

Inaugural dissertation
for
obtaining the doctoral degree
of the
Combined Faculty of Mathematics, Engineering and Natural Sciences
of the
Ruprecht - Karls - University
Heidelberg

Presented by
Saskia Tauch, M.Sc.
born in Heilbronn-Neckargartach
Oral Examination: 27$^{\text{th}}$ April, 2023

Communication between tumour cells and fibroblasts in the tumour microenvironment during melanoma progression

Referees: Prof. Dr. Peter Angel

Prof. Dr. Jochen Utikal

This picture is dedicated to Bettina Kast.

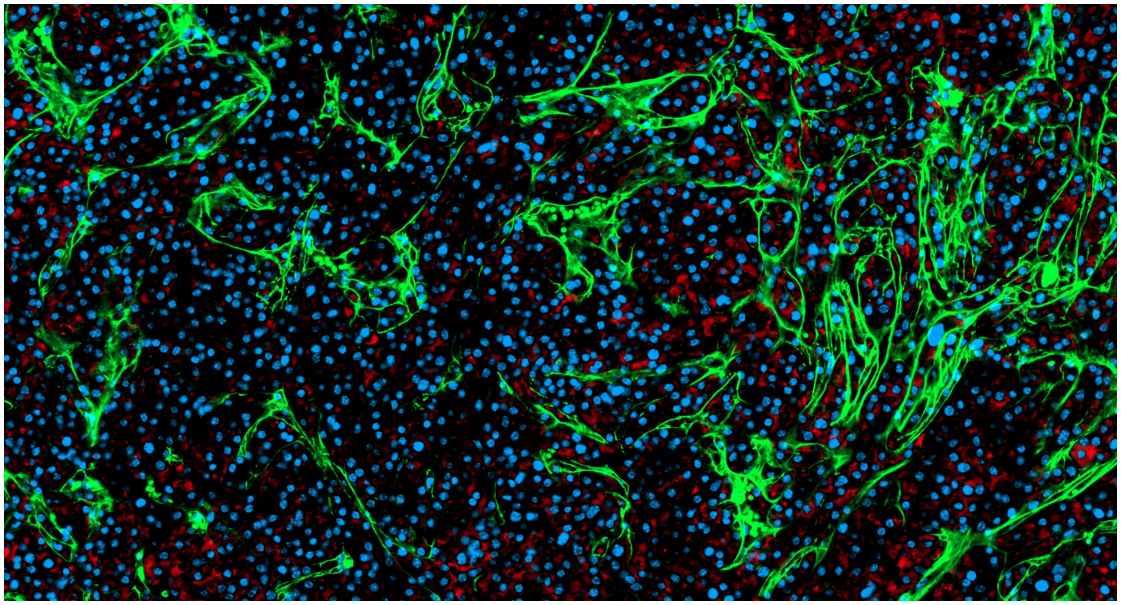

Contents

1 Abstract

Malignant melanoma (MM) represents the most aggressive and deadly form of skin cancer relating to only about 5 % of all skin cancers, but accounting for about 65 % of skin cancer deaths. Current therapies mainly focus on targeting melanoma cells directly; however, other cell types, including cancer-associated fibroblastic cells (CAFs), forming the tumour microenvironment (TME) support cancer progression. Moreover, they also play an important role in tumour relapse and therapeutic resistance. Thus, targeting CAFs has recently entered the limelight of cancer therapy. However, molecular mechanisms underlying the interplay between melanoma cells and CAFs at the site of the primary tumour and especially in the TME of distant metastases remain largely elusive. Therefore, in order to identify novel players in melanoma progression, I aimed at defining and analysing alterations in the genetic programs of CAFs during various phases of MM. To achieve this, I employed an improved mouse model of MM development, progression and metastasis. In a first step, I investigated the effect of CAF- specific loss of PDPN on primary tumour growth. In a second, more comprehensive approach, cells from the tumour stroma at primary tumour and lung metastatic sites were isolated applying an optimised protocol for tissue dissociation at low temperatures and isolation of viable single cells, followed by scRNA sequencing.

Fibroblast-specific *Pdpn* deletion was very efficient and did not affect PDPN expression in other cell types. However, growth curves and survival in experiments, in which a size matched criteria was employed, did not show any effect due to loss of *Pdpn*. Thus, I conclude, that PDPN might serve as a marker for certain CAF subtypes in other studies, and, could be used as a prognostic marker, but is not crucial for growth of murine melanoma primary tumours. Analysis of the generated scRNA sequencing data revealed approximately 230.000 viable cells, reflecting the whole spectra of cell types commonly known to be present in the tumour microenvironment. Thus, the applicability of the here developed protocol for single cell suspensions for scRNA sequencing could be validated. For in depth analysis of CAFs, normal fibroblasts and CAFs were isolated *in silico*. Comparing tumour site specific gene signatures showed an immune regulatory profile for CAFs related to lung metastasis and a mesenchymal profile for the CAF subset related to the primary tumour site. Further investigation of CAF heterogeneity led to the discovery of a, in MM previously undiscovered, VEGFα CAF subset, which is specifically

present within primary tumour CAFs and exhibits an angiogenesis-specific marker expression pattern. Strikingly, metastasis CAFs are marked by a very specific gene signature, which is associated with *Saa3* expression and related signalling. First mechanistic studies regarding putatively *Saa3* inducing signal transduction pathways, indicate IL1β signalling to play a central role in the activation of *Saa3* in the metastatis CAF subset. Interestingly, MPP6 has been described to mediate the pro-tumourigenic function of SAA3 in PDAC CAFs, which was based on the upregulation of MPP6 in SAA3 null CAFs and subsequent functional experiments. Indeed, my data showed mutually exclusive expression of *Saa3* and *Mpp6* in CAFs. Thus, MPP6 might be an antagonist to SAA3 not only in the context of PDAC but also in MM.

Hence, the central conclusions of my thesis are (1) that the proposed target PDPN is not applicable for MM and (2) that VEGFα and SAA3 related signalling could be identified as novel CAF-specific targets in MM primary tumours and metastasis, respectively.

1.1 Zusammenfassung

Das maligne Melanom (MM) umfasst 5 % aller Hautkrebsfälle, verursacht aber ca. 65 % aller mit Hautkrebs in Zusammenhang stehender Todesfälle und stellt daher die tödlichste und aggressivste Form von Hautkrebs dar. Die aktuell verfügbaren Therapien sind meist auf eine gezielte Bekämpfung der Tumorzellen ausgerichtet. In der direkten Umgebung des Tumors, der sogenannten Tumormikroumgebung (TME), befinden sich jedoch noch andere Zellarten, wie z.B. tumor-assoziierte Fibroblasten (CAF), welche das Tumorwachstum, Therapieresistenzen und das Wiederauftreten von Tumoren begünstigen. Dementsprechend werden neue Therapien vermehrt gegen die TME und CAFs ausgerichtet. Jedoch sind die molekularen Mechanismen, welche dem Zusammenspiel von MM Zellen und CAFs zugrunde liegen, insbesondere in Fernmetastasen, noch weitgehend unaufgeklärt. Um neue Einflussfaktoren auf die Enwicklung des Melanoms zu identifizieren, welche potenzielle Angriffspunkte für neue Therapien darstellen könnten, war es das Ziel meiner Thesis Veränderungen im genetischen Program von CAFs in unterschiedlichen Phasen der MM Entwicklung zu definieren und zu analysieren. Hierfür wurde ein optimiertes Mausmodell für das Voranschreiten und die Metastasierung des MM eingesetzt und daran der Effekt von CAF-spezifischem Verlust von PDPN auf das Wachstum des Primärtumors untersucht. Mit einer zweiten, umfassenderen Herangehensweise, untersuchte ich die Zellen der Primärtumor- und Metastasenumgebung mittels scRNA Sequenzierung (Einzelzellanalyse). Hierfür isolierte ich lebendige Zellen mit einem optimierten Protokoll zur Vereinzelung von Zellen bei niedrigen Temperaturen.

Die CAF-spezifische Deletion von *Pdpn* war effizient und spezifisch, da keine anderen Zellarten betroffen waren. Allerdings zeigten Experimente, in welchen die Größe des Primärtumors als Endpunktkriterium verwendet wurde, keinen Effekt von PDPN auf das Wachstum der Tumore oder das Überleben der Mäuse. Somit scheint PDPN zwar als Marker für bestimmte CAF Untergruppen und als prognostischer Marker für Therapien zu fungieren, aber nicht essentiell für das Wachstum von MM Primärtumoren zu sein. Die Analyse der erhobenen scRNA-Sequenzierdaten ergab einen Datensatz mit ca. 230.000 lebendigen Zellen, welche das breite Spektrum der Zellarten in der Tumorumgebung widerspiegelten. Dies bestätigte, dass das optimierte Protokoll für eine Zellvereinzelung bei kalten Temperaturen zur Probenaufarbeitung für scRNA-Sequenzierungsexperimente erfolgreich angewendet werden kann. Für eine gezielte Analyse von CAFs, wurden

diese, zusammen mit normalen Fibroblasten *in silico* isoliert. Der Vergleich von organspezifischen Gensignaturen, ergab ein immunregulatorisches Profil für CAFs aus der Lungenmetastase und ein mesenchymales Expressionsmuster für CAFs aus dem Primärtumor. Weitere Untersuchungen der CAF Heterogenität offenbarten eine bisher im MM Primärtumor noch nicht identifizierte VEGFα CAF Population, deren Expressionsmuster mit Angiogenese in Verbindung steht. Bemerkenswerterweise haben CAFs aus Metastasengewebe ein spezifisches Genexpressionsmuster, welches in Zusammenhang mit SAA3 Signalwegen steht. Erste Analysen deuten darauf hin, dass die Expression von *Saa3* in Metastasen-CAFs über den IL1β/ IL1R Signalweg aktiviert wird. Interessanterweise konnte in CAFs aus PDAC gezeigt werden, dass MPP6 in SAA3-negativen CAFs hochreguliert wird und somit ein Faktor in der Regulation der tumorförderlichen Aktivität von SAA3 darstellt. Auch in Metastasen-CAFs schließt sich die Expression von *Saa3* und *Mpp6* größtenteils gegenseitig aus. Daraus lässt sich ableiten, dass MPP6 vermutlich auch in MM ein Antagonist zu SAA3 darstellt.

Folglich ergibt sich als Kernaussage für meine Thesis, (1) dass der vorgeschlagene Therapieangriffspunkt PDPN nicht auf MM übertragbar ist, und (2) dass die VEGFα- und SAA3 Signaltransduktionswege als neue CAF-spezifische Therapieaangriffspunkte in MM dienen könnten.

2 Introduction

2.1 Skin development and architecture

The skin is the largest organ and the outermost layer of the body, as such it is also it's first defence barrier [Watt, 2014].

Structurally, the skin can be divided into the epidermis and the dermis [Nguyen and Soulika, 2019]. Both layers have a distinct composition of cells, which is schematically visualised in Figure 2.1. Within the epidermis, keratinocytes make up the majority of cells. Among the other cell types of the epidermis are melanocytes, Langerhans cells and Merkel cells. Additionally, the epidermis contains three epidermal appendages: (1) sweat glands (2) hair follicles and (3) nails [Nguyen and Soulika, 2019; Watt, 2014]. Linked to different grades of keratinocyte maturation, the epidermis can be further divided into three sub-layers. Of these, the innermost layer, the *stratum basale*, comprises proliferating basal keratinocytes. During differentiation, keratinocytes diverge from the basement membrane, undergo morphological changes and build first the *stratum spinosum*, then the *stratum granulosum*, and finally, as the cornified outermost layer, the *stratum corneum*. The *stratum corneum* plays a central role in the skins defense structure. As such, it provides not only a physical protection shield, but also regulates the hydration of the skin [Nguyen and Soulika, 2019].

Underneath the epidermis lies the dermis, including mainly fibroblasts, but also immune- and endothelial cells. Being a connective tissue, the dermis has a small proportion of cells and is mostly made up by collagens and elastic fibres. Moreover, the dermis is required for the nutrient supply of the skin, since the epidermis doesn't contain vessels [Nguyen and Soulika, 2019; Watt, 2014]. The dermis can also be separated into different layers: Right below the basement membrane starts the papillary dermis, which is characterised by a high amount of fibroblasts. The second dermal layer is the reticular dermis, which, in contrast to the papillary dermis, is much thicker and mainly contains collagens. The hypodermis is the lowest dermal layer, containing mainly white adipocytes [Nguyen and Soulika, 2019; Watt, 2014].

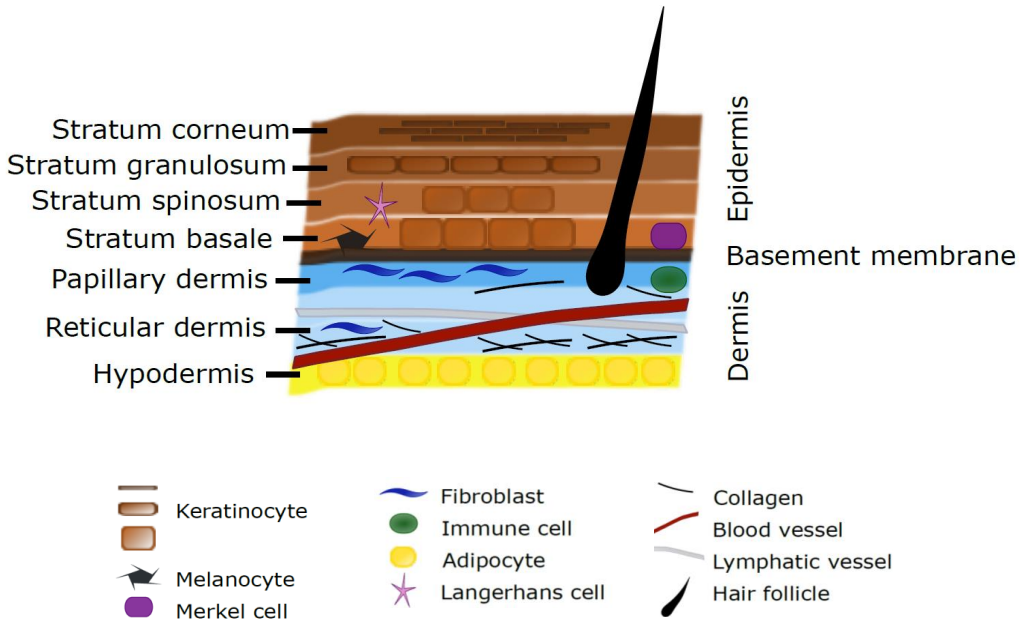

Figure 2.1: **Schematic representation of the skin architecture.** The epidermis consists of the three layers *stratum corneum*, *stratum granulosum*, *stratum spinosum* and *stratum basale*. Underneath follow the dermal layers: papillary dermis, reticular dermis and hypodermis. Epidermis and dermis are separated by the basement membrane.

Since the skin is the first line of protection towards mechanical and chemical forces, it is likely be affected by tissue damage leading to diseases such as cancer. Skin cancer can be divided into melanoma and non-melanoma cancers. The latter class comprises e.g. basal cell carcinoma (BCC), squamous carcinoma (SCC) and Merkel cell carcinoma (MCC) [Cives et al., 2020].

2.2 Malignant Melanoma

The name melanoma originates from the Greek words *melas* "dark" and *oma* "tumour", and was first mentioned by Hippocrates in the 5th century BC [Urteaca and Pack, 1966].

2.2.1 Epidemiology and risk

Although malignant melanoma (MM) accounts for only about 5 % of all skin cancer cases, it is responsible for more than 65 % of all deaths related to skin cancer,

and thus, is a very aggressive type of skin cancer [Davey et al., 2021; Domingues et al., 2018; Ransohoff et al., 2016]. This is aggravated by the fact that the global incidence of MM not only continuously increases, but increases at a faster pace than other tumour-related diseases. Moreover, the median age at diagnosis of MM, which is 57 years, is notably younger as compared to other solid tumours, like for example lung cancer, with 70 years being the medium age of diagnosis. This further underlines the severity of MM [Davey et al., 2021; Schadendorf et al., 2015].

MM arises from genetic and epigenetic mutated melanocytes, the melanin producing cells in the skin. Melanocytes emerge from the neural crest and are located in the basal layer of the epidermis or at hair follicles (Figure 2.1)[Davey et al., 2021]. Under physiological conditions, melanocytes protect the skin from UV light by producing the photoprotective pigment melanin. UV light, in turn, is the major environmental risk factor causing MM. Additionally, phenotypical characteristics like the presence of many or atypical moles, red hair and fair skin also contribute to an increased risk of developing MM. In line with this, geographic regions closer to the earth's equator report more MM cases compared to the ones further away [Davey et al., 2021].

Genetically, MM is familial inherited by germ-line mutations in 5-12 % of all cases. In such cases MM goes along with an increased risk of internal cancers, like pancreatic cancer [Ransohoff et al., 2016]. Germ-line mutations in loci of genes like *CDKN2A, CDK4, POT1,* and *TERT*, so called high-risk mutations, create a 60% to 90% likelihood to develop MM for those patients [Ransohoff et al., 2016]. In contrast, sporadic MM, embracing about 90 % of all MM cases, are driven by low- or moderate-risk mutations in e.g. the *BRAF* gene.

The different stages of MM progression and metastasis can be described according to the Clark model (Figure 2.2), starting with a benign nevus (1) which is limited in growth yet but may transform into a premalignant dysplastic nevus (2) [Clark et al., 1984]. Marked by unlimited hyperplasia, a nevus enters the radial-growth phase (3), followed by penetration of the basement membrane within the vertical-growth phase (4) and eventually metastasis (5). Genetic and epigenetic mutations drive the progression through the multiple steps.

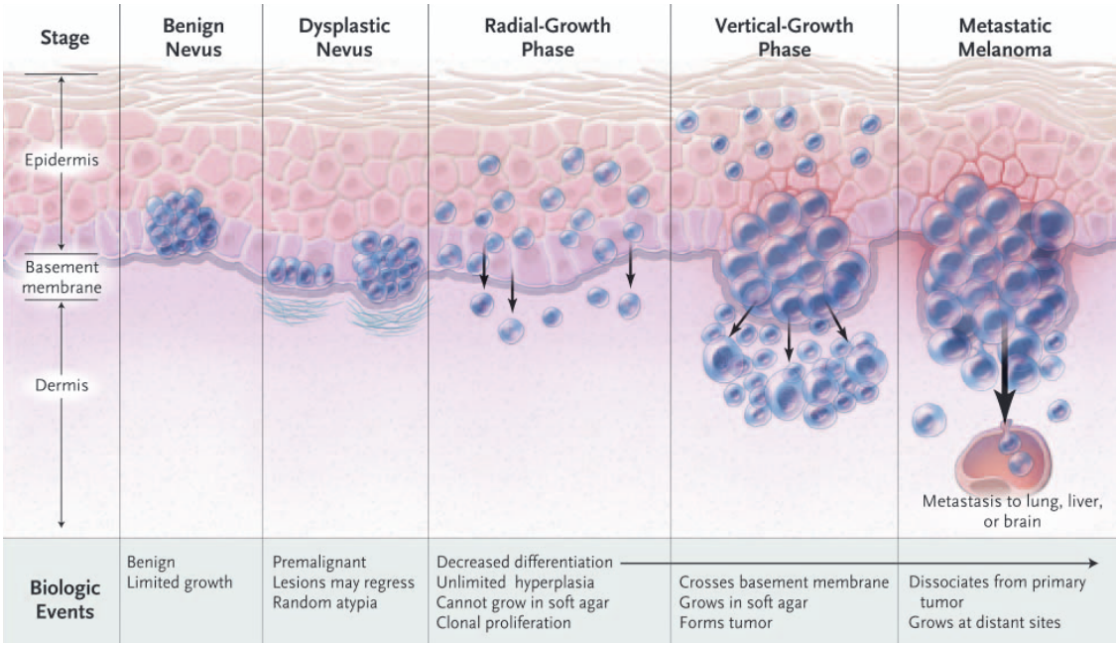

Figure 2.2: **The Clark model of MM disease progression.** (1) Benign nevus, (2) dysplastic nevus, (3) radial-growth phase, (4) vertical-growth phase, (5) metastasis. Adapted from Miller and Mihm [2006].

In the Clark model, all steps are depicted to follow a linear sequence, which is not strictly true for all cases, noting that spread of metastases can already occur in patients with small primary tumours [Bedrosian et al., 2000]. However, metastasis in MM is a complex multifactorial mechanism and since broadly spread metastasis to distant organs (e.g. lung, brain, liver and bone) is the main factor contributing to lethality of MM patients, lots of research has been invested into a better understanding of the underlying processes [Zbytek et al., 2008].

Interestingly, in 4-12 % of patients with melanoma metastases, no primary tumour could be identified [Damsky et al., 2014]. On the other hand, MM metastases can appear a long time after the corresponding primary tumour had been resected. The latter process is described in literature as metastatic dormancy. During metastatic dormancy, disseminated tumour cells supposedly stay in a relatively non-proliferative state until they manage to overcome the obstacles hindering the formation of macrometastases, which can take up to 45 years [Damsky et al., 2014]. Moreover, autopsies reveal higher rates of metastases than found during clinical examination of living patients, indicating that not all disseminated melanoma cells become relevant in the clinical picture. Accordingly, e.g. 10-20 % of patients present at the hospital with liver metastases, while in 54-77 % of patients liver metastases are detected during autopsy [Damsky et al., 2014; Lee, 1980; Patel et al., 1978]. This does further underline that there are still missing pieces of the puzzle.

Multiple factors and mechanisms, such as the cell- intrinsic process of epithelial-to- mesenchymal transition (EMT) are thought to play a central role in metastasis of epithelial tumours. During this process, epithelial cells gradually acquire mesenchymal traits while losing epithelial characteristics, making cells more motile and invasive [Kalluri and Weinberg, 2009]. However, melanocytes originate from the neural crest, and as such, though resembling differentiated epithelial cells in some ways, don't share the same differentiation program. The melanocytic differentiation is mainly regulated by the MITF and WNT/ β-catenin signaling pathways, which are both dysregulated in MM. A clear connection between those pathways and MM metastasis has not been established, yet [Davey et al., 2021].

2.3 Tumour microenvironment

In the early phase of cancer research, hypotheses were built from a reductionist point of view: Cancer is a disease made from cancer cells alone and all characteristics of the disease go directly back to the genetics of cancer cells themselves. By the end of the twentieth century, researchers realised that cancers are more complex, rather like tissues or even organs, containing, besides tumour cells, many other types of cells [Weinberg, 2014]. Nowadays, the diversity of non-malignant cell types and matrix components within a tumour is described as tumour microenvironment (TME). The TME embraces infiltrating immune cells, cancer-associated fibroblastic cells and endothelial cells, together they can make up to 90 % of a tumour (Figure 2.3) [Weinberg, 2014]. Recent research shows that the non-malignant cells of the TME are almost, if not as important as cancer cells for cancer initiation, progression, relapse and therapeutic resistance [Hanahan and Coussens, 2012]. In terms of MM progression, processes such as the accumulation of mutations and alterations of the TME contribute to successful metastasis in MM [Falzone et al., 2016; Chiriboga et al., 2016; Moro et al., 2014]. Extracellularly, matrix metalloproteinases (MMPs) have been shown to pave the way for invading MM cells by degrading the extracellular matrix (ECM) and basement membrane, thereby releasing cytokines and growth factors, which in turn further promote invasion of tumour cells [Davey et al., 2021; Moro et al., 2014].

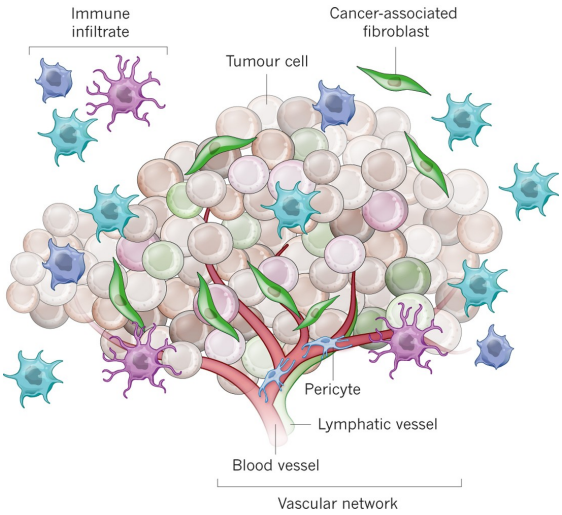

Figure 2.3: **The tumour microenvironment.** Tumours don't consist entirely of cancer cells. Many other cell types, like infiltrating immune cells, cancer-associated fibroblasts and endothelial cells, form the so called tumour microenvironment. Adapted from Junttila and de Sauvage [2013].

2.3.1 TME cells contribute to the hallmarks of cancer

Heterotypic signalling, like the communication of tumour calls with non-malignant cells, is no exception only occurring in the context of a tumour. Cross-talk between different cell types also happens under physiologic conditions, such as wound healing or embryonic development. It is mediated and stimulated by cytokines, chemokines, growth factors, and matrix remodelling enzymes such as MMPs [Balkwill et al., 2012]. During cancer progression, cancer cells take over such physiological processes and use them to fulfil the needs of a tumour. One example for hijacking a physiological process, which is based on heterotypic signalling is angiogenesis, the process of blood vessel formation. It is induced by angiogenic factors, which are secreted by non-endothelial cells, followed by PDGF and HB-EGF production in endothelial cells to attract pericytes and vascular smooth muscle cells. Together, pericytes and vascular smooth muscle cells build the outer layer of vessels, facilitating structural stability. Subsequently they secrete VEGF and Ang-1, which are both required for endothelial cell survival. This shows exemplified the mode of action how multiple cell types work together to form endothelial vessels. In the context of cancer, the process gets boosted e.g. by the secretome of cancer cells themselves, since angiogenesis is required to deliver nutrients and oxygen throughout the growing tumour mass [Weinberg, 2014].

The above described process of (neo-) angiogenesis is one of eight challenges - the so called 'hallmarks of cancer'- a tumour must master or circumvent to ensure further pathogenic progression. In 2000, Hanahan and Weinberg introduced six hallmarks as a set of concepts, which tumours have in common, later, in 2011 two further hallmarks were added [Hanahan and Weinberg, 2011]. In total, the hallmarks of cancer are: (1) Sustaining proliferative signaling, (2) evading growth suppressors, (3) avoiding immune destruction, (4) enabling replicative immortaility, (5) activating invasion and metastasis, (6) inducing angiogenesis, (7) resisting cell death, (8) deregulation cellular energetics. Strikingly, Hannahan and Weinberg depict the large contribution of TME cells to fulfil these hallmarks (Figure 2.4). Interestingly, cancer-associated fibroblasts (CAFs) contribute to almost each hallmark of cancer, indicating a central role in cancer progression [Hanahan and Coussens, 2012].

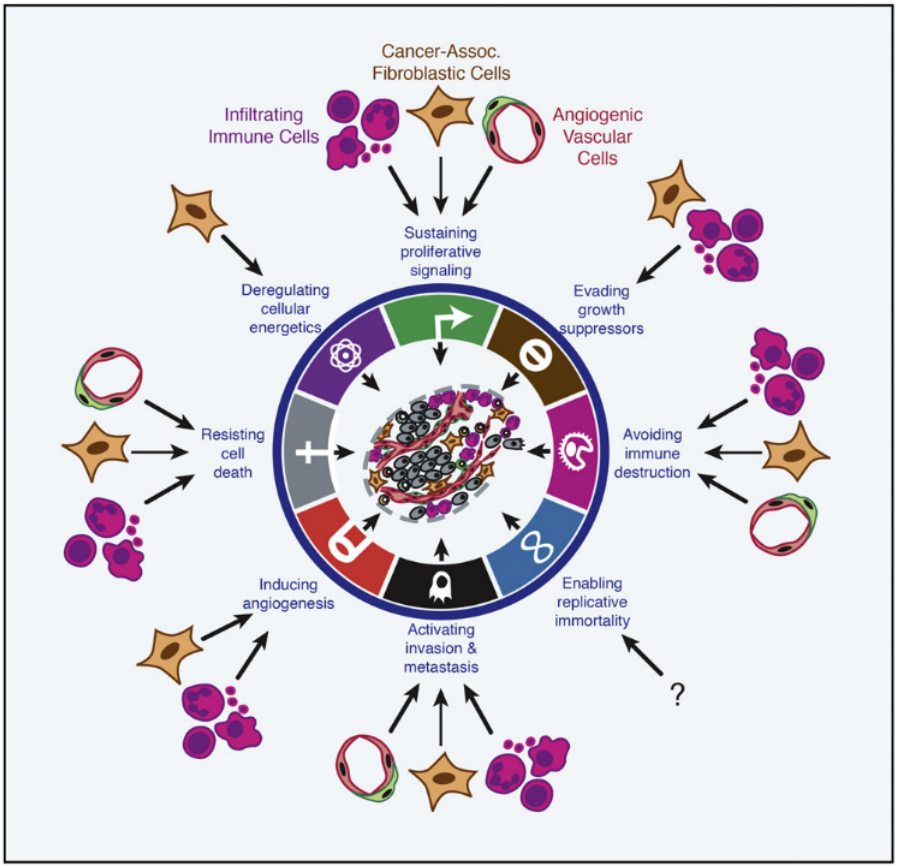

Figure 2.4: **Contribution of TME cells to the hallmarks of cancer.** Adapted from Hanahan and Coussens [2012]

2.3.2 Cancer-associated fibroblasts

Cancer-associated fibroblasts (CAFs) are thought to be similar to myofibroblast, which can be found under physiological conditions in the context of wound healing. Which, again, hints towards another physiological process, which tumours convert to their own use, leading to the description of cancer as a constitutive wound healing process (reviewed in Deyell et al. [2021]).

CAFs are highly heterogeneous and represent the most abundant and active stromal cell population in the TME. Based on the great heterogeneity within CAFs, multiple strategies are usually applied to identify this group of cells: (1) morphological features (elongated, spindle shaped) (2) negative selection for other linage markers (epithelial, endothelial and leukocyte) (3) positive selection for one or multiple CAF marker (αSMA, FAP, PDGFR) [Ping et al., 2021].

In line with the heterogeneity in marker gene expression, many different cell types have been described as sources for CAFs. Besides the recruitment and activation of resident fibroblasts [Fukino et al., 2004], it has been shown that bone marrow mesenchymal cells transdifferentiate into CAFs [Quante et al., 2011]. Moreover, resident epithelial and endothelial cells are able to become CAFs by epithelial to mesenchymal transition (EMT) or endothelial to mesenchymal transition (EndMT), respectively [Petersen et al., 2003; Zeisberg et al., 2007]. The myriad of cells of origin, which are described for CAFs, led to the idea to describe CAFs as a dynamic cell state, instead of a cell type [Madar et al., 2013].

Having shown, CAFs to be very heterogeneous in terms of appearance and origin, what about their role in cancer? CAFs seem to be cellular all-rounders, based on the many functions, which literature grants them. CAFs not only secrete cytokines and growth factors but also remodel the ECM, thereby releasing even more factors, which were previously bound within the matrix. Collectively, these soluble factors lead to the promotion of (1) tumour growth, (2) inflammation, (3) angiogenesis and (4) metastasis [Sahai et al., 2020; Tirosh et al., 2016; Zhou et al., 2015; Hanahan and Coussens, 2012].
Remarkably, CAFs exert pro-tumourigenic functions not only via their secretome, but also in direct cell-cell contact with tumour cells. Labernadie et al. showed in 2017 that a mechanically active heterotypic E-cadherin/N-cadherin adhesion complex between CAFs and cancer cells promotes collective invasion into the surrounding tissue [Labernadie et al., 2017].
However, the role of CAFs is not clearly and solely pro-tumourigenic, since remodelling of the ECM is not necessarily associated with pro-tumourigenic functions. Indeed, besides releasing soluble factors from the ECM CAFs can also reshape the matrix to pave the way for metastatic spread or to form a barrier against infiltration of tumour cells or therapeutic agents. On the other hand, however, the ECM can also be modified to build a "restrictive barrier", which hinders tumour cells from further invading a tissue [Ping et al., 2021].

2.3.3 CAFs in melanoma

In the context of melanoma, CAFs are often called melanoma-associated fibroblasts (MAFs). Interestingly, normal dermal fibroblasts suppress progression of MM development at early stages, whereas at later stages melanoma cells actively

recruit primary skin fibroblasts and increase their activation and matrix deposition. In this context, co-culture and *in vivo* experiments provide evidence that MAFs promote melanoma cell proliferation [Zhou et al., 2015]. Moreover, it has been suggested that MAFs contribute to MM drug resistance, as shown by work from Hirata et al., who demonstrated that MAFs contribute to BRAF inhibitor resistance by aiding in the reactivation of ERK/MAPK pathway via matrix modifications, which in turn activate the integrin β1/FAK/Src signaling in melanoma cells [Hirata et al., 2015]. Additionally, Lakins and colleagues proposed that MAFs specifically suppress $CD8^+$ T cells in the TME by expressing FASL and PD-L2 and thus, inhibit anti-tumoural immune responses [Lakins et al., 2018]. The potential of MAFs to affect immunotherapy outcome is supported by the finding of Wong et al. that CAF profiles of patients before treatment are associated with melanoma immunotherapy outcome in patients [Wong et al., 2019].
However, the above described functions were mostly revealed by *in vitro* experiments analysing CAFs in their entirety, thus, cellular heterogeneity on the single cell level and associated molecular mechanisms underlying the interplay between melanoma cells and MAFs *in vivo* remain largely unexplored.

2.3.4 scRNA sequencing leads to a new understanding of CAF heterogeneity

In recent years, the introduction of single cell (sc) RNA sequencing has lifted CAF research onto another level. In 2009, Tang et al. published the first report of transcriptome sequencing, applied on single blastomeres from 4-cell-embryo-stage [Tang et al., 2009]. Since then, the technique has rapidly developed into approaches, which allow parallel RNA sequencing of tens of thousands of single cells [Hu et al., 2018]. While bulk RNA sequencing only allows the analysis of the average gene expression within a certain population, scRNA sequencing has the big advantage that the transcriptome of each cell can be assessed individually, thereby emphasising differences within a population. Research on heterogeneous cell groups, such as CAFs, vastly benefits from this development [Kanzaki and Pietras, 2020].

Before the big era of scRNA sequencing started, Öhlund et al. were among the first who attempted to categorise CAF sub-clusters in murine pancreatic cancer. Based on immunofluorescence stainings of FAP, αSMA and IL6, they identified a myofibroblastic (myCAF) and an inflammatory (iCAF) CAF group [Öhlund

et al., 2017]. Later, the same group confirmed the finding of myCAFs and iCAFs in human and murine PDAC by scRNA sequencing and further defined associated transcriptional profiles [Elyada et al., 2019]. Additionally, a third CAF population was described as antigen-presenting CAFs (apCAFs). This CAF subset seems to be able to activate $CD4^+$ T cells in an antigen-specific manner [Elyada et al., 2019].

Other studies, like the one from Friedman et al. on murine breast cancer related CAFs, followed [Friedman et al., 2020]. Here, CAFs were divided into two main groups by their expression of *Pdpn* (pCAFs) and *S100a4* (sCAFs). Both, pCAFs and sCAFs contain multiple smaller subgroups. The presence of these CAF types was validated on human tissue sections and the ratio between pCAFs and sCAFs was correlated with clinical outcome, i.e. high percentage of pCAFs resulted in shorter recurrence-free and overall survival of patients.

Interestingly, the Teichmann laboratory investigated CAF heterogeneity at different time points in murine primary B16.F10 melanomas [Davidson et al., 2020]. This revealed the three populations of immune, desmoplastic and contractile CAFs, differentiated by the expression pattern of α*SMA*, *CD34*, *Pdgfr*α and *Pdpn*. Albeit Davidson et al. uncovered interesting facts about MM associated CAFs, their study focussed on primary tumours and no sample of distant metastasis was included. Thus, the critical question, if metastasis CAFs have a distinct targetable profile, remains open.

2.4 MM diagnosis and current therapies

Since melanomas look similar to normal moles by visual criteria, the ABCDE rule has been incorporated for visual screening of suspicious lesions. Applying the ABCDE rule, the assymetry, border irregularity, colour heterogeneity, diameter and evolving of a lesion are investigated [Lopes et al., 2022]. According to the current guidelines, melanoma is classified by TNM staging (T: tumour size, N: spread to nearby lymph nodes; M: distant metastasis [Gershenwald et al., 2017]). This classification differentiates patients with local disease (stage I and II), from patients with affected lymph nodes (stage III) and patients with advanced melanoma where metastasis has reached distant organs (stage IV). Factors, which help to determine the respective stage include tumour thickness (Breslow depth), mitotic rate, presence of ulceration, presence of microsatellites and in-transit lesions, metastatic spread to lymph nodes and distant organs [Jenkins and Fisher, 2021]. Additional screening for BRAF mutations is applied for stage III patients to decide if im-

munotherapy or targeted therapy should be applied.

Mostly, when presented in the clinics, cutaneous melanomas are localised stage I diseases and therefore, can be successfully treated by surgical excision [Joyce and Skitzki, 2020]. However, the prognosis for metastatic melanoma is much worse. For a long time radio- and chemotherapy were the only treatment options for advanced melanoma, but within the last decade, treatment approaches have vastly improved by the development of immuno- and targeted therapy [Lopes et al., 2022].

2.4.1 Immunotherapy

The general idea of immunotherapy is to activate the immune system and stimulate it to target cancerous cells. The first immunotherapy agent (interleukin 2, IL-2) was already approved by the U.S. Food and Drug Administration (FDA) in the 1990s. About two decades later, the first immunological checkpoint inhibitors (ICIs), ipilimumab, nivolumab and pembrolizumab were approved by the FDA and later by the European Medicines Agency (EMA) [Jenkins and Fisher, 2021]. Ipilimumab is an antagonist of the cytotoxic-T lymphocytes antigen 4 (CTLA-4), while nivolumab and pembrolizumab are antagonists of the programmed cell death protein 1 (PD-1). Since 2020 the two agents atezolizumab, an antagonist of programmed cell death ligand 1 (PD-L1), and relatlimab-rmbw, an antagonist of lymphocyte activation gene-3 (LAG-3), got approved by the FDA but not yet by the EMA [Lopes et al., 2022]. CTLA-4 and PD-1 are expressed in T cells and inhibit their activation [Steininger et al., 2021]. Many tumour cells, like melanoma cells, highly express the PD-1 ligand PD-L1, which supports immune evasion by inhibiting T cell activation via PD-1. Blocking the PD-1 axis alone or in combination with CTLA-4 can enhance immune cell stimulation against tumour cells [Steininger et al., 2021]. Larkin et al. could show that the combined administration of nivolumab and ipilimumab leads to an overall survival at 5 years of 52 %, compared to 44 % and 26 % for single administration of nivolumab or ipilimumab, respectively [Larkin et al., 2019]. However, remarkable efficacy of immune checkpoint therapies is still restricted to only a cohort of patients, due to innate or required resistances [Lopes et al., 2022]. Noteworthy, immunotherapies lead to a number of immune-related adverse events (irAEs) like skin rash, vitiligo, diarrhea, hyperthyroidism or hypothyroidism [Lopes et al., 2022].

2.4.2 Targeted therapy

In contrast to immunotherapy, which generally aims to activate the immune system, targeted therapy exploits alterations within tumour cells.

As already mentioned above, the *BRAF* gene is a common site for mutations in melanoma patients, being found in approximately 50 % of melanoma cases. The BRAF protein is a part of the mitogen-activated protein kinase (MAPK)/ extracellular signal-regulated kinases (ERK) signalling pathway, which is an important regulator of cell proliferation. Important members of the MAPK/ERK cascade include downstream of a receptor tyrosine kinase (RTK) the proteins RAS, RAF, MEK and ERK [Lopes et al., 2022]. Mutations in proteins, which are modules of this pathway lead to hyperactivation of cell proliferation in melanoma cells [Domingues et al., 2018]. Besides BRAF, other pathway components like NRAS and NF1 show mutations in 25 and 14 % of patients, respectively [Lopes et al., 2022]. Targeting these mutations aims to decrease melanoma cell proliferation. Since 2011 three different BRAF inhibitors (Vemurafenib, Dabrafenib, Encorafenib) and MEK inhibitors (Trametinib, Cobimetinib, Binimetinib) were approved by the FDA and EMA for single or combinatorial application [Lopes et al., 2022]. Different combinations of BRAF- and MEK inhibitors lead to response rates of 60-70 % and progression-free survival rates of 30-40 % after 18 months [Dummer et al., 2018; Robert et al., 2015; Larkin et al., 2014]. Nevertheless, similar to immunotherapy, targeted therapies also cause side effects such as fatigue, diarrhea or photosensitivity [Lopes et al., 2022]. Moreover, therapy efficacy is restricted by development of resistance mechanisms within 12 months [Lopes et al., 2022; Rajani et al., 2019].

Interestingly, in the year 2020, the FDA even approved the triple application of Cobimetinib (MEK inhibitor), Vemurafenib (BRAF inhibitor) and Atezolizumab (anti-PD-L1 antibody), to combine the best of targeted- and immunotherapy in one approaches [Lopes et al., 2022].

However, various resistance mechanisms have emerged, causing therapeutic inefficacy by exploiting biological plasticity of melanoma cells [Czarnecka et al., 2020; Domingues et al., 2018]. Moreover, there is still a big cohort of MM patients, which doesn't respond to approved therapies. Hence, further therapeutic targets for MM are still urgently needed.

2.5 Objective

Current therapeutic options for advanced melanoma still leave a large cohort of patients in which treatment does not lead to long-term remission or in other cases not even to significant response to the administered compounds. Immuno- and targeted therapies mainly focus on fighting against melanoma cells directly, but harnessing stromal cells of the TME, such as CAFs, as therapeutic target has recently entered the limelight of cancer therapy.

Hence, the aim of this project is to define and functionally analyse alterations in the genetic program of CAFs during various phases of MM. Therefore, I will use an improved mouse model of MM development, progression and metastasis. As a first approach I will specifically investigate the role of PDPN in CAFs in the TME of primary tumours, since it has been described as CAF sub-population marker and in the same context as a prognostic marker for patient survival. In a second, more generalistic approach, tumour stroma at primary tumour and metastatic sites will be isolated (along with tumour tissue) and analysed by scRNA sequencing. This will enable me to identify CAF sub-populations and their corresponding genetic signature, thereby uncovering alterations between CAFs of the primary tumour and of lung metastasis. In depth analysis of metastasis related CAFs and their transcriptional profile will potentially unravel novel targets for advanced melanoma therapies.

3 Methods

3.1 Animal experiments

3.1.1 Housing of mice

All mouse experiments and procedures were approved by the local government authorities (Regierungspräsidium Karlsruhe, G321/19 and G139/20). To perform the experiments, mice were transferred into experimental barriers of the animal facility at the DKFZ. Mice were housed in individually ventilated cages under specific pathogen-free conditions, at 21 °C, 50-60 % humidity, controlled 12 h light cycles and *ad libitium* food and water supply.

3.1.2 MT-ret derived syngraft model for MM

MT-ret allografts fragments (in vivo passage 2) were obtained from the group of Hellmut Augustin (DKFZ, Heidelberg) and were biobanked at -196 °C in DMEM/F12, HEPES (Thermo Fisher Scientific), supplemented with 10 % FCS and 10 % DMSO, and re-transplanted in 8-10 weeks old female C57BL/6N mice for in vivo expansion [Gengenbacher et al., 2020]. Fragments of the third passage were used for all experiments. MT-ret tumour fragments (Ø = 3 mm) were orthotopically transplanted into 8-10 week old mice of the respective genotype. Tumour volume was measured by vernier calliper at least three times a week (V= L x H x W; V: volume, L: length, H: height, W: width). Surgical resection of all primary tumours occurred at a cut-off volume of 550 mm^3. During transplantation of tumour fragments and resection of primary tumours, mice were anaesthetised with isoflurane (O2 Flow 2 l/min, 1,5-2 Vol % isoflurane). To prevent mice from becoming hypothermic, mice were placed on a heating mat during surgery. Additionally, eyes were covered with eye ointment to avoid dehydration. For higher precision, mice were shaved around the transplantation/ resection site. For analgesia, 2 mg/kg of bodyweight Metacam® (Meloxicam, Boehringer Ingelheim) was injected s.c. 30 min prior to surgery as well as 24 and 48 hours post surgery. Following primary tumour resection, all mice were monitored by MRI for metastasis development.

3.1.3 CAF specific PDPN KO

The tumour experiment was performed as described above for the MT-ret derived syngraft model for MM. In order to induce the knockout of *Pdpn* in CAFs, 100

mg/kg bodyweight tamoxifen in oil was injected (i.p.) on days 3, 6, 9 and 16 after the transplantation. Control groups received the same volume of oil instead of tamoxifen.

3.1.4 Magnetic resonance imaging

Magnetic resonance imaging (MRI) measurements were performed by the DKFZ small animal imaging core facility, using a Bruker BioSpec 3Tesla (Ettlingen, Germany) with the ParaVision software V1.1. During the measurement, mice were anaesthetised with 3.5 % sevoflurane in air. In order to detect leasions, T2 weighted imaging was performed with a T2 Turbo RARE sequence and for volume measurements a T1 measurement was performed with the T1 FLASH sequence and the contrast agent ProHance.

3.2 scRNA Sequencing

3.2.1 Tissue dissociation

First, tissues underwent mechanical dicing using scissors, followed by enzymatic dissociation applying an enzyme mix consisting of LiberaseTM (0.25 U/ml), Collagenase D (0.6 U/ml), Dispase II (4.5 U/ml) and DNaseI (50 U/ml) for 45 min rotating in the cold room. The suspension was then passed through a syringe by back loading to further dissociate remaining tissue parts, first without cannula and then applying an 18G cannula. Single cells were separated by centrifugation and re-suspended in DMEM containing 1 % BSA and 2.5 mM EDTA to stop the enzymatic activity. Afterwards, red blood cells were lysed with ACK buffer. Since metastases in the MT-Ret derived syngraft model develop approximately two months after the resection of the primary tumour, dissociated samples were cryopreserved. Therefore, cells were collected by centrifugation, re-suspended in freezing medium (90 % FCS + 10 % DMSO) and transferred into cryostatic tubes (1.8 ml per tube and 1 million cells per ml). Cells were slowly frozen at -80 C, using a Mr Frosty.

Prior to FACSort and library preparation, cryopreserved single cells were rapidly thawed in a 37 °C water bath and transferred into a 50 ml falcon tube. Cells were stepwise diluted by adding a total of 30 ml of pre-warmed DMEM containing 2 % BSA. After centrifuging the cell suspension two times for 5 min at 300 x g, 28

ml supernatant was removed, cells were re-suspended in the remaining 2 ml and further washed by adding 5 ml of fresh medium. Cells were again centrifuged two times for 5 min at 300 x g and then re-suspended in 1 ml FACS buffer. After centrifuging one more time for 4 min at 1000 x g and 4 °C, cells were either re-suspended in FACS buffer for FACSort or for prior surface marker staining in Fc-block. The above described protocol for dissociation and cryopreservation was developed based on recommendations from 10x Genomics (CG00039 Rev D) and multiple protocols described in literature [Wutschka et al., 2021; O'Flanagan et al., 2019; Guerrero-Juarez et al., 2019; Rinkevich et al., 2015]

3.2.2 Flow cytometry for analysis of cells

To determine putative CAF proportions in dissociated samples, cells were re-suspended the cell pellet in 50 µl Fc-block (CD16/32; 1:100 in FACS buffer), incubated 10 min on ice in the dark. Then, 50 µl FACS buffer supplemented with 2x antibody CD45-FITC (BD 553080, final dilution 1:100), CD31-FITC (ebioscience 110319, final dilution 1:400), EpCAM-FITC (BioLegend 118207, final dilution 1:200) and TER119-FITC (BD 557915, final dilution 1:50) were added, mixed by vortexing and incubate 20 min on ice in the dark. To wash the sample, 900 µl FACS buffer were added. After centrifuging for 4 min at 1000 x g and 4 °C the cell pellet was re-suspended in 500 µl FACS buffer. Immediately before the sort DAPI was added 1:1000 (DAPI stock 10 mg/ml).

3.2.3 Flow cytometry for sorting of cells

To deplete $CD45^+$ cells, cells were re-suspended the cell pellet in 50 µl Fc-block (CD16/32; 1:100 in FACS buffer), incubated 10 min on ice in the dark. Then, 50 µl FACS buffer supplemented with 2x antibody CD45- APC/Cy7 (30-F11, BioLegend 103115, final dilution 1:100) were added, mixed by vortexing and incubate 20 min on ice in the dark. To wash the sample, 900 µl FACS buffer were added. After centrifuging for 4 min at 1000 x g and 4 °C the cell pellet was re-suspended in 500 µl FACS buffer. Immediately before the sort DAPI was added 1:1000 (DAPI stock 10 mg/ml). $DAPI^-$, $tdTomato^+$ $APC\text{-}Cy7^-$ cells were sorted into DNA low binding tubes containing 200 µl PBS + 0.04 % BSA + 0.1 mM EDTA.

3.2.4 Library preparation and sequencing

Library preparation was performed in the facilities of the scOpen Lab at the DKFZ. After sorting, cell suspensions were transferred to normal Eppis and centrifuged twice for 4 min at 800 x g. For library preparation, single cells were processed by using the Chromium Next GEM single cell 3' GEM, Library and Gel Bead Kit v3.1 together with the Chromium Next GEM Chip G Single Cell Kit, following manufacturer's protocols. Sequencing of the libraries was performed by the next-generation sequencing (NGS) Core Facility at the DKFZ on a NovaSeq 6000.

3.3 Bioinformatical analysis

The bioinformatical analyses of processing, quality control, uniform manifold approximation and projection and cell cycle analysis were performed by Dr. Joschka Hey (DKFZ, Heidelberg), followed by biological analysis and interpretation by myself.

3.3.1 Processing and Quality control

Fastq files were merged and data was then processed by using the Cellranger version 6.1.1 and the GRCm38 mouse genome assembly as reference. Further processing was performed with the R package Seurat 32 v 3.2.2 [Stuart et al., 2019]. For quality control the data was filtered for the features 'number of genes detected in each cell', 'total number of molecules detected within a cell', 'percentage of mitochondrial RNA', 'percentage of ribosomal RNA' to remove dead or dying cells and multiplets from the dataset. Since the data contained multiple tissues, quantiles were used as cut offs.

3.3.2 Uniform manifold approximation and projection (UMAP)

The dataset was visualised by applying the RunUMAP function of Seurat 32 v 3.2.2 with the first 17 dimensions for the whole dataset and the first 12 dimensions for the fibroblasts subset of the data [Stuart et al., 2019]. As method for dimensional reduction for UMAP input, principal component analysis (PCA) was used. Marker genes for each cluster were identified by using the FindAllMarkers function, setting the parameters in a way that only genes, which were expressed in at least 25 % of cells within a cluster and logarithmic fold change of at least 0.25.

3.3.3 Cell cycle analysis

Cell cycle analysis was performed as described by Tirosh et al. [2016]. The relative expression of a set of 43 G1/S and 55 G2/M genes was assessed for each cell to generate a cell cycle scores and assign the corresponding cell cycle phase.

3.3.4 Gene ontology term analysis

For gene ontology (GO) term analysis, the top marker genes with an adjusted P-value smaller than 0.01 and an average log2 fold change bigger than 1 was uploaded into the metascape online-tool and analysed for GO term enrichment [Zhou et al., 2019].

3.4 Histology

3.4.1 Tissue fixation, processing and sectioning

Dissected organs were fixed in 4 % PFA/DPBS at 4 °C for about 24 h. In a next step, organs were transferred into plastic tissue cassettes and placed in 70 % Ethanol for storage at 4 °C until further processing. Samples were fully automated processed for paraffin embedding with the Vacuum Infiltration Processor (Sakura), following the protocol listed below. Subsequently, tissues were transferred into metal molds for paraffin embedding. After solidifying on a 4 °C cooling plate, blocks were removed from the molds and stored at RT. Sectioning was performed by Bettina Kast or by myself with the sliding microtome SM2012 R (Leica). 6 µm thick sections were first smoothened in a 40 °C water bath and then transferred to glass slides and dried at 42 °C O/N.

Table 1: Vacuum Infiltration Processor program

Step	Temperature	Time	Cycle
70 % EtOH	35 °C	60 min	1
80 % EtOH	35 °C	90 min	1
90 % EtOH	35 °C	90 min	2
96 % EtOH	35 °C	90 min	2
100 % Isopropanol	35 °C	90 min	2
Xylene	40 °C	120 min	2
Paraffin	58 °C	120 min	4

3.4.2 Immunofluorescence staining

First, sections were deparaffinised and rehydrated, by performing the following steps:

In a next step, antigens were retrieved by heat mediated antigen retrieval in 10 mM citric buffer (pH 6.0) for 15 min at 95 °C followed by a washing step in PBS for 5 min. Before further incubations, tissue sections were encircled with an ImmEdge Pen™ (Vector Laboratories). To prevent unspecific binding of antibodies, sections were blocked with 10 % goat serum in PBS for 1 hour at RT. After blocking, sections were stained with primary antibodies at 4 °C O/N. Pri-

Table 2: Pre-processing steps for immunofluorescence staining

Step	**Substance**	**Time**	**Process**
1	Xylene 1	10 min	deparaffinisation
2	Xylene 2	2 min	
3	96 % EtOH	2 min	rehydration
4	80 % EtOH	2 min	
5	70 % EtOH	2 min	
6	60 % EtOH	2 min	
7	PBS	2 min	

mary antibody was removed and sections washed 3 x for 15 min in PBS. Next, sections were incubated with fluorophore-labelled secondary antibodies for 2 h at RT, washed 3 x for 15 min in PBS counterstained with Hoechst 33342 and washed again 3 x for 15 min in PBS before mounting in fluorescent mounting medium (Dako).

Images of stained tissue sections were acquired with the Axio Scan.Z1 (Zeiss, Oberkochen) and afterwards processed with the Zen Blue Software.

4 Materials

4.1 Mice

Table 3: Mouse strains

Mouse strain	Description	Origin
C57Bl/6N	wildtype	Janvier
PDPN$^{fl/fl}$col1A2-creER(T)	Inducible expression of Cre in mesenchyme derived cells combined with floxed *Pdpn* allele	P. Angel, DKFZ
Col1A2-creER(T)	Inducible expression of Cre in mesenchyme derived cells	Zheng et al. [2002]
Gt(ROSA)26Sor$^{tm4(ACTB-tdTomato,-EGFP)Luo}$/J	Ubiquitous expression of td-Tomato	Muzumdar et al. [2007]

4.2 Antibodies and compounds

Table 4: Primary antibodies for immunofluorescence

Antigen	Host species	Dilution	Company
PDPN (clone8.1.1)	syrian hamster	1:100	ebioscience 14034182
αSMA-FITC	mouse	1:500	Sigma-Aldrich F3777

Table 5: Secondary antibodies for immunofluorescence

Antigen	Host species	Dilution	Company
Syrian hamster IgG	goat	1:200	Jackson ImmunoResearch 107-165-142

Table 6: Fluorophore-labelled antibodies for flow cytometry

Antigen	**Fluorophore**	**Dilution**	**Company**
CD45	APC/Cy7	1:100	BioLegend 103115
CD45	FITC	1:100	BD 553080
CD31	FITC	1:400	ebioscience 110319
EpCAM	FITC	1:200	BioLegend 118207
TER119	FITC	1:50	BD 557915

Table 7: Compunds for immunofluorescence and flow cytometry

Compound	**Dilution**	**Company**
Hoechst 33342	1:1000	chemodex CDX-B0030
DAPI	1:1000	Thermo Fisher D1306

4.3 Biomolecular reagents and enzymes

Compound	**Company**
Collagenase D	Roche, Switzerland
Dispase II	Gibco/ Thermo Fisher Scientific, USA
DNase I	Sigma Aldrich, USA
LiberaseTM	Roche, Switzerland
Normal Goat Serum	Vector Laboratories, USA

4.4 Buffers

Buffer	Composition
ACK erythrocyte lysis buffer (pH 7.2-7.4)	150 mM NH_4Cl 10 mM $KHCO_3$ 0.1 mM EDTA
Blocking buffer for immunofluorescence	10 % goat serum in PBS
Citric buffer (pH 6.0)	1.8 mM citric acid 8.2 mM sodium citrate
FACS buffer	1 % BSA in PBS
FACS collecting buffer	0.04 % BSA 0.1 mM EDTA in PBS
10x PBS (pH 7.2)	1.5 M NaCl 27 mM KCl 82 mM Na_2HPO_4 x 2 H_2O 17 mM NaH_2PO_4 x H_2O

4.5 Chemicals and reagents

Compound	Company
Ammonium chloride (NH_4Cl)	Merck, Germany
Bovine serum albumin (BSA)	PAA, AUstria
Calcium chloride (CaCl)	Merck, Germany
Citric acid	AppliCHem, Germany
Dimethylsulfoxid (DMSO)	Biomol, Germany
Disodium phosphate (Na_2HPO_4)	Honeywell Fluka, Germany
Ethanol	VWR, France
Ethylenediamine-tetraacetat (EDTA)	Roth, Germany
Fluorescent Mountng Medium	Dako/ AGilent, USA
Isopropanol (2-propanol)	Fisher Chemical, UK
Paraformaldehyde	Roth, Germany
Potassium chloride (KCl)	Roth, Germany
Potassium bicarbonate ($KHCO_3$)	Merck, Germany
Sodium chloride (NaCl)	Fisher Scientific, UK
Sodium dihydrogen phosphate (NaH_2PO_4)	Neolab, Germany
Tamoxifen	Sigma Aldrich, USA
Triton-X-100	AppliCHem, Germany
Xylene	VWR, France

4.6 Equipment

Item	Company
Animal Trimmer Aesculpa®	Braun, Germany
Axio ScanZ.1 Slidescanner	Zeiss, Germany
BD FACS Canto™ II	Becton Dickinson, Germany
BD FACS Aria™ I	Becton Dickinson, Germany
Cauteriser	Fine Science Tools, Germany
Cauteriser Tips	Fine Science Tools, Germany
Centrifuge Heraeus FRESCO17	Heraeus Sepatech, Germany
Centrifuge Variofuge 3.0R	Heraeus Sepatech, Germany
Digital Caliper	RS Pro, Germany
Embedding machine Tissue-Tek TEC	Sakura, USA
Fine scale XS205 Dual Range	Mettler Toledo, Germany
Heating mat Bosotherm 2000	Bosch+Sohn, Germany
Isoflurane gas vapoiser Vapor 19.3	Dräger, Germany
Magnetic stirrer/ heat plate Variomag Montherm	H+P Labortechnik, Germany
pH meter 765 Calimatic	Knick, Germany
Pipettes (Pipetman)	Gilson, USA
Pipettes (Eppendorf research)	Eppendorf, Germany
Pipettor Pipetboy acu	Integra Biosciences, Swizerland
Silicon mat	René Remie Surgical Skill Centre, The Netherlands
Shaker SD5D	CAT Laboratories, Germany
Slide staining tray	Pyramid innovation, UK
Surgical hooks	René Remie Surgical Skill Centre, The Netherlands
Surgical tools	Fine Science Tools, Germany
Water bath	GFL, Germany
Vortex	Bender and Hobein/IKA, Germany
Vacuum Infiltration Processor	Sakura, Germany

4.7 Consumables

Item	Company
BD Micro-Fine™+ U-100 Insuline syringes	Becton Dickinson, USA
Cell strainer (70 µm)	Corning, USA
Conical centrifuge tubes 15 mL	Corning, USA
Conical centrifuge tubes 50 mL	Corning, USA
Cover slips	Th. Geyer, Germany
CryoTube™ vials	Thermo Fisher, Denmark
DNA LoBind Tube 1.5 ml	Eppendorf, Germany
Embedding cassette Histosette	Simport, The Netherlands
Feather disposal scalpel	Feather, Japan
Foam biopsy pads Surgipath®	Leica, The Netherlands
ImmEdge Pen™	Vector Laboratories, USA
Needle 18G x 1.5"	Medoject, Slovak Republic
Reaction tubes (1.5 mL)	Sarstedt, Germany
Povidone Iodine Braunol®	B. Braun Melsungen AG, Germany
Sugi®	Kettenbach, Germany
Suture Ethilon (4-0/5-0)	Ethicon, UK
Syringes 1 mL	B. Braun Melsungen AG, Germany

4.8 Software

Software	Company
BD FACS Diva™	Becton Dickinson, Germany
FlowJo V10	Tree Star, Inc., USA
GraphPad Prism 7.05	GraphPad SOftware, Inc., USA
ImageJ	National Institutes of Health, USA
Inkscape 0.92.3	Inkscape Project, USA
Texmaker 5.1.2	Pascal Brachet
Office 2013	Microsoft, USA
ZEN2.3 (blue edition)	Zeiss, Germany

5 Results

5.1 MT-ret derived syngraft model for MM represents a suitable model to investigate CAFs

Many mouse models for MM fail to faithfully mimic all steps of the human MM progression by lacking the robust development of metastases at defined distant sites within a certain time frame. Moreover, murine MM tumours show less vascularisation, but more necrotic areas than human MM tumours [Gengenbacher et al., 2017]. The MT-ret derived syngraft model, established by Gengenbacher at al., overcomes these problems, thus, representing an optimised *in vivo* system to study MM in mice [Gengenbacher et al., 2020]. In this model, a fragment from a tumour, which spontaneously developed in MT-ret mice (Tg(Mt1-RET)304Ina; Iwamoto et al. [1991]) was initially transplanted subcutaneously onto the skin of 8-10-week-old female C57BL/6N mice (Figure 5.1A). The resulting primary tumour was cut into fragments and cryo-preserved. By doing so, Gengenbacher at al. established a biobank with fragments, which could be used for further transplantations. I received fragments from their biobank and expanded them *in vivo* to generate my own biobank. The new fragments were transplanted in the same way like for the expansion onto the skin of 8-10-week-old mice. After 3-4 weeks, the primary tumour was resected, to prevent a high burden due to its size (Figure 5.1A).

The resection entailed several obstacles: (1) high vascularisation of the tumour resulted in big vessels coming from the left upper and lower limb. Closing these vessels, to prevent on the one hand haemorrhage of the mouse and on the other hand spread of cycling tumour cells in the abdominal cavity, needs a lot of exercise; (2) the primary tumour attached and sometimes even grew into the peritoneum, consequently, the area of peritoneum, which was attached to the tumour needed to be removed as well. I had noticed that even if the tumour was just attached to and didn't grow into the peritoneum, it was better to remove that part of the peritoneum after all to prevent early recurrence of metastases in this area, which would lead to a premature endpoint to avert higher burden for the animal.

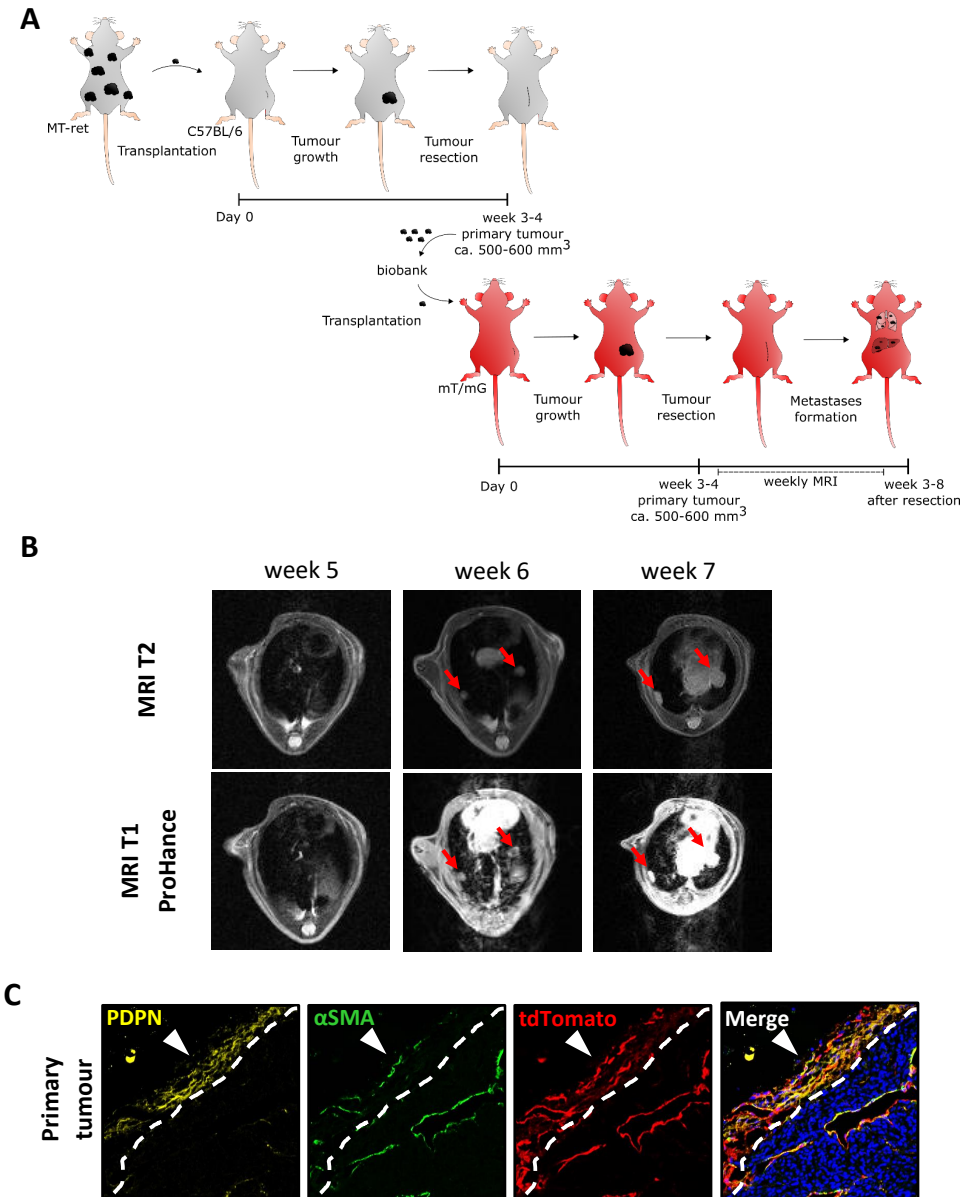

Figure 5.1: **MT-ret derrived syngraft model for MM.** (A) Schematic representation of the MT-ret derived syngraft model. (B) Whole-body MRI screening approach: representative images for lung lesions, without (upper) and with contrast agent ProHance (lower). Time points in weeks after resection. Data produced jointly with small animal imaging core facility. (C) Immunofluorescence staining of PDPN (yellow) and αSMA (green) and endogenous tdTomato (red) expression in the TME of a primary tumour engrafted in a mT/mG mouse (exemplarily indicated by white arrowhead). Dashed line indicates the tumour/ TME margin. Time point of resection= day 20. Data was produced jointly with Lena Weiß, a bachelor student in the laboratory.

Distant metastases developed on average within two months after resection. Similar to the human situation, metastases occur most frequently in the lymph nodes, the lung and the liver [Gengenbacher et al., 2017]. For these reasons, the MT-ret model was chosen for studying the role of CAFs in MM progression and metastasis development.

Metastasis occurrence and growth needed to be closely monitored, hence, mice were subjected to weekly MRI starting from three weeks after the resection. A whole-body MRI screening method was established to this aim. In doing so, I also tested if metastases will be enriched for the contrast agent ProHance, since this would make exact volume measurements possible. Indeed, lesions in the lung appeared to be enriched for ProHance. The time series in figure 5.1B shows metastasis growth starting approximately 5-6 weeks after resection of the primary tumour. Metastases were measurable for the first time at the 6 weeks time point, which was two weeks before this mouse reached the endpoint.

For an easy distinction in further analyses on a single cell level between host and tumour cells, the mT/mG mouse line (Gt (ROSA)26Sor$^{tm4(ACTB\text{-}tdTomato,\text{-}EGFP)Luo}$/J; Muzumdar et al. [2007]) was used as host mouse in my studies. In these mice, membrane-localised tdTomato is expressed in every cell, since its gene was inserted in the ubiquitously expressed ROSA locus under the control of the β actin (ACTB) promoter, whereas cells of the transplanted tumour fragment are unlabelled. In order to ascertain that all fibroblasts within the TME of the applied MM mouse model derive from the host mouse (tdTomato^{+}) and do not originate from the transplanted tumour fragment (tdTomato^{-}), I performed immunofluorescence (IF) staining of the common fibroblast marker proteins Podplanin (PDPN) and α-smooth muscle actin (αSMA) on tissue sections of a primary tumour engrafted in a mT/mG mouse (Figure 5.1C). Both markers co-localise with endogenous tdTomato expression in the stroma of a primary tumour and there is no cell, which is positive for one or both markers but negative for tdTomato. In contrast, MM cells do not express tdTomato.

Finally, since the objective was to use the MT-ret derived syngraft model for my studies in tumour- and metastasis- derived CAFs, and since there is currently very little data on CAFs in this model, it was necessary to further investigate their abundance and marker expression. Therefore, I performed an IF staining for the fibroblast markers αSMA and PDPN on tissue sections of primary tumours and metastases, developed in mice transplanted with a MT-ret tumour fragment. Figure 5.2 shows that the whole TME surrounding the primary tumour, as well as liver and lung metastases, is positive either for one or for both markers, indicating, that CAFs are an abundant stromal cell population in the MT-ret derived syngraft model.

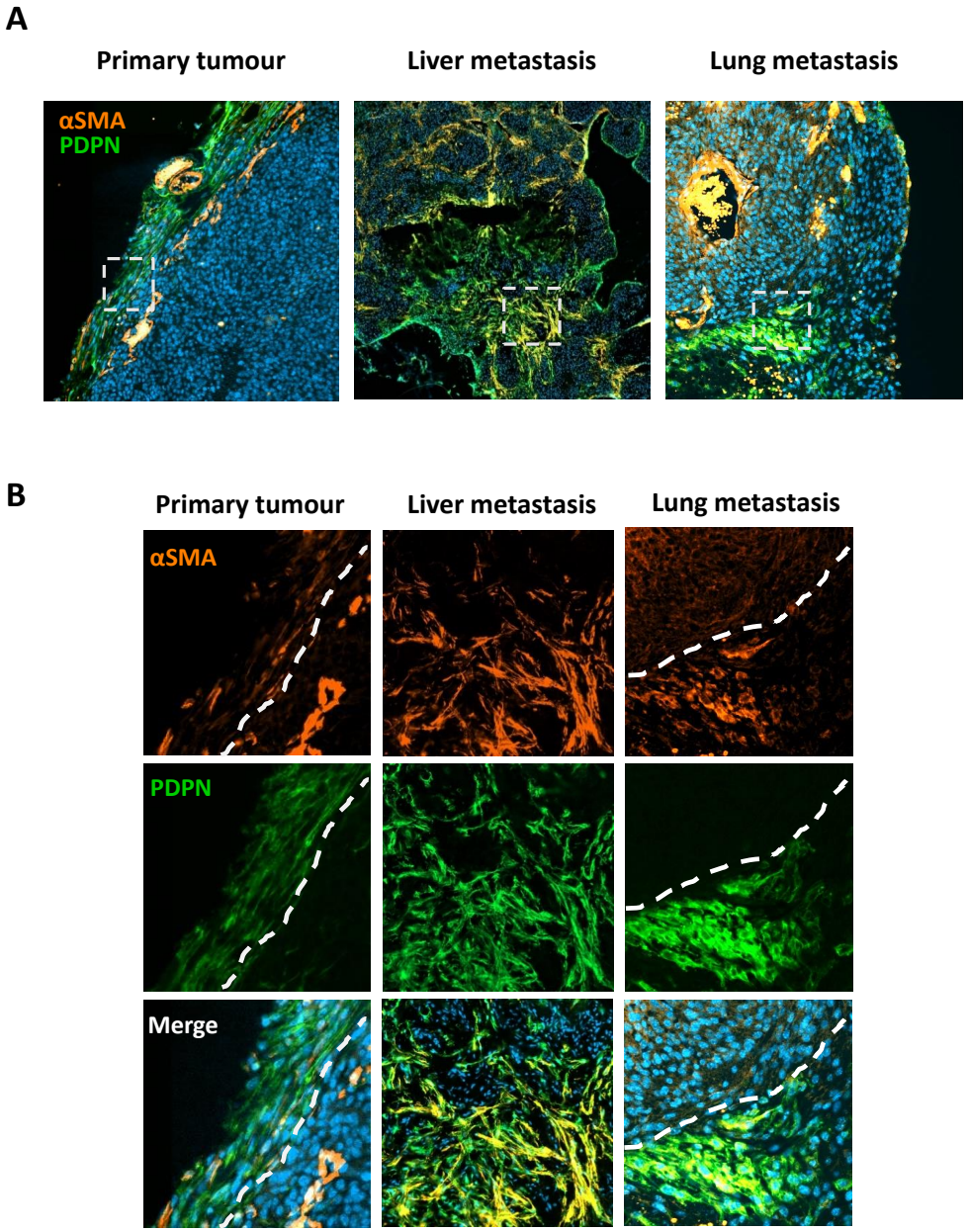

Figure 5.2: **CAFs are an abundant population within the TME of the MT-ret derived syngraft model.** Immunofluorescence staining of PDPN (green) and αSMA (orange) on tissue sections of a primary tumour, a lung metastasis and a liver metastasis. Time point of tumour resection= day 24; time point of liver metastasis= 24 days after primary tumour resection; time point of lung metastasis= 30 days after primary tumour resection. (A) Overview image of stained primary tumour (left) and liver metastasis (right) tissue. (B) Higher magnification of the highlighted rectangle in A. Dashed line indicates the tumour/ stroma margin. Primary tumour data was produced jointly with Lowis Kemm, a bachelor student in the laboratory.

5.2 CAF specific loss of *Pdpn* does not affect tumour growth

After initial characterisation of CAFs in the TME of the applied mouse model, I could show that a subset of CAFs is positive for PDPN. PDPN is a transmembrane protein, which is expressed on tumour cells and/or CAFs. In 45% of MM patients PDPN is expressed in CAFs, which correlates with bad prognosis, including a higher risk to develop lymph node metastases and shorter progression free survival (PFS) [Kan et al., 2014]. Moreover, the *in vivo* study of Hoshino et al. reveals a supporting effect of PDPN-high fibroblasts, co-injected with tumour cells, on tumour formation and metastasis in murine adenocarcinoma [Hoshino et al., 2011]. Recently, PDPN has been shown to be a relevant marker to distinguish CAF subtypes identified by scRNA sequencing in B16.F10 primary tumours [Davidson et al., 2020]. In another scRNA sequencing study, in which PDPN was used as CAF subset marker (pCAFs), a correlation between high proportions of pCAFs and a bad prognosis for patient survival in breast cancer was found [Friedman et al., 2020]. Therefore, I wanted to functionally address the role of CAF specific PDPN in tumour growth in the MT-ret derived syngraft model for MM.

To tackle this, I combined the afore-mentioned MM mouse model with a mouse strain in which *Pdpn* can be deleted specifically in fibroblasts via the inducible Col1α2-creER(T) (Figure 5.3A/ Zheng et al. [2002] and Wutschka et al. [2021]). The initial genotypes in figure 5.3A correspond to the control genotypes PDPN$^{fl/fl}$ and Col1A2-creER(T). After two generations of breeding, the desired genotype PDPN$^{fl/fl}$col1A2-creER(T) (Figure 5.3A genotype (4), thereafter called Knockout: KO) was generated. Upon tamoxifen administration at day 3, 6 and 9 after transplantation of the MT-ret tumour fragment, *Pdpn* shall be deleted in all activated CAFs. These time points were chosen for two reasons: (1) to induce the Cre in fibroblasts as soon as they got activated by tumour cells; (2) to avoid overburden of mice right after the transplantation with parallel injection of pain medication and tamoxifen. Introduction of a tamoxifen booster injection at day 16 after transplantation is thought to ensure *Pdpn* deletion in newly recruited or activated CAFs (Figure 5.3B). Immunofluorescence staining of PDPN showed an efficient reduction of PDPN protein in CAFs of tamoxifen treated KO mice compared to PDPN$^{fl/fl}$ mice (Figure 5.3C left). PDPN was not reduced in either the Col1A2-creER(T) or in the oil treated control groups (data not shown). Importantly, this deletion is specific for fibroblasts as shown by PDPN-positive lymphatic vessels in the TME

(Figure 5.3C left, Breiteneder-Geleff et al. [1999]) and is sustained until the size of the primary tumour reaches the end point criteria around day 21 (Figure 5.3C right).

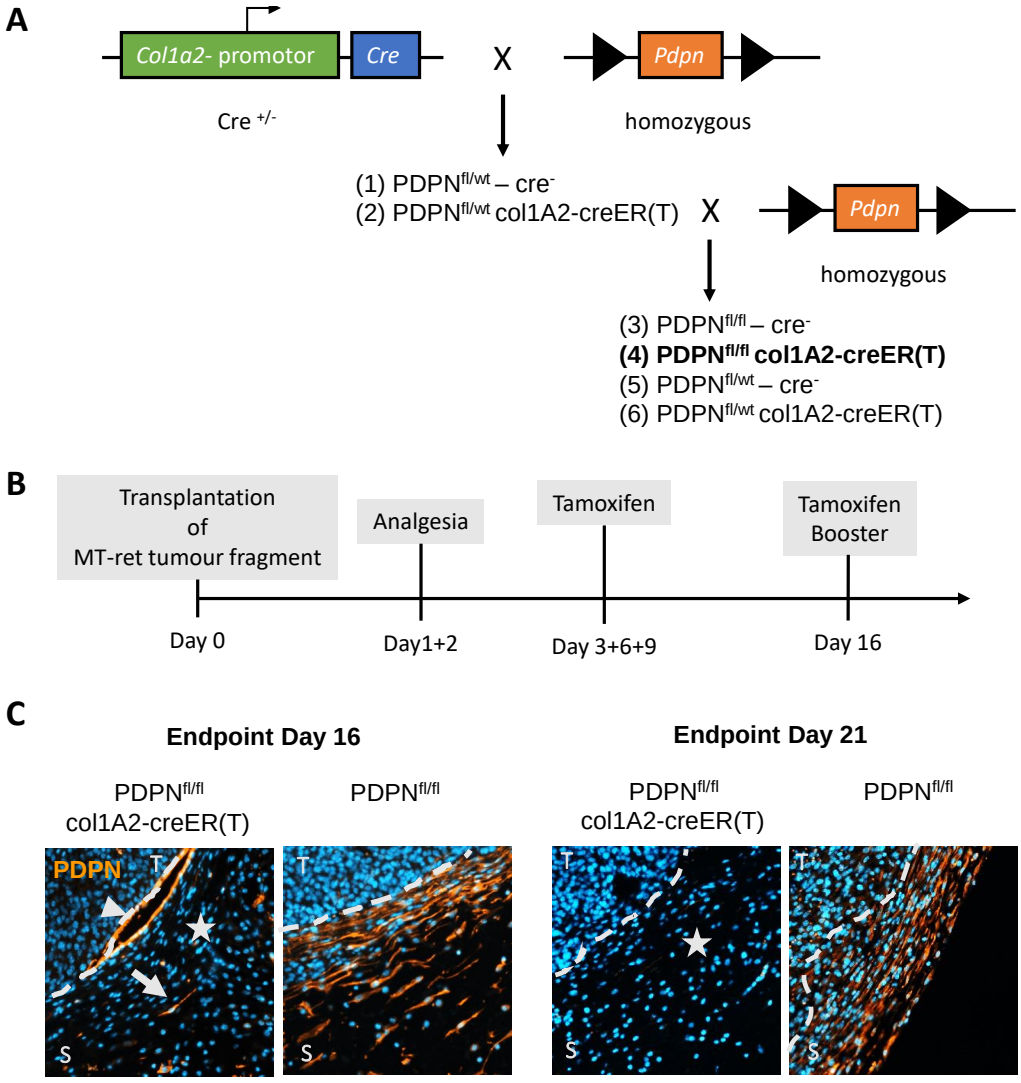

Figure 5.3: **PDPN KO in CAFs is stably maintained throughout primary tumour growth.** (A) Mating scheme for the applied mouse strain. (B) Schematics of tamoxifen treatments after transplantation of a tumour fragment. Control groups were treated with oil at the same time points. (C) Immunofluorescence staining of PDPN on primary tumours with (PDPN$^{fl/fl}$ col1A2-creER(T)) and without fibroblast specific *Pdpn* deletion (PDPN$^{fl/fl}$) at day 16 after transplantation (left) and at day 21 after transplantation (right). Arrow indicates PDPN-positive CAFs in PDPN$^{fl/fl}$ col1A2-creER(T) mice. Star indicates area with PDPN-negative CAFs. Arrow head indicates PDPN-positive lymph vessel as internal control for KO specifity. Dashed line indicates tumour margin. S= stroma; T= tumour.

In order to determine if loss of *Pdpn* in CAFs would lead to reduced primary tumour growth, I measured the tumour volume and monitored the time until the end point size was reached (Figure 5.4). Comparing the time until the tumour size reached the end point criteria, which is depicted as Kaplan–Meier survival plot in Figure 5.4A, shows that KO mice did not survive longer (median survival (mS)= 22 days) than control mice ($PDPN^{fl/fl}$/ mS= 21 days or col1A2-creER(T)/ mS= 21.5 days). Further, I wanted to investigate if primary tumour growth had stalled or slowed down and closed up to the control tumours only at the end. In figure 5.4B the tumour volumes are plotted for each time point. Until approximately day 22, tumours from all groups had a linear growth pattern. During this time, tumours of KO mice (purple) grew at a similar rate like $PDPN^{fl/fl}$ (black x). Tumours from oil treated $PDPN^{fl/fl}$col1A2-creER(T) mice (black dots) grew slower than all other groups until day 24. However, this was not an effect, which was specific for all oil treated groups, since tumours of oil treated Col1A2-creER(T) mice (green) grew similarly to the ones of tamoxifen treated mice. Between day 20 and day 24, many tumours reached the end point size, and thus, only a few tumours, which grew slower than the rest, were still measurable at day 24 - 29. Taken together, the comparison shows that contrary to the initial literature-based hypothesis, tumour growth in KO mice had not slowed down in relation to the control groups.

Additionally, when mice reached the end point, lymph nodes were visually inspected for metastases. However, none of the mice had a macroscopically visible lymph node metastasis. Thus, it was only possible to analyse the effect of *Pdpn* loss on primary tumour growth, at this end point.

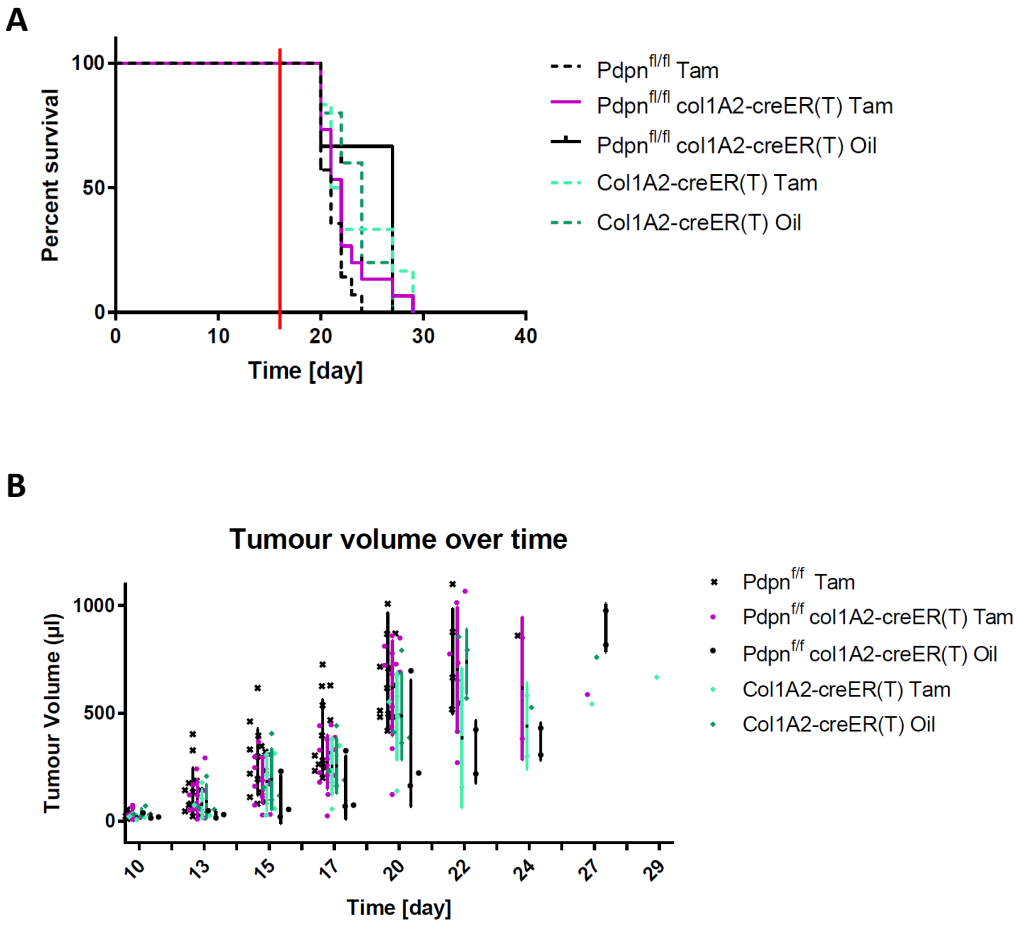

Figure 5.4: **CAF specific deletion of *Pdpn* does not reduce primary tumour growth in the MT-ret derived syngraft model.** (A) Survival analysis of animals of the indicated genotypes. Endpoint was determined by size (*diameter* $\leq$ 15 mm and *volume* $\leq$ 1000 µl) of the primary tumour. n(PDPN$^{fl/fl}$ Tam)=14/ mS= 21 days; n(PDPN$^{fl/fl}$ col1A2-creER(T) Tam)=15/ mS= 22 days; n(Col1A2-creER(T) Tam)=6/ mS= 21.5 days; n(PDPN$^{fl/fl}$ col1A2-creER(T) Oil)=3/ mS= 27 days; n(col1A2-creER(T) Tam)=6; n(col1A2-creER(T) Oil)=5/ mS= 24 days. Red line indicates time point of tamoxifen booster injection. (B) Tumour volume (in µl) over time (in days) corresponding to the mice in (A).

5.3 Preparing single cell suspensions by applying a newly established dissociation protocol at low temperatures

Since PDPN, as an already published marker of a subset of CAFs within the primary tumour with putatively prognostic properties, did not affect primary tumour growth in mice, I sought to find new CAF-specific genes with relevance for CAF function in MM formation and progression. For this purpose, in depth characterisation of CAFs by dissecting the cellular heterogeneity of CAFs in the TME of the MT-ret derived syngraft model for MM was performed in an unbiased way by scRNA sequencing. In doing so, I wanted to focus especially on the differences between CAFs in the primary tumour and lung metastasis to unravel potentially novel CAF related targets for advanced melanoma.

Therefore, I had to establish a protocol, which allowed me to dissociate different tissues into single cells, since all available protocols were optimised for one specific tissue only. Taking into account that, by processing samples into single cell suspensions for scRNA sequencing, the proportion of certain cell populations may vary due to different grades of robustness towards the dissociation protocol, I aimed for a protocol, which is on the one hand as gentle as possible but also as effective as necessary. On the other hand, RNA quality and cell intrinsic responses to enzymatic and mechanical forces needed to be taken into consideration. O'Flanagan and colleagues show that the stress response of cells during the process of tissue dissociation can be reduced by applying a protocol at cold temperatures [O'Flanagan et al., 2019]. Hence, I tested different combinations of enzymes, enzyme concentrations, incubation times, mechanical dissociation techniques and cryo-preservation options, which were described in the literature, at cold temperatures (on ice/ in the cold room), to get the highest possible yield of CAFs. By doing this, I finally developed the following work-flow at 4°C (Figure 5.5A): first, mechanical dicing of the tissues using scissors, followed by enzymatic dissociation applying an enzyme mix consisting of Liberase^{TM}, Collagenase D and Dispase II for 45 min rotating in the cold room. The suspension was then passed through a syringe by back loading to further dissociate remaining tissue parts. Single cells were resuspended in DMEM containing BSA and EDTA to stop the enzymatic activity. Afterwards, red blood cells were lysed. Since metastases in the MT-ret derived syngraft model develop approximately two months after the resection of the primary tumour, dissociated samples needed to be cryo-preserved until all sam-

ples are collected to allow parallel downstream processing of all samples, thereby, reducing batch effects.

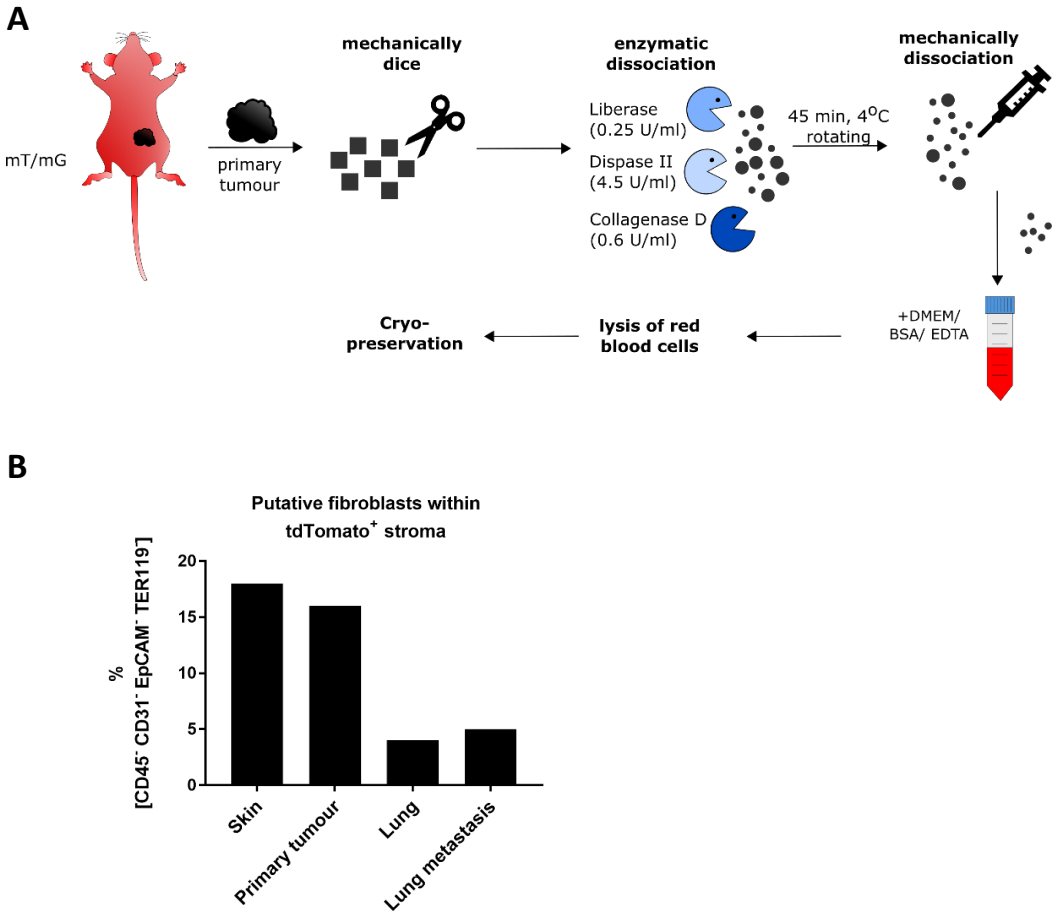

Figure 5.5: **scRNA sequencing sample preparation.** (A) Schematic re-presentation of the optimised protocol for isolation of single cells at low temperatures. (B) Putative fibroblast populations in challenged and unchallenged tissues. Bars show the percentage of putative fibroblasts within the tdTomato positive stromal fraction.

A main readout for the suitability of a protocol is the proportion of recovered fibroblasts in the processed samples. To determine putative fibroblast and CAF proportions, FACS analysis was performed. Due to the fact that there is not one single marker, which labels all normal fibroblasts and CAFs, negative selection for linage markers (CD45, CD31, EpCAM, TER119) is commonly performed and was applied here to identify putative fibroblasts by FACS [Bartoschek et al., 2018]. The described dissociation protocol and FACS panel were applied to samples of the

primary tumour and lung metastases, as well as to their unchallenged counterparts skin and lung. Figure 5.5B shows the percentage of putative fibroblasts in each of these tissues. Comparison of the numbers reveals that the overall proportion of putative fibroblasts and CAFs, do not differ appreciably between unchallenged and tumour samples. However, in samples from the primary tumour (16 %) and unchallenged skin (18 %), the percentage of CAFs and fibroblasts, respectively, is higher compared to samples from lung metastasis (4.5 %) and unchallenged lung (3.5 %). Nevertheless, in all conditions the percentage of putative fibroblasts is likely high enough to apply the established dissociation protocol for scRNA sequencing samples.

5.4 scRNA sequencing data mirrors heterogeneous tumour tissue composition

I could show by IF stainings of primary tumour and metastasis tissue sections that CAFs are abundant in the TME of the MT-ret derived syngraft model. Moreover, FACS analysis indicates that fibroblasts and CAFs remain at a high frequency in the TME cell fraction after dissociation into single cells.

In a next step, to investigate CAF heterogeneity and corresponding expression patterns, scRNA sequencing was performed on samples from primary tumours of tumour bearing mice and corresponding lung metastases (Figure 5.6A). Tissues were dissociated into single cells and cryo-preserved according to the protocol described in Figure 5.5A until all relevant specimens could be collected. Thawed samples were then FACSorted for tdTomato positive stromal cells from the host and tdTomato negative tumour cells. Furthermore, in three replicates CD45 positive cells were depleted by FACS to additionally enrich fibroblasts and CAFs. Library preparation was performed using the 10x Chromium Next GEM Single Cell 3' GEM, Library and Gel Bead Kit v3.1 followed by sequencing on a NovaSeq 6000. In order to process all samples, four runs of library preparation and sequencing were performed. Care was always taken to ensure that a primary tumour and its corresponding lung metastasis were in the same run. Thus, expression differences between primary tumour and metastasis due to technical aspects could be excluded.

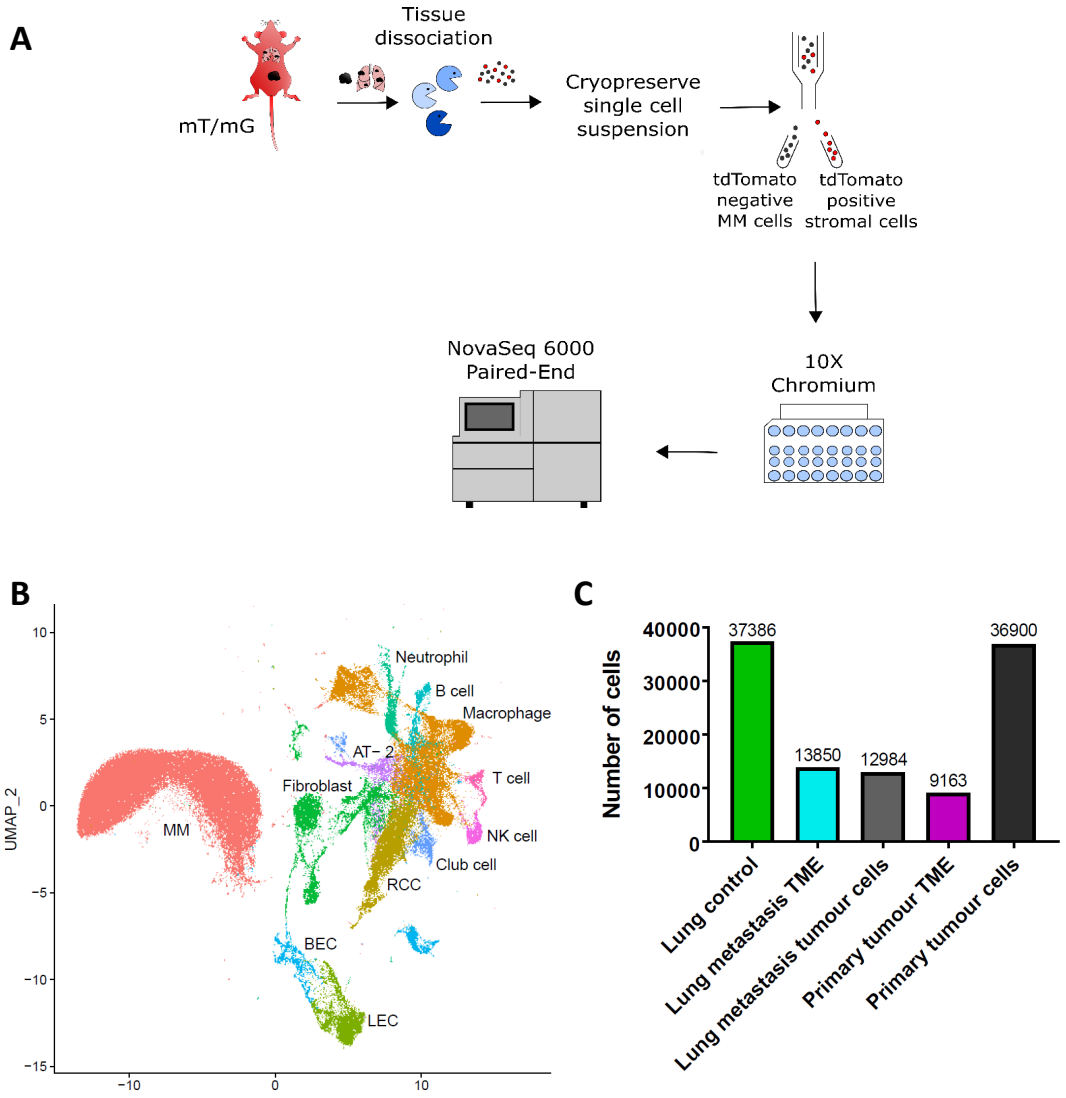

Figure 5.6: **Cellular composition of unchallenged lung and MM tissue.** (A) Schematic overview of the work-flow of the scRNA sequencing sample preparation. It took a total of four rounds of library preparation and sequencing to process all samples. (B) Cell clusters from 10x Genomics scRNA-sequencing analysis visualised by Uniform Manifold Approximation and Projection (UMAP) with cells colour coded for cell type. Analysis was based on data processed by Dr. Joschka Hey.(C) Number of cells per tissue, which passed QC.

After quality control metrics (e.g. genes per cell and percentage of mitochondrial genes) were applied, 227.146 cells remained in the data set and clustered into 12 cell type cluster (Figure 5.6B). Figure 5.6C shows the contribution per tissue type, which were 37.368 cells from the unchallenged lung controls, 13.850 cells from the lung metastasis TME, 12.984 metastasis tumour cells, 9.163 cells from the primary tumour TME and 36.900 primary tumour cells.

Collectively, these cells reflected the breadth of cell types within a tumour tissue. According to commonly known linage markers, I identified MM cells (*Cited1, Cd63, Dct*), fibroblasts (*Mgp, Dcn, Col1a1*), blood- (BEC; *Pecam, Cd34, Vwf*) and lymphatic endothelial cells (LEC; *Lyve1, Tmem100, Cldn5*) as well as immune cells including macrophages (*Lyz2, Chil3, Ccl6*), neutrophils (*S100a9, S100a8, Il1b*), B cells (*Cd79a, Cd79b, Igkc*), NK cells (*Nkg7, Gzma, Ccl5*) and T cells (*Cd3g, Il7r, Trac*). Lung specific cell types like alveolar type II cells (AT-2; *Sftpb, Sftpd, Slc34a2*), club cells (*Scgb3a2, Scgb1a1, Scgb3a1*) and respiratory ciliated cells (RCC; *Tmem212, Sec14l3, Ccdc153*) were also present (Figure 5.7).

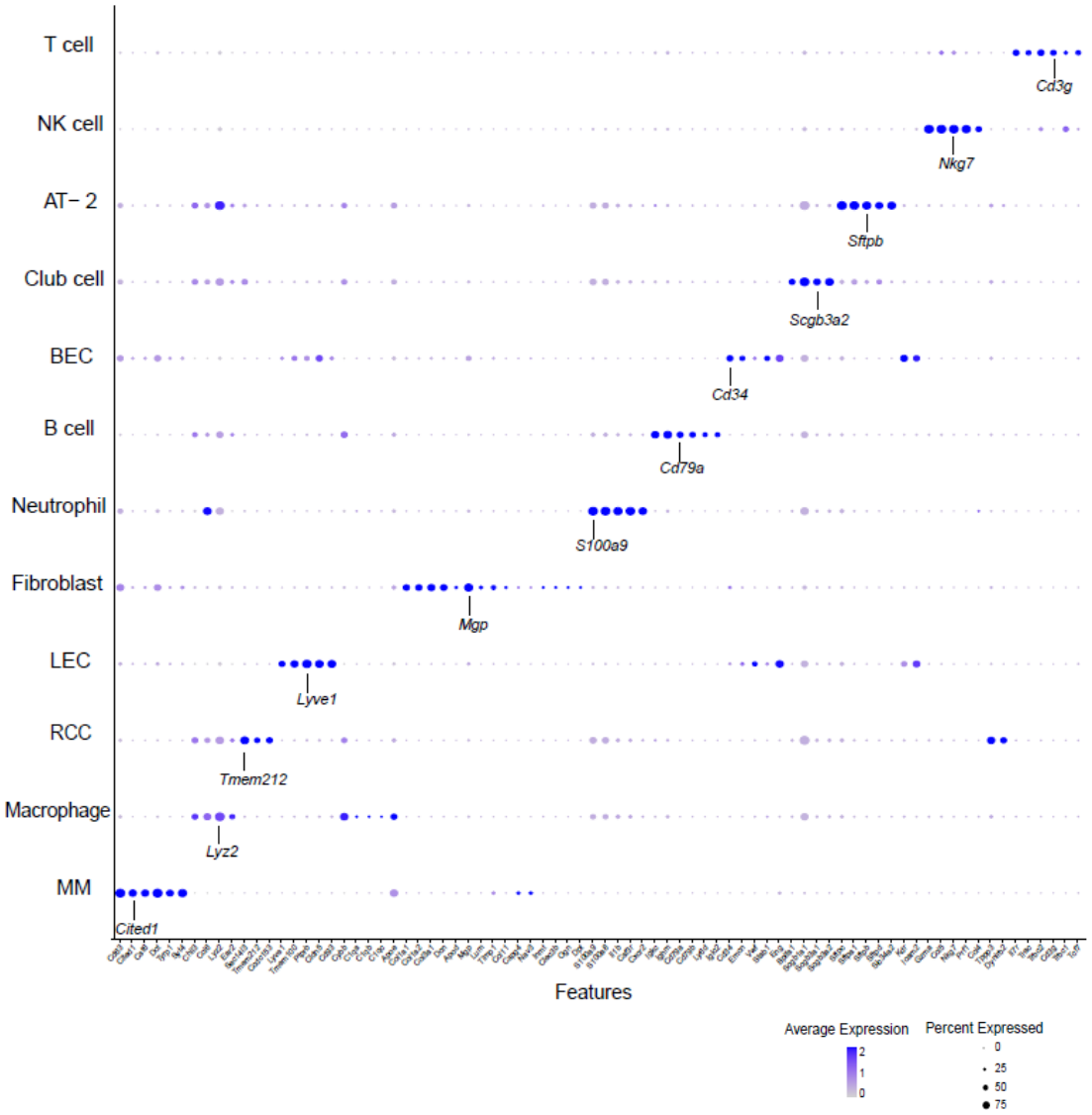

Figure 5.7: **Expression of linage marker genes of different cell types.** Dotplot shows the expression of selected linage markers across all cell types. Size of dot indicates the percentage of cells within a cluster, which express the gene. Colour reflects the average expression. Data was produced jointly with Dr. Joschka Hey.

Extracting MM cells and non-malignant cells into two separate UMAP plots allows for more detailed distinction of clusters within the two groups of cells. For MM cells high intra- and inter- tumour heterogeneity has been described in literature [Tirosh et al., 2016]. In line with this, figure 5.8A shows that MM cells formed three distinct groups. To investigate if this was driven by tumour site specific differences, cells were colour coded by their tissue of origin, revealing that one group was exclusively derived from primary tumour samples, one was metastasis specific and the one in between was a mixture of both tissues (Figure 5.8B).

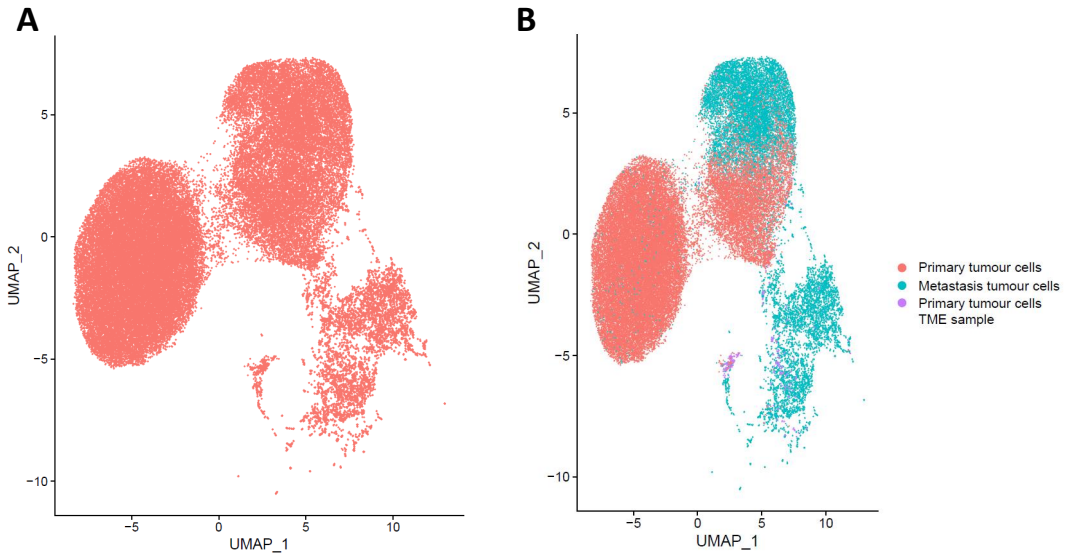

Figure 5.8: **scRNA sequencing reveals distinct MM cell cluster for primary tumours and metastases.** (A) MM cluster extracted from Figure 5.6B with cells colour coded for tissue of origin (B). Data was produced in collaboration with Dr. Joschka Hey.

In regards to non-malignant cells, examining the composition and tissue of origin of non-malignant cells reveals that macrophages mainly derived from the unchallenged lung control tissue with a separate group of macrophages from both, primary tumour and lung metastasis (Figure 5.9). Similarly, endothelial cells and fibroblast formed separate clusters for each tissue. However, cells from the different tissues were evenly distributed in the clusters for NK and T-cells. Inspecting lung specific cell type clusters, it occurred that RCC, club cells and AT-2 cells not only originated from unchallenged lung control samples but also from metastasis samples. Taken together, this indicates, that my dataset not only harbours the potential to assess tumour/ metastasis- specific genetic signatures of CAFs but also of MM cells, endothelial cells and macrophages.

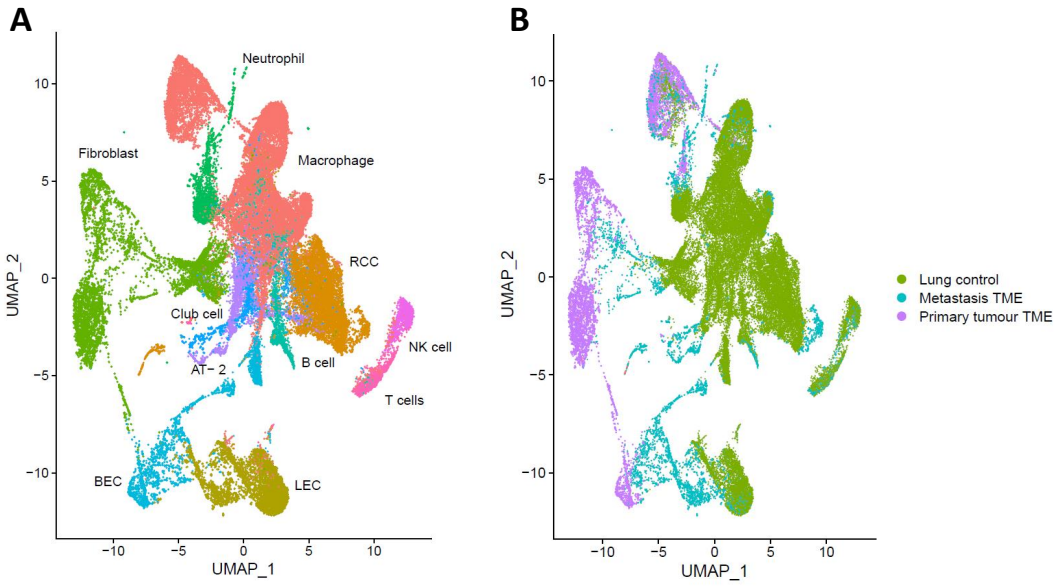

Figure 5.9: **scRNA sequencing data reflects breadth of TME composition for MM primary tumours and metastases.** TME and lung ctrl cluster extracted from figure 5.6B with cells colour coded for cell type (A) and tissue of origin (B). Data was produced jointly with Dr. Joschka Hey.

5.5 scRNA-sequencing allows identification of distinct CAF clusters

Aiming to investigate CAF heterogeneity in more detail, I analysed clusters, which expressed a set of fibroblast markers including collagens (*Col1a1*, *Col1a2* and *Col3a1*), extracellular matrix proteins (*Mgp*) and proteoglycans (*Dcn* and *Lum*). As shown in figure 5.10B, those markers are exclusively expressed by fibroblasts and no other cell type. Thus, confirming that most contaminating cells from other cell types like immune, epithelial, endothelial and MM cells were excluded *in silico* from the data set before performing fibroblast specific analysis.

Clustering of the isolated cells resulted in 11 clusters for normal fibroblasts and CAFs, which are visualised in figure 5.10A. Creating a heatmap with the top marker genes for each cluster, demonstrated a definite separation of the clusters based on their marker gene expression. For many clusters affiliation to known fibroblast types could be assigned on the basis of the expressed marker genes (Figure 5.10C). Lung specific fibroblast types like alveolar and peribronchial fibroblasts could be designated by the expression of *Npnt*, *Mfap4*, *Fmo2*, *Inmt* and *Hhip*, *Mustn1*, *Enpp2*, respectively (Figure 5.10C/D). Upregulation of the genes *Rgs5*, *Myh11* and *Myl9* identified a smooth muscle cell (SMC) cluster. Buechler et al. propose that advential and parenchymal fibroblasts are universal fibroblast types, which serve as a source for specialised fibroblasts, both, advential (*Pi16* and *Ly6a*) and parenchymal (*Col15a1* and *Fbn2*) fibroblasts were present in my data [Buechler et al., 2021]. Extracellular matrix (ECM) fibroblasts were named after their high expression of extracellular matrix related genes like *Tnxb*, *Col3a1*, *Col1a2* and *Fbn1*. Interestingly, clustering revealed the presence of a subset, which expressed strongly *Vegfa*, which I termed VEGFα CAFs.

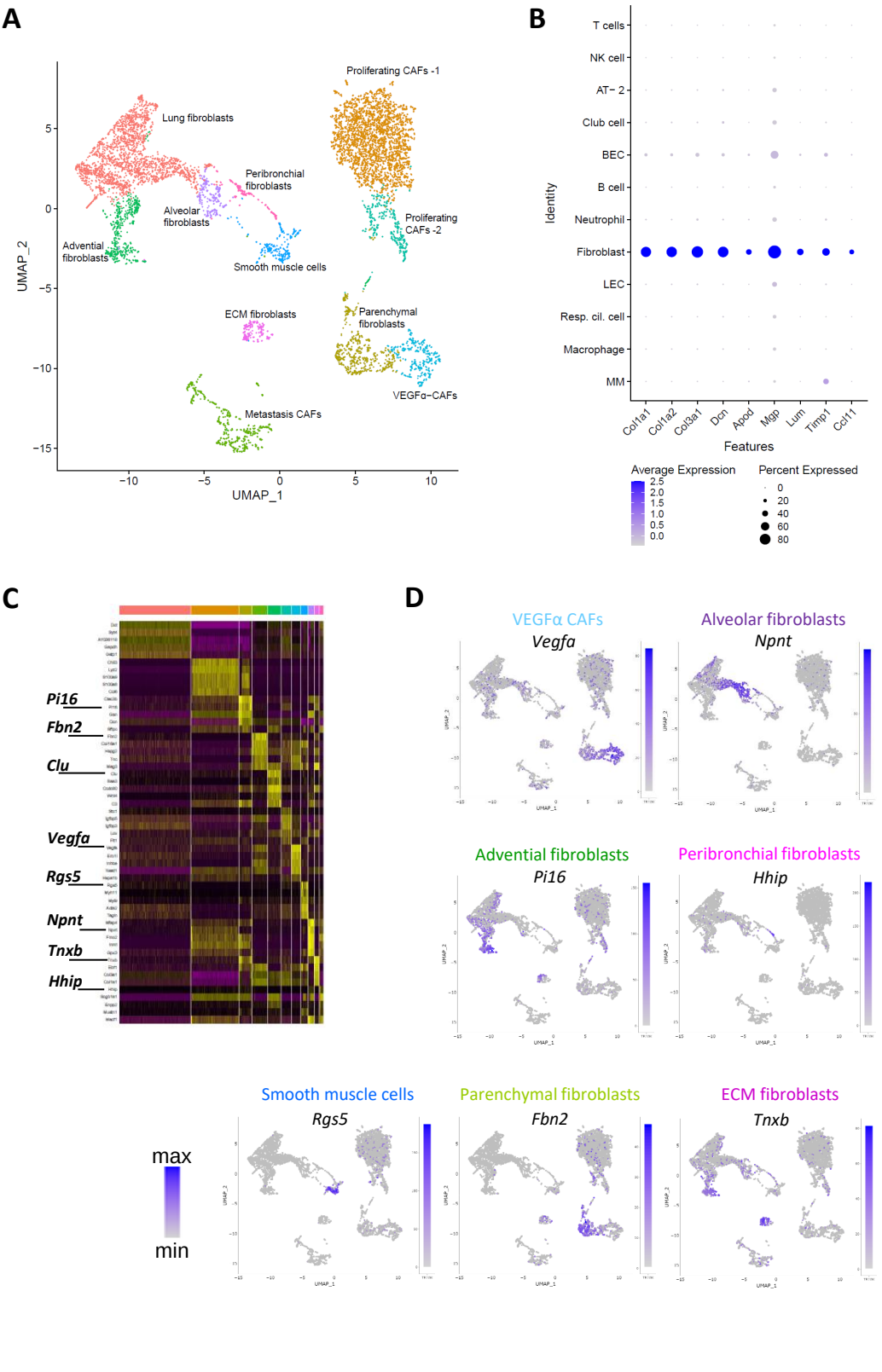
A
Proliferating CAFs -1
Lung fibroblasts
Peribronchial fibroblasts
Alveolar fibroblasts
Proliferating CAFs -2
Advential fibroblasts
Smooth muscle cells
ECM fibroblasts
Parenchymal fibroblasts
VEGFα−CAFs
Metastasis CAFs
UMAP_2
UMAP_1
B
T cells
NK cell
AT− 2
Club cell
BEC
B cell
Neutrophil
Fibroblast
LEC
Resp. cil. cell
Macrophage
MM
Identity
Col1a1
Col1a2
Col3a1
Dcn
Apod
Mgp
Lum
Timp1
Ccl11
Features
Average Expression
Percent Expressed
C
Pi16
Fbn2
Clu
Vegfa
Rgs5
Npnt
Tnxb
Hhip
D
VEGFα CAFs
Vegfa
Alveolar fibroblasts
Npnt
Advential fibroblasts
Pi16
Peribronchial fibroblasts
Hhip
Smooth muscle cells
Rgs5
Parenchymal fibroblasts
Fbn2
ECM fibroblasts
Tnxb
max
min

Figure 5.10: **Putative fibroblast populations identified in unchallenged lung and melanoma tissue.** (A) Fibroblast cluster extracted from figure 5.6B with cells colour coded for sub-clusters. (B) Expression of fibroblast marker genes across all cell types. Size of dot indicates the percentage of cells within a cluster, which express the gene. Colour reflects the average expression. (C) Heatmap showing the top 5 marker genes for all fibroblast sub-cluster. (D) Selected marker genes, which were used to annotate sub-clusters. Colour code indicates level of gene expression. (A)-(C) Analysis was based on data processed by Dr. Joschka Hey.

VEGFA is a member of the vascular endothelial growth factor (VEGF) family, which contains the five ligands VEGFA, VEGFB, VEGFC, VEGFD and placenta growth factor (PlGF). The coresponding VEGF receptors VEGFR-1, VEGFR-2 and VEGFR-3 are mainly expressed on blood endothelial cells, non-endothelial cells and lymphatic endothelial cells, respectively. The function of binding to VEGFR-1 makes VEGFA to the main regulator of angiogenesis. Blood vessel formation, in turn, is one of the hallmarks of cancer and is required for nutrient and oxygen supply of tumour cells [Apte et al., 2019; Hanahan and Weinberg, 2011]. This prompted me to further explore the transcriptional profile of this cluster.

5.6 VEGFα CAFs in murine MM primary tumours harbour an angiogenesis signature

First, I investigated if other marker genes of this cluster were also related to angiogenesis (Figure 5.11A). Indeed, N-myc downstream regulated gene 1 (*Ndrg1*) has been shown to be involved in VEGFA induced angiogenesis [Watari et al., 2020]. Furthermore, the heat shock proteins HSPA1A and HSPA1B are known to be induced by hypoxia, which is a prerequisite condition for angiogenesis [Daugaard et al., 2005].

In a next step, I wanted to further confirm the angiognesis gene signature by performing gene ontology (GO) term analysis, which is a method to investigate the enrichment of gene sets related to biological processes. This revealed, besides fibroblast specific GO terms such as 'regulation of cell-matrix adhesion', other terms, which are in line with the above mentioned angiogenesis related genes. The analysis also indicates an upregulation of TGF-β, EGFR1 and HIF-1 signalling pathways, which are important for blood vessel formation (Figure 5.11B).

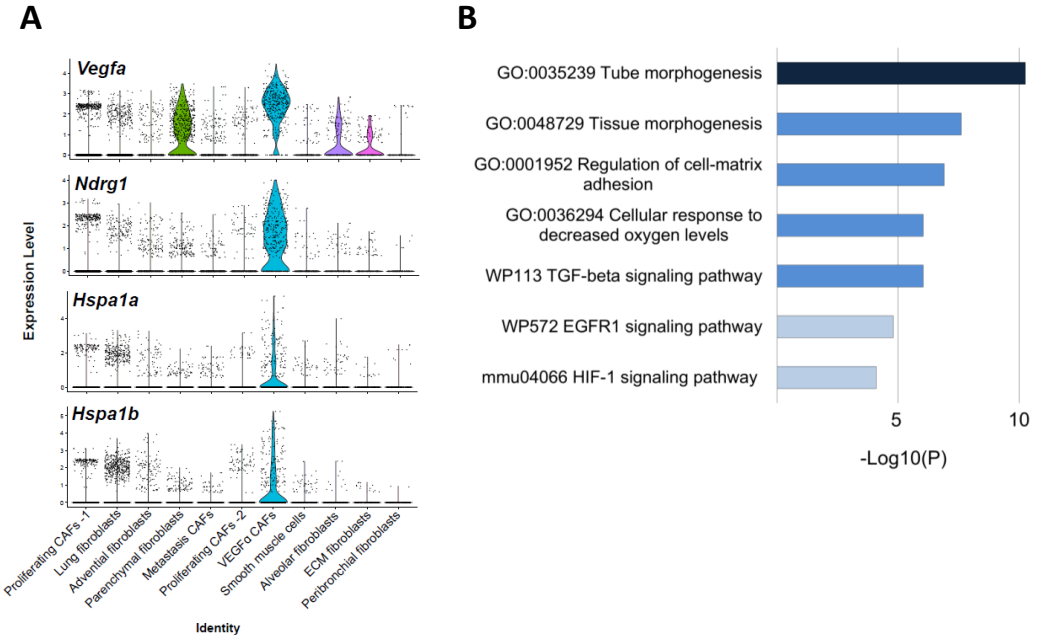

Figure 5.11: **VEGFα CAFs have an angiogenetic transcriptional profile.** (A) Violin plots show expression of angiogenesis specific marker genes of VEGFα CAFs for all CAF sub populations. Data was pre-processed by Dr. Joschka Hey and further analysed by myself. (B) GO term analysis with the top marker genes with an adjusted P-value < 0.01 and an average log2 fold change > 1 (Metascape: Zhou et al. [2019]).

Interestingly, Bartoschek et al. also identified CAFs with a vasuclar signature (vCAFs) and found a cycling CAF population (cCAFs), which clustered together with vCAFs and, shown by IF staining on tissue sections, to be surrounded by vCAFs [Bartoschek et al., 2018]. Therfore, I investigated if my dataset also contained proliferating CAFs, which might be related to VEGFα CAFs. Analysing the expression level of genes activated during different states of the cell cycle, showed two highly proliferative CAF populations for which a functional annotation according to marker gene expression was not possible, before (Figure 5.12). Hence, these clusters were named 'proliferating CAFs-1 and -2'. Compared to the other CAF subsets, the proliferating CAF-1 cluster was the largest one, and, together with the proliferating CAF-2 cluster, made up the majority of primary tumour CAFs (3429 proliferating CAFs vs. 611 parenchymal fibroblasts and 383 VEGFα CAFs).

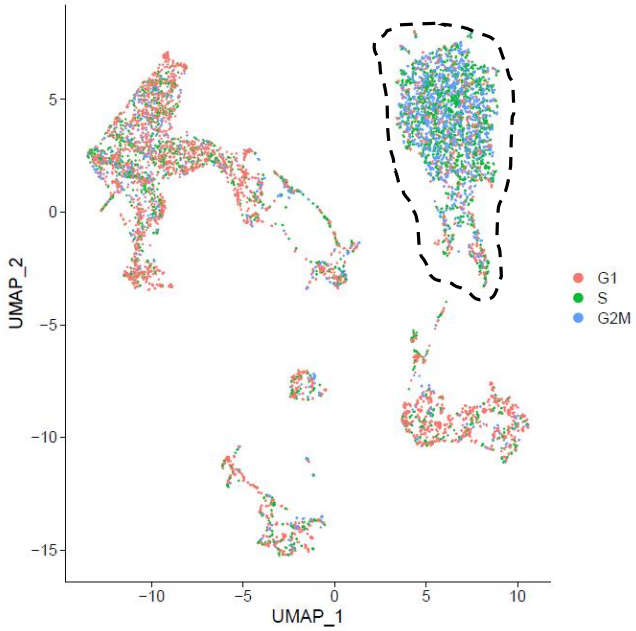

Figure 5.12: **Cell cycle analysis reveals highly proliferative CAF populations within the primary tumour.** Colour code indicates in which cell cycle phase cells were: G1 (red), S (green), G2/M (blue). Dashed line encircles highly proliferative clusters. Data was produced jointly with Dr. Joschka Hey.

5.7 CAF subsets can be clearly separated by their tissue of origin

I next set out to determine whether metastasis specific CAFs have a gene signature, which functionally clearly distinguishes them from primary tumour CAFs. To identify which cell clusters contain metastasis CAFs, cells were colour coded according to their tissue of origin, which was determined by the samples from which the cells were derived (Figure 5.13A/B).

Alveolar and peribronchial fibroblasts come from unchallenged lung control tissue and from lung metastasis samples. Highlighting the tissue of origin revealed one fibroblast cluster, which only contained cells from the lung control. This cluster didn't have a clear marker gene signature for functional annotation and, thus, was named according to its tissue origin 'lung fibroblasts'.

Parenchymal fibroblasts and proliferating CAFs 1 and 2 mainly derive from the primary tumour TME (611, 3004 and 397 cells) and rarely from the metastasis TME (19, 13 and 15 cells). VEGFα CAFs and ECM fibroblasts are clusters, which exclusively contain cells from the primary tumour TME. In contrast, SMC and advential fibroblasts derive from all three tissues (21 and 445 cells lung control, 130 and 56 cells metastasis TME and 130 and 34 cells primary tumour TME).

One cluster consisted mainly of CAFs from the metastasis TME (521 cells) and a few cells from lung control tissue (13 cells) and the primary tumour TME (16 cells), and therefore was called 'metastasis CAFs'.

I could identify a transcriptional profile, which was specific for all subsets deriving mostly from one certain tissue type (Figure 5.13C). Clusters containing primarily fibroblasts from unchallenged lung tissue, strongly expressed *Gsn*. Metastasis CAFs exhibit an immunogenic signature, expressing *Cxcl12* and *Apoe*, while all clusters with a majority of primary tumour CAFs were positive for the mesenchymal marker *Postn*.

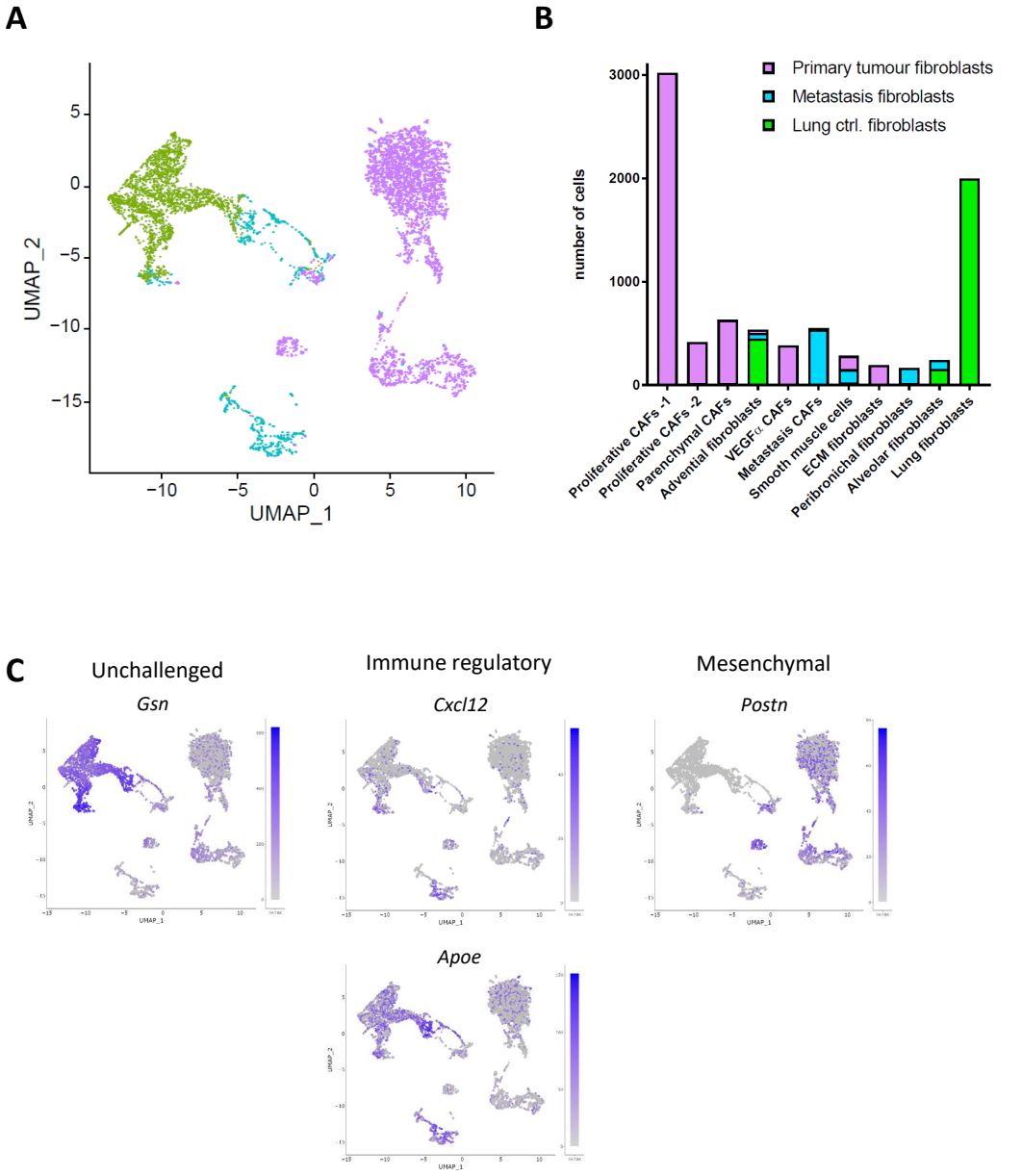

Figure 5.13: **Tissue specific transcriptional profiles of fibroblast subsets.** (A) Colour code indicates from which tissue a cell derived: Cells from unchallenged lung tissues in green, cells from lung metastasis in blue and cells from primary tumour tissue in purple. Data was produced under the guidance of Dr. Joschka Hey. (B) Quantitative representation of (A). (C) Distribution of tissue specific expression patterns of *Gsn*, *Cxcl12*, *Apoe* and *Postn*. Colour code indicates level of gene expression.

5.8 The pro-tumourigenic gene *Saa3* is exclusively expressed in metastasis CAFs

Having identified one specific metastasis CAF subset, I investigated its transcriptional profile in more depth. By exploring the expressed marker genes for this cluster, I found *Cxadr* and *Lgals7* (encoding proteins involved in cell-cell and cell-matrix interactions) to be upregulated, as well as *Clu* (encoding an extracellular chaperone) and *Calca* (encoding a vasodilator). In addition, *Wnt4* and *Wt1* genes were highly expressed (Figure 5.14A). WNT4 regulates the canonical and non-canonical β-catenin pathways and WT1 is on the one hand a tumour suppressor but on the other hand also involved in development of different organs like kidney, gonads and lung [Zhang et al., 2021; Wilm and Muñoz-Chapuli, 2016]. In line with this, many developmental GO terms were upregulated (Figure 5.14B).

Moreover, metastasis CAFs express the pro-tumourigenic gene *Saa3*. Serum Amyloid A (SAA) proteins are acute phase proteins, which are, under physiological conditions, induced as a response to systemic inflammation. However, in the context of tumour development SAA3 has been described to regulate the formation of a metastatic niche in liver and lung, and to act as a chemoattractant for monocytes and neutrophils. In the literature, many receptors, including TLR2, TLR4, and RAGE, have been described to bind SAA3 and transfer its stimulus to intracellular signalling pathways [Lee and Beatty, 2021; Hansen et al., 2015]. SAA3 receptors are expressed on a broad range of cell types, indicating the importance of SAA3 in many biological processes. For instance, SAA3 has been shown to induce the expression of multiple matrix metalloproteinases (MMPs) and cytokines like S100A4/8/9, G-CSF, IL-6, IL-1β, TNF, which is also reflected by the upregulated GO terms. In turn, many of these molecules can lead to *Saa3* expression via NF-κB signalling [Lee and Beatty, 2021; Hansen et al., 2015].

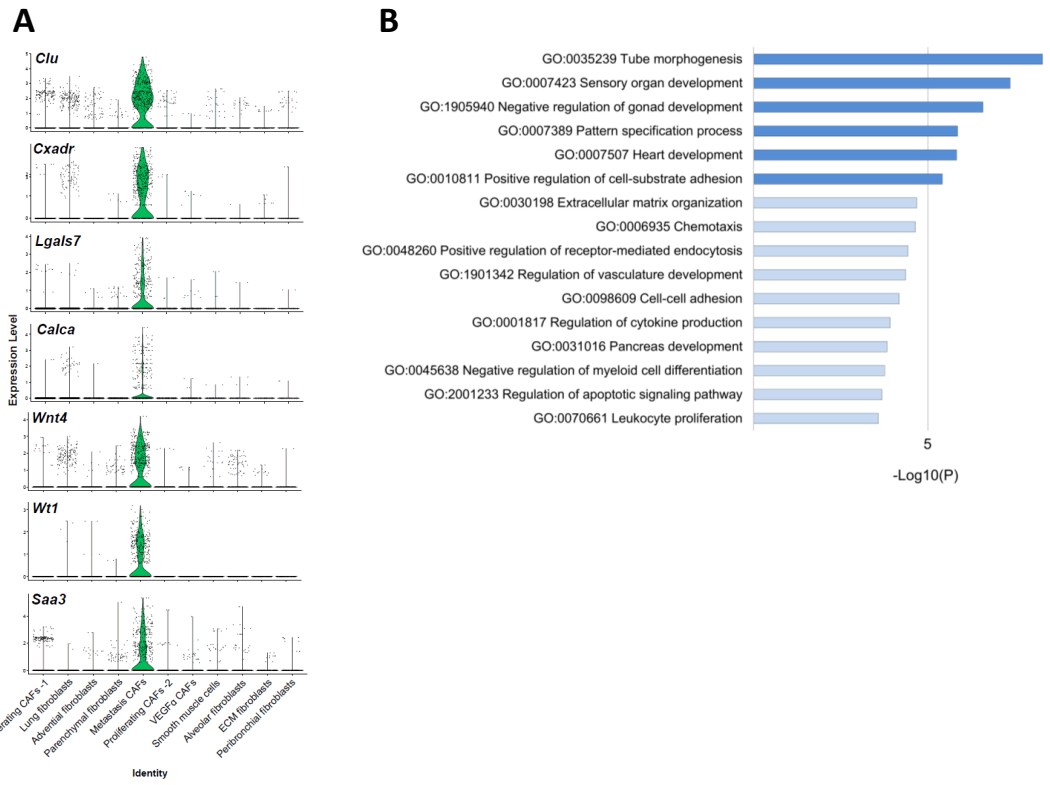

Figure 5.14: **Gene signature of metastasis CAFs exhibits developmental and immunogenic features.** (A) Violin plots show expression of the top marker genes of metastasis CAFs for all CAF sub populations. Data was pre-processed by Dr. Joschka Hey and further analysed by myself. (B) GO term analysis with the top marker genes with an adjusted P-value < 0.01 and an average log2 fold change > 1 (Metascape:Zhou et al. [2019]).

In order to find out how *Saa3* expression got induced in metastasis CAFs, I investigated the presence of the above described ligands and their receptors (Figure 5.15A). Interestingly, among the contemplable ligands, *Il1b*, *Tnf* and *S100A4* were the only ones, which were expressed in my data (Figure 5.15A). *Il1b* was mainly expressed by neutrophils and macrophages, while its corresponding receptor *Il1r1* was broadly expressed in metastatic CAFs and less frequently in other CAFs and normal fibroblasts. *Tnf* was expressed in a salt- and- pepper pattern throughout all immune cell clusters except the NK cell cluster. In line with that, the TNF receptor *Tnfrsf1a* was expressed in a similar pattern and at a uniform level in all CAF and normal fibroblast clusters. Of all putative ligands, *S100a4* was expressed most prominently. Each cell type expressed *S100a4* to a certain extent. In contrast, most of the potential receptors for S100A4 are not expressed on CAFs, only *Tlr4* was expressed sparsely in metastasis CAFs.
Since SAA3 is mostly regulated via the NF-κB pathway and also acts by activating it, I explored if members of this pathway were expressed in metastasis CAFs [Hiratsuka et al., 2008]. Indeed, figure 5.15B shows that NF-κB (*Nfkb1*) itself and IκB (*Nfkbia*) were both expressed in metastasis CAFs in a similar distribution like *Saa3* (Figure 5.15B).

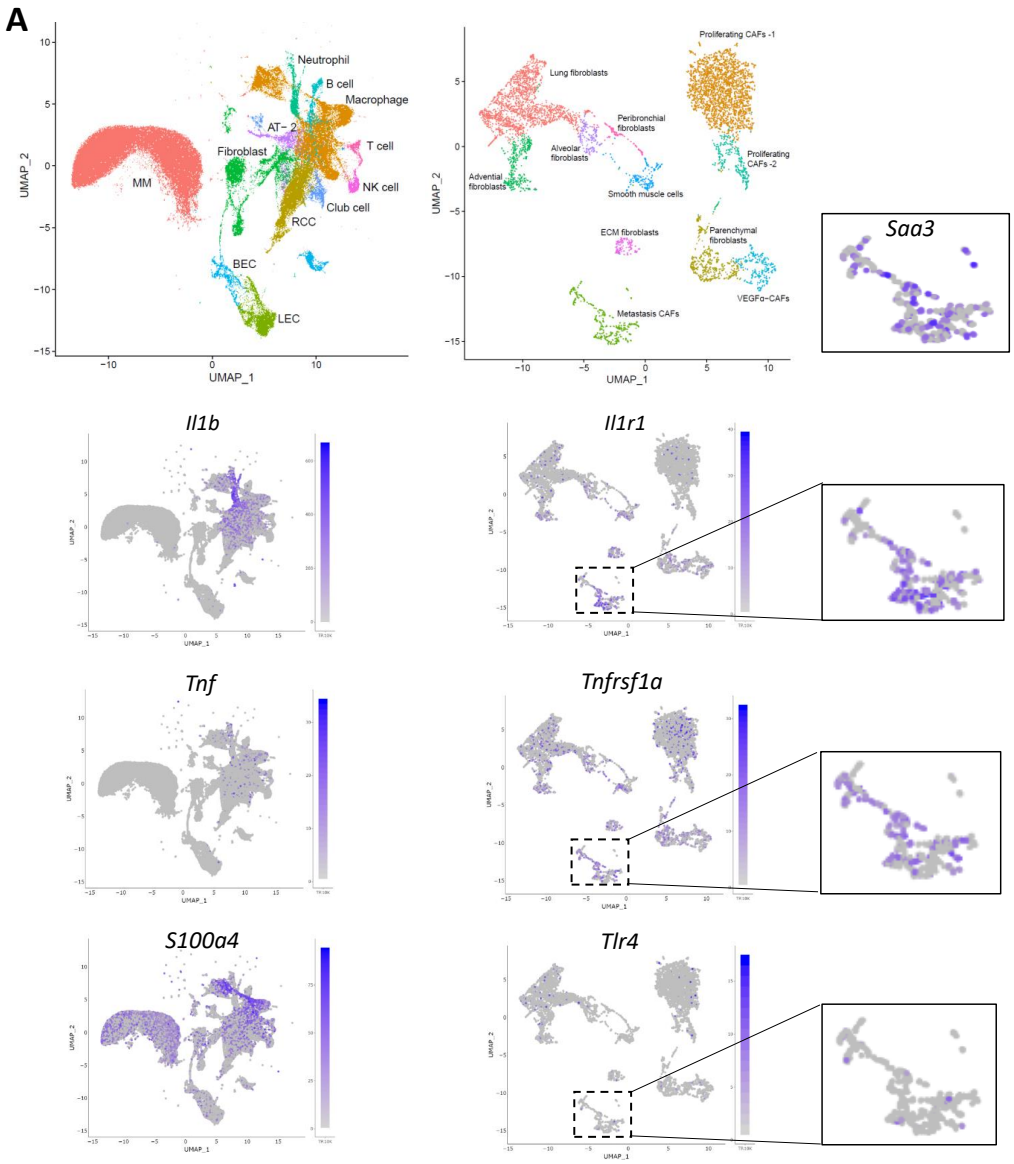
A
Neutrophil
B cell
Macrophage
AT− 2
Fibroblast
T cell
MM
NK cell
Club cell
RCC
BEC
LEC
UMAP_1
UMAP_2
Proliferating CAFs -1
Lung fibroblasts
Peribronchial fibroblasts
Alveolar fibroblasts
Proliferating CAFs -2
Advential fibroblasts
Smooth muscle cells
ECM fibroblasts
Parenchymal fibroblasts
VEGFα-CAFs
Metastasis CAFs
Saa3
Il1b
Il1r1
Tnf
Tnfrsf1a
S100a4
Tlr4
B
Nfkb1
Saa3
Nfkbia (IkBa)

Figure 5.15: ***Saa3* expression in metastasis CAFs is potentially induced by Il1β signalling.** (A) Top row: overview of all cell type (left) and CAF (right) clusters. For details, see figure 5.6B and figure 5.10A. Below: expression of putative ligands in all cells (left) and expression of corresponding receptors on fibroblasts (middle), with a magnification of the metastasis CAF cluster (right). (B) Expression pattern of *Nfkb1* and *Nfkbia* in metastasis CAFs. Magnification of metastasis CAF cluster and comparison to *Saa3* expression in the middle. Colour code indicates level of gene expression.

5.9 Expression of *Mpp6* and *Saa3* negatively correlate in metastasis CAFs

My data show that *Saa3* is a specific marker for metastasis CAFs and suggests that its expression is induced via the IL1R1 related signalling pathway. Strikingly, GO term analysis indicates that *Saa3* expression strongly shapes the properties of metastasis CAFs, since many of the upregulated terms relate to biological functions of SAA3. Correspondingly, Djurec et al. propose a pro-tumourigenic capacity specifically for *Saa3* positive CAFs in pancreatic tumours [Djurec et al., 2018]. In their model *Saa3* positive CAFs promote tumour growth, while *Saa3*-null CAFs suppress it. They identified Mpp6, a member of the palmitoylated membrane protein subfamily of the peripheral membrane-associated guanylate kinases (MAGUK), to play a central role this mechanism. Thus, I analysed and compared the expression pattern of *Mpp6* in metastasis CAFs. Interestingly, *Mpp6* was also highly, but mutually exclusive expressed with *Saa3* (Figure 5.16).

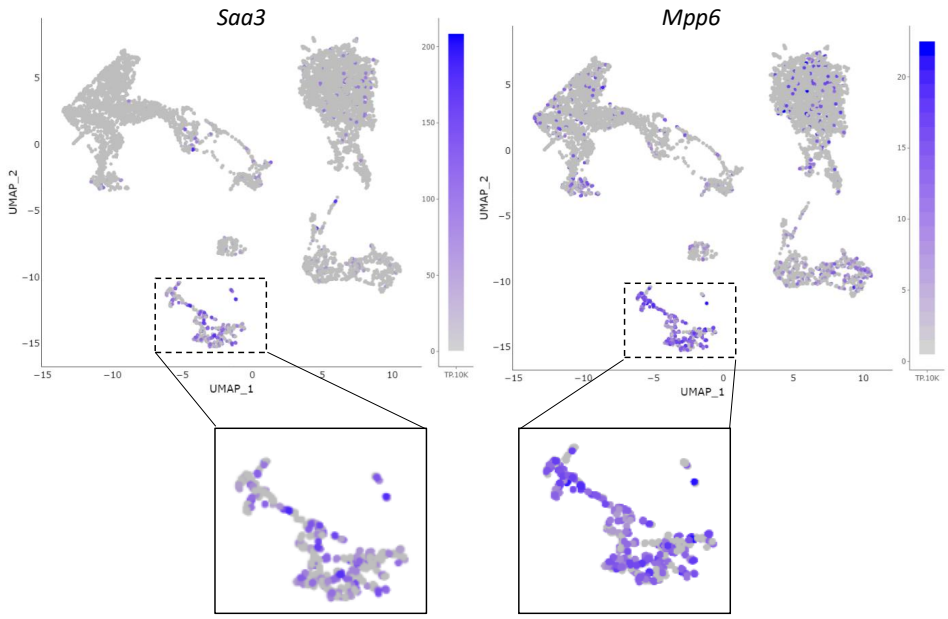

Figure 5.16: **Metastasis CAFs express *Saa3* and *Mpp6* in a mutually exclusive pattern.** Overview of *Saa3* and *Mpp6* expression in CAF clusters and magnification of the metastasis CAF cluster. For details, see figure 5.10A. Colour code indicates level of gene expression.

6 Discussion

Despite great improvements in the therapy of advanced melanoma, MM is still a very deadly type of skin cancer with a continuously increasing global incidence [Davey et al., 2021; Schadendorf et al., 2015]. Metastasis in distant organs plays a central role in the lethality of MM patients [Zbytek et al., 2008]. Since researchers have started to apprehend the importance of non-malignant cells of the TME, in terms of cancer progression and metastasis, hopes were raised to develop further therapy options by targeting the TME. Therefore, I aim to gain detailed insights into the interplay between melanoma cells and CAFs, as CAFs represent the most abundant and active component of the TME. Here, scRNA sequencing offers a new tool for in depth analysis and comparison of genetic programs and putative functions of present CAF populations.

Collectively, I could show that, surprisingly, primary tumour growth in the MT-ret derived syngraft model is independent of PDPN in CAFs, albeit the fact, that this protein represents a hallmark of at least a subset of CAFs and, thus, was proposed to play a crucial role in CAF function. Moreover, scRNA sequencing data showed that sample preparation with the here established protocol at low temperatures, including a cryo-preservation step, conserved cell type heterogeneity of tumour tissues. The analysis of approximately 8.400 normal fibroblasts and CAFs resulted in 11 clusters of which at least 4 clusters corresponded to CAF populations and the remaining clusters to normal fibroblasts. Primary tumour CAF subsets exhibited a mesenchymal profile, while metastasis CAFs expressed the immune regulatory markers *Cxcl12* and *Apoe*. Further analysis of marker expression patterns showed that one subset of primary tumour CAFs strongly expressed *Vegfa* and other angiogenesis related marker genes. Most interestingly, the metastasis CAF cluster had a very distinct signature, which was linked to *Saa3* related signalling. The data suggests that *Saa3* expression was activated by Il1β signalling. Additionally, I found that *Saa3* and *Mpp6* were mutually exclusive expressed in metastasis CAFs, indicating Mpp6 as a possible antagonist of Saa3.

6.1 Targeting CAF-specific PDPN directly does not inhibit MM primary tumour growth

In many tumour entities, like lung SCC, or lung, breast and pancreas adenocarcinomas, PDPN expressing CAFs were shown to correlate with bad prognosis [Suzuki et al., 2022]. Moreover, Hoshino et al. link the expression of PDPN in CAFs to promotion of tumour progression and metastasis [Hoshino et al., 2011]. Analysis of samples from cancer patients, divided into PDPN- high and PDPN-low groups, revealed a connection of PDPN-positive CAFs with an immunosuppressive TME [Suzuki et al., 2022]. These examples elucidate the relevance of PDPN-positive CAFs in many cancers.

The findings of this thesis however, clearly show by functional means, that although PDPN has been indicated to be a crucial factor for the pro-tumourigenic function of CAFs, *Pdpn* KO in CAFs didn't inhibit growth of murine MM primary tumours.

On a molecular level, PDPN, as a transmembrane protein, has multiple ways of interaction with other proteins. It can lead to stimulation of surface proteins on other cells, like CLEC-2 on platelets and immune cells, leading to enhanced activation and motility [Astarita et al., 2012]. Alternatively, PDPN can interact with other transmembrane proteins on the same cell, such as CD44 [Astarita et al., 2012]. Additionally, it has been shown that PDPN leads to cell migration and invasion via the intracellular ERM (ezrin, radixin, moesin)-protein - Rho-A - ROCK axis [Martín-Villar et al., 2006]. Interestingly, Rho-A signalling can be induced not only via PDPN. Based on that, one could consider that compensation mechanisms might have developed, which keep Rho-A and ROCK active but don't rely on PDPN. In line with that is the work of Gaggioli et al., which postulates that Rho and ROCK function is required in leading fibroblasts to open a path in which tumour cells could follow [Gaggioli et al., 2007]. Strikingly, they state that it is Integrin-α5, which activates Rho-A. Thus, one explanation for the lacking effect of *Pdpn* KO in CAFs on tumour growth could be that reduced PDPN - ERM-protein - Rho-A - ROCK signalling can be compensated by Integrin-α5 - Rho-A - ROCK signalling. Similarly, Baars et al. showed that PDPN is not required in keratinocytes during re-epithelialisation of wounds, albeit its striking upregulation in keratinocytes around the wound margin [Baars et al., 2015]. Consequently, they

also concluded, that ERM proteins got activated via another protein in the case of *Pdpn* KO.

Taken together PDPN-related signalling seems to be involved in many processes, but targeting PDPN does not necessarily interfere with all of these processes. Thus, PDPN itself might not be the pathway component, which can be used as a therapeutic target in MM.

6.2 scRNA sequencing data partially match previously published CAF categories

The data show the presence of at least three CAF clusters within the TME of the primary tumour and one CAF cluster within lung metastasis. Marker expression patterns of these clusters suggest that published categorisations for CAFs are not fully compatible with the clusters described here.

In the study of Davidson et al., CAFs in B16.F10 based melanoma primary tumours were investigated [Davidson et al., 2020]. The marker genes, which were used to clearly distinguish the three CAF populations from another (α*SMA*, *CD34*, *Pdgfr*α, *Pdpn*), were all expressed throughout the here described CAF clusters, but in a salt and pepper pattern. Therefore, the distinct marker gene distributions of α*SMA*, *CD34*, *Pdgfr*α and *Pdpn*, corresponding to the described immune, desmoplastic and contractile CAFs were not present. There are several reasons, which might explain discrepancies between these two MM CAF studies. First, Davidson et al. used a different mouse model in which the latest end point was earlier compared to the end point in the present model (day 11 vs. ca. day 21). This attribute provided tumour cells in the present model more time to recruit and reprogram CAFs, potentially resulting in more or different CAFs, like it is the case in late stage tumours, when compared to early stages [Wang et al., 2021b].

Another possible explanation for the occurring differences could be that not only CAFs from one tumour entity contributed to the data but unchallenged lung fibroblasts together with CAFs from multiple tissues (primary tumour and lung metastasis). This might change the clustering and the definition of marker genes, which are upregulated in one CAF cluster as compared to all other fibroblast clusters [Ntranos et al., 2019]. In contrast, Davidson et al. investigated primary

tumours at multiple time points and didn't include metastases of distant organs, like lung or liver into their analysis. They were trying to include cells from unchallenged skin, however, at the end there were only 45 skin cells among all analysed cells, which is too little for significant conclusions.

Lastly, technical variability was probably introduced by using different library preparation platforms. While Davidson at al. applied the plate-based Smart-seq2, which allows sequencing of transcriptomes of a small amount of cells in great depth, I used the droplet-based 10X Genomics Chromium (10X) platform, where more cells can be sequenced at the same time but with a smaller sequencing depth [Wang et al., 2021a]. This also contributed to a big difference in the number of analysed CAFs. In the here presented data, 8.411 normal fibroblasts and CAFs were identified, while Davidson et al. sequenced a total of 4,627 cells of which only 454 cells were fibroblastic cells. Consequently, I could potentially identify more clusters, and thus, also rare CAF types, since my data contained much more cells and a certain amount of cells per cluster is required for statistical significant conclusions. The advantage of Davidson et al. was the possibility to analyse also weakly expressed genes within their clusters. Together, these three technical facts of different methods, sequencing depths and amounts of cells represent a major impact on variation in the data. However, since the aim of my dissertation was primarily to dissect cellular heterogeneity of CAFs, rather than analysing weakly expressed genes, it still seems that the 10X platform was the right choice.

Considering that there are already discrepancies in CAF classifications between two studies, which both investigated CAFs in murine MM, it seems natural that classifications from different tumour entities are not easily transferable to one another either, due to additional tissue specific differences. Nevertheless, it is worthwhile to discuss the differences and similarities of here described CAF populations to some other studies:

Metastasis CAFs expressed *Clu* and *Saa3* among the top marker genes for this cluster, which were described for apCAFs by Elyada et al. [Elyada et al., 2019]. However, MHCII related genes like *Cd74* or *H2-Ab1*, which were characteristic, too for apCAFs, were only weakly expressed. On the other hand, metastasis CAFs expressed markers of iCAFs such as *Cxcl12*. Gene signatures of CAFs related to the primary tumour TME were generally more similar to myofibroblastic CAFs (myCAFs), since e.g. *Tnc* and *Igfbp3* were broadly expressed and among the top

5 marker genes for the clusters of parenchymal fibroblasts and proliferating CAFs-2, respectively. This comparison shows, that the CAF classes defined by Elyada et al. fit partially, but not entirely, to the ones identified here. The analysis of Elyada et al. might be more similar to the here presented data as compared to Davidson et al., for two reasons. First, because Elyada et al. also used the 10X platform, and second, because they included cells from adjacent normal tissue into their analysis, like I included unchallenged lung cells.

Interestingly, the CAF populations defined by Bartoschek et al. have even more similarities to the here identified CAF subset functions [Bartoschek et al., 2018]. In the study of Bartoschek et al. 716 CAFs isolated from murine breast cancer (MMTV-PyMT mice) were grouped into vascular (vCAF), matrix (mCAF), cycling (cCAF) and developmental (dCAF) CAFs. In this study, GO-term analysis, using the top 150 differently expressed genes per cluster, was applied for the nomenclature of the CAF clusters. Congruently with the cluster names, in vCAFs GO sets for vascular development and angiogenesis were enriched, while it were ECM and EMT GO sets for mCAFs, cell cycle GO terms for cCAFs and tissue development and morphogenesis GO terms for dCAFs. I clearly identified proliferating CAFs-1 and -2, which correspond to cCAFs, since in both groups the genes for G2/M and S cell cycle phases were upregulated. mCAFs are similar to ECM fibroblasts in my data and vCAFs are enriched for similar GO terms like VEGFα CAFs. Lastly, metastasis CAFs partially have a developmental signature, as shown by the expression of *Wnt4* and *WT1*, and developmental GO terms. Thus, using these criteria metastasis CAFs are similar to dCAFs. Seeing such resemblances is rather surprising since Bartoschek et al. used the Smart-seq2 platform and investigated CAFs in a different tumour entity. Therefore, one could conclude that functional annotation based on GO term enrichment analysis, which itself has a large number of genes as input, might be broader applicable and transferable between different studies than classifications based on a small set of marker genes.

Overall, this comparison indicates that CAF classifications described in literature are not universally applicable for different mouse models or different tumour entities (Kanzaki 2020). However, similar experimental set-up and classifications based on GO set enrichment seem to enable comparison of CAFs analysed in different studies.

6.3 CAF derived VEGFα as potential therapeutic target

The findings of this dissertation suggest that there is at least one specific CAF population within the melanoma primary tumour TME, which specifically induces angiogenesis, and thus, supports nutrient supply for tumour cells.

I found that this specific subset - VEGFα CAFs - strongly expressed *Vegfa*. Binding of VEGF-A to it's receptors induces endothelial cell division, leading to vessel formation [Apte et al., 2019]. Moreover enrichment of the terms 'Tube morphogenesis', 'TGF-beta signaling pathway' and 'EGFR1 signaling pathway' further supported the potential task of this cluster for vessel formation. The expression of *Hspa1a* and *Hspa1b*, which are heat shock proteins induced by hypoxia, and the enrichment of the GO terms 'Cellular response to decreased oxygen levels' and 'HIF-1 signaling pathway' indicated that hypoxia induced the expression of *Vegfa* most likely via HIF-1.

Interestingly, the anti-VEGF drug bevacizumab is already included in multiple clinical trials for melanoma stage III/ IV therapies, further underlining the potential of CAF secreted VEGF as therapeutic target [Lopes et al., 2022].

Bartoschek et al. suggested that vCAFs originate from pericytes and detach from vessel proximity due to hypoxia [Bartoschek et al., 2018]. Indeed, pericyte markers *Cspg4* and *Pdgfrb* were expressed in VEGFα CAFs, while *Rgs5* was only weakly expressed. This might indicate a pericyte origin and a subsequent downregulation of certain pericyte markers.

6.4 scRNA sequencing data hints towards multiple putative origins of metastasis CAFs

Identifying the sources of CAFs has been the focus of many investigations. The data of this thesis suggests different putative sources of metastasis CAFs:

Analysing the contribution of normal fibroblasts and primary tumour/ metastasis related CAFs to the distinct fibroblast subsets lead to a rough separation of clusters into a group of clusters, which mainly contained cells from primary tumours, from lung metastases or unchallenged lung tissue. However, the metastasis CAF cluster contained also a small amount of fibroblasts from the lung control and the primary tumour. Both contributions were less than 1 % of all cells within

this cluster. Therefore, a statistically significant conclusion cannot be drawn at this point. Nevertheless, the distribution of lung control and the primary tumour cells within the metastasis CAF cluster was mutually exclusive (see Figure 5.13A). Interestingly, the small branch on the left side of the metastasis CAF cluster was initially identified as a separate cluster, which was merged with the rest of the metastasis cluster to assure statistical significance by appropriate cluster sizes of more than 100 cells per cluster. This small branch is the area in which lung control cells were located, while primary tumour cells were in the area of the initially second and bigger cluster (right part). Thus, sequencing of more metastasis CAFs could potentially lead to two separate clusters, which correspond to different CAF sources. Consistently, the advential fibroblast cluster, which has been described by Buecheler et al. as universal fibroblast subtype, which can serve as a source for specialised fibroblasts in healthy and diseased conditions, contained fibroblasts from metastasis samples [Buechler et al., 2021]. Consequently, advential fibroblasts must have been in close proximity to metastases, and thus, potentially got activated and became metastasis CAFs.

On the other hand, it has been shown that CAFs travel together with tumour cells to metastatic sites, supporting tumour cell survival within the circulation and formation of the metastatic niche [Hurtado et al., 2020; Duda et al., 2010]. The presence of a small amount of primary tumour-related CAFs within the metastasis CAF cluster and of CAFs derived from metastasis samples in the clusters of parenchymal fibroblasts and proliferatng CAFs-1 and 2, allows room for the theory that CAFs from the primary tumour travelled together with MM cells to the lung. Moreover, parenchymal fibroblasts have been described by Buecheler et al., similar to advential fibroblasts, as universal fibroblast population, which can evolve into other fibroblasts types [Buechler et al., 2021].

Contrasting all of the above, metastasis CAFs broadly express bone marrow-derived mesenchymal stem cell (BM-MSC) markers like *Clu*, thus, BM-MSCs appear as another possible source for metastasis CAFs. This is in line with BM-MSCs beeing often listed as CAF sources in literature [Sahai et al., 2020; Quante et al., 2011].

Taken together, the arguments listed above underline the complexity of the question of CAF origin. Albeit lacking of significant proof, the data suggests that metastasis CAFs have multiple sources and potentially derive from BM-MSCs,

local lung fibroblasts and CAFs from the primary tumour.

6.5 SAA3 related signalling offers metastasis CAF-specific therapeutic intervention points

The anaylsis of metastasis CAFs revealed that *Saa3* is among the top marker genes for this cluster. This is intriguing, since SAA3 is associated with immune regulatory pro-tumourigenic functions and SAA3 related signalling offers therapeutic intervention points.

The fact that *Saa3* is mainly present in metastasis CAFs and barely in primary tumour CAFs or normal fibroblasts, supports the theory that SAA3 is involved in the formation of the pre-metastatic niche in the lung [Hansen et al., 2015].

Furthermore, the enrichment of the 'chemotaxis' GO term, along with the high expression of *Saa3* and *Cxadr* exclusively in the metastasis CAF cluster suggests that metastasis CAFs induce the recrution of neutrophils and macrophages to the site of lung metastasis. In turn, IL1b, which is mainly produced by neutrophils within my data, potentially induces *Saa3* expression. This indicates a reciprocal interaction of neutrophils with metastasis CAFs via SAA3 and IL1β . Strikingly, Munir et al. showed that neutrophils get recruited to CAF rich areas in tumours [Munir et al., 2021]. They proposed that CAF derived amyloid β induced neutrophils to release pro-tumourigenic tumor-induced extracellular traps (t-NET), consisting of chromatin bound DNA and proteins, in a CD11b dependent manner. Such t-NETs consequently enhance CAF expansion and activation [Munir et al., 2021]. Based on that, I propose the hypothesis of a feedforward loop in which neutrophil derived Ilb induces *Saa3* in CAFs, which leads to further neutrophil recruition and NET formation, followed by renewed CAF activation. Whether SAA3 was, along with amyloid β, involved in the initial neutrophil recruition, or whether *Saa3* expression is a result of otherwise recruited neutrophils and only further enhanced neutrophil recruition, is undeterminable at the current point of the project. However, both proteins, SAA3 and amyloid β, are linked to NF-κB signalling, suggesting at least a simultaneous mode of action or even autocrine/ paracrine activation of one another [Hiratsuka et al., 2008; Sato et al., 2021].

In terms of therapeutic options for targeting SAA3 and its related signalling,

a specific inhibitor for SAA3 is not available, yet. Since SAA3 acts via multiple receptors, which are expressed on a broad range of cell types, it is also difficult to generally inhibit SAA3 action by blocking only one certain receptor. Moreover, *Saa3* expression can be induced by multiple ligand-receptor combinations. Thus, it is crucial to identify the relevant receptor in the respective situation. The data here indicates that IL1β/IL1R1 signalling could be an exploitable intervention point, since it seems to specifically activate *Saa3* expression in metastasis CAFs. Strikingly, the IL1R antagonist anakinra is already being tested in a clinical trial for PDAC (NCT02021422), and thus, could be transferable to MM trials.

I also found that *Mpp6*, which is thought to regulate the pro-tumourigenic function of SAA3, is expressed at a high level in the metastasis CAF cluster.

In line with the study from Djurec et al., which shows that *Mpp6* is upregulated in *Saa3* null CAFs, *Mpp6* and *Saa3* are barely expressed in the same cells of the metastasis CAF cluster [Djurec et al., 2018]. Since in their study *Mpp6* high CAFs exert an anti-tumourigenic phenotype, one could conclude, that the same was true for *Mpp6* high metastasis CAFs in the present study. If so, the question arises, whether levels of *Mpp6* and *Saa3* changed in a time dependent manner or whether there were two locally distinct groups of metastasis CAFs. The theory of a time dependent process, in which metastasis CAFs first exhibited high levels of *Mpp6* along with tumour suppressive functions, and then transformed into pro-tumourigenic CAFs with high levels of *Saa3*, would be in line with the observation, that normal dermal fibroblasts suppress tumour cells at early stages [Zhou et al., 2015]. However, this would argue against the hypothesis, that CAFs from the primary tumour travelled along with tumour cells to the metastatic site, since such CAFs clearly had to be tumour cell supportive.

Eventually, both, *Mpp6* and *Saa3* high CAFs are evenly distributed within the metastasis CAF cluster, indicating that the levels of *Mpp6* and *Saa3* do not result in entirely different expression patterns.

6.6 Limitations, future perspectives and conclusion

Whilst my thesis covers a comprehensive analysis of CAFs within the primary tumour and especially metastasis of murine melanoma (Figure 6.1), a few limitations remained. To determine if the identified signature of metastasis CAFs is general for metastasis in all organs or specific for lung metastasis, metastasis samples from

other organs, like liver could be included into the scRNA sequencing experiment. In view of the fact that SAA3 plays a role in the formation of the pre-metastatic niche, it would be insightful to compare the composition of CAFs in early stages of primary tumour development and corresponding pre-metastatic niches of lung metastasis to the current data. Lastly, to gain clinical relevance of the here presented findings, validation of the presence of CAF signatures in human samples by scRNA sequencing experiments would be essential. However, most of the above could and will be compensated by investigating the questions via immunofluorescence staining on corresponding tissue sections.

This project harbours a great potential for further analysis and proof of here proposed hypothesises.

To gain data, which helps to understand if Integrin-α5 signalling could compensate PDPN signalling in CAFs, FACS analysis on CAFs isolated and cultured from tumour bearing PDPN KO and control mice have to be performed. In a first step, the protein level of Integrin-α5 shall be assessed in PDPN KO and control CAFs. If this revealed an upregulation of Integrin-α5 in PDPN KO CAFs, functional assays, like the application of Rho and ROCK inhibitors or downregulation of Integrin-α5 by siRNAs, would follow.

Moreover, the general localisation of the here defined CAF clusters would reveal additional insights into their interactions with tumour and TME cells. This will be tackled by performing immunofluorescence staining and in situ hybridisation of the described marker genes on tissue sections. This will also show if cycling CAFs are in close proximity of VEGFα CAFs, and thus, could serve as proliferating reservoir of VEGFα CAFs.

In order to explore neutrophil recruition to lung metastasis and potential vicinity to metastasis CAFs, neutrophil markers will be visualised along with metastasis CAF markers by immunofluorescence staining. Moreover, presence of t-NETs will be investigated by staining of myeloperoxidase (MPO) und Citrullinated histone H3 (CitH3).

Collectively, my thesis gives in depth insights into CAF heterogeneity at the site of the melanoma primary tumour, and unprecedented, at metastatic sites. I could

show, for the first time, that a defined CAF subset exists within the melanoma primary tumour, which exhibits an angiogenesis signature, and thus, most likely, supports neoangiogenesis. Moreover, I was able to identify a unique expression pattern of metastasis CAFs, which highlighted novel CAF specific therapy targets, like IL1R. I also showed that markers for CAF subsets, such as PDPN, not necessarily serve as therapeutic intervention point.

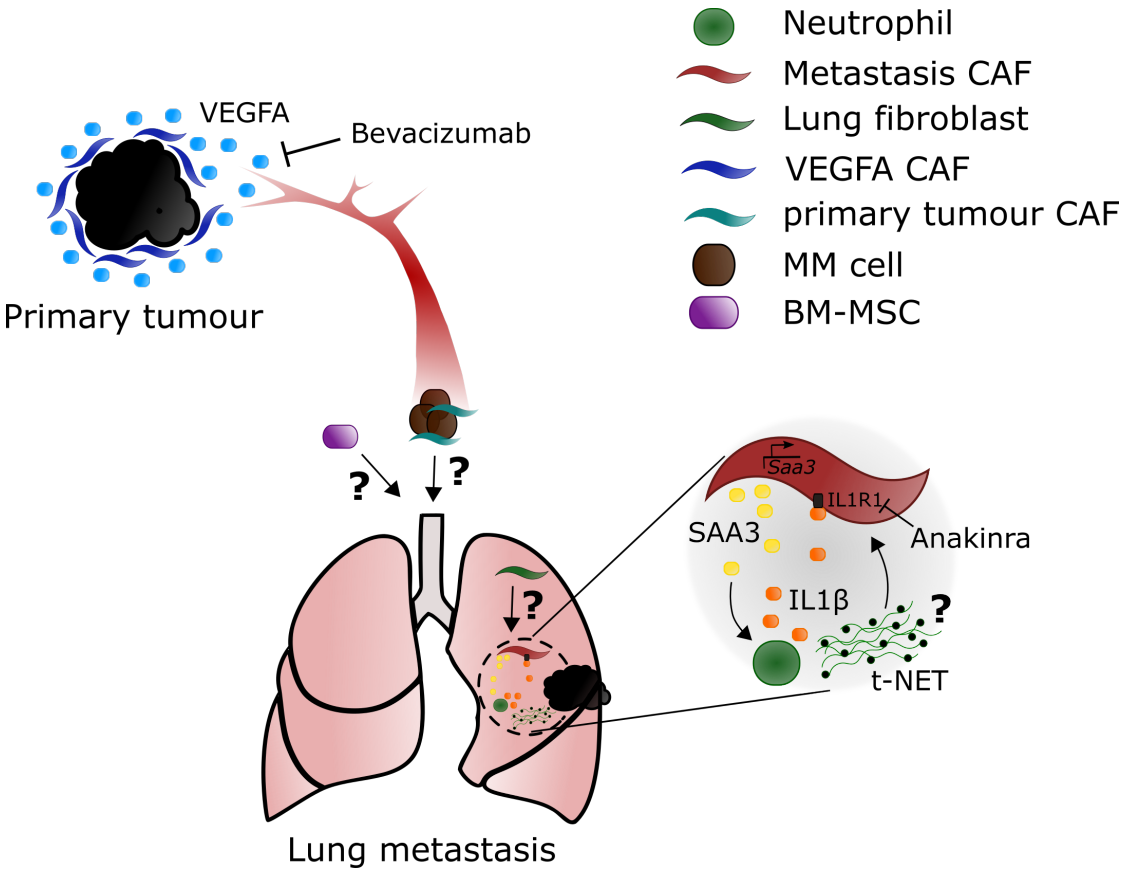

Figure 6.1: **Graphical abstract summarising the central results of this work.**

7 Acknowledgements

I want to give thanks to each and everyone who companioned me during my PhD and contributed to it.

First of all, I would like to express my gratitude to Prof. Dr. Peter Angel for giving me the opportunity to conduct my PhD studies in his laboratory and for his support during the last four years. You gave me a lot of freedom and showed trust in me to design my project and to realise my own ideas. Also a great thank you for putting together such a great team.

I am grateful to Prof. Dr. Jochen Utikal for being a valuable member of my TAC and for being my second supervisor.

Moreover, I would like to thank Dr. Karin Müller Decker and Prof. Dr. Thomas Wieland for being examiners in my PhD defence.

I would like to thank our collaboration partners Prof. Dr. Christoph Plass and Dr. Joschka Hey, for their bioinformatical support and analysis.

A huge thank-you goes to the whole Angel laboratory including Ekaterina, Macrina, Sabrina, Lena, Melanie, Jule, Sören and Melli.

There are no proper words to describe my gratefulness to Betty. I could not have imagined any better team member. Bettina Kast, thank you for being an awesome technician, a discussion partner, a big sister, a realist, a mice whisperer and so much more. You contributed to the successful finalisation of my PhD in so many ways.

Moreover, I would like to thank Lena W. and Lowis for the great experience of supervising the two of you during your internship in our lab and for your valuable contribution to my PhD project.

I am also very grateful that Yana has become a part of my daily life at the DKFZ. Having you in my office has brought me a lot of joy and greatly enriched the last year, thank you.

All of you together, generated an environment, which enabled me to not only survive my PhD but also to have a great time in the lab. Together with you, I

collected countless wonderful memories inside and outside the lab. You are more than colleagues to me, you became dear friends of mine.

I would like to show appreciation to my family, you supported me during, and if necessary, distracted me from my PhD. Thanks to my dad for supporting me throughout my educational journey. Thanks to Thorsten for his bioinformatical interest in my PhD project and support even on holidays. Thanks to my mum for always believing in me. Thanks to Sabine for advice and support in life. Thanks to my siblings, Lisa and Michael, and their other halves Michi and Emanuel, for listening, supporting and encouraging me. Thanks to my little nephew Noah, for cheering me up during the final phase of my thesis. Thank you Petra, Harald and Simon for always being very interested in my PhD. Thank you for your support and all the enriching conversations. Last but certainly not least, I want to express my indescribable gratefulness and appreciation to Alex, for having you by my side, for your support, love and abundance of patience. I promise you that you will not have to hear anything about mouse experiments for a while.

8 Abbreviations

αSMA	alpha smooth muscle actin
Ang-1	angiopoietin-1 protein
apCAF	antigen presenting CAF
Apoe	apolipoprotein E
AT-2	alveolar type 2
BC	before christ
BCC	basal cell carcinoma
BEC	blood endothelial cell
BM-MSC	bone marrow-mesenchymal stem cell
BRAF	B-Rapidly Accelerated Fibrosarcoma protein
CAF	cancer-associated fibroblast
Calca	calcitonin related polypeptide alpha
cCAF	cycling CAF
Ccdc153	coiled-coil domain containing 153
Ccl5/6	C-C motif chemokine ligand 5/6
CD31	cluster of differentiation31
CDK4	cyclin-dependent kinase 4
CDKN2A	cyclin-dependent kinase inhibitor 2A
Chil3	chitinase-like 3
Cldn5	claudin5
Col1a1	collagen1a1
CTLA4	cytotoxic T-lymphocyte associated protein 4
Cxadr	coxsackievirus and adenovirus receptor
Cxcl12	CXC-motiv-chemokin 12
dCAF	development CAF
Dcn	decorin
ECM	extracellular matrix
EGFR1	epidermal growth factor receptor 1
EMA	european medicines agency
EMT	epithelial-to-mesenchymal transition
EndMT	endothelial-to-mesenchymal transition
Enpp2	ectonucleotide pyrophosphatase/phosphodiesterase 2
EpCAM	epithelial cell adhesion molecule

ERK	extracellular signal-regulated protein kinase
ERM	ezrin, radixin, moesin
FACS	fluorescence-activated cell sorting
FAK	focal adhesion kinase
FAP	fibroblast activating protein
Fbn1/2	fibrillin-1/2
FDA	U.S. Food and Drug Administration
Fmo2	flavin containing dimethylaniline monoxygenase 2
FSP-1	fibroblast-specific protein 1
GO	gene ontology
Gsn	gelsolin
Gzma	aranzyme A
HB-EGF	heparin-binding EGF-like growth factor
Hhip	hedgehog-interacting protein
HIF-1	hypoxia induced factor 1
Hspa1a/b	heat shock protein 1a/b
iCAF	inflammatory CAF
Igkc	Immunoglobulin Kappa Constant
IL1b/6	Interleukin 1b/6
IL1R	Interleukin 1 receptor
Inmt	indolethylamine N-Methyltransferase
irAEs	immune-related adverse events
KO	knock out
LAG-3	lymphocyte-activation gene 3
LEC	lymphatic endothelial cell
Lgals7	galectin 7
Lum	lumican
Lyve-1	lymphatic vessel endothelial hyaluronan receptor 1
Lyz2	lysozyme C
MAFs	melanoma-associated fibroblast
MAPK	mitogen-activated protein kinase
mCAF	matrix CAF
MCC	merkel cell carcinoma
MEK	Mitogen-activated protein kinase kinase
Mfap4	microfibril-associated glycoprotein 4

Mgp	matrix Gla protein
MITF	microphthalmia-associated transcription factor
MM	Malignant Melanoma
MMP	matrix-metalloprotease
MPP6	M-phase phosphoprotein 6 homolog
MRI	magnetic resonance imaging
mT/mG	membrane-targeted Tomato/membrane-targeted GFP
MT-ret	metallothionein-I-ret
Mustn1	musculoskeletal, embryonic nuclear protein 1)
myCAF	myfibroblastic CAF
Myh11	myosin heavy chain 11
Myl9	myosin light chain 9
Nfkb1	nuclear factor kappa B subunit 1
Nfkbia	nuclear factor kappa B inhibitor a
NK cell	natural killer cell
Nkg7	natural killer cell granule protein 7
Npnt	nephronectin
pCAF	PDPN CAF
PD1	programmed cell death protein 1
PDAC	pancreatic ductal adenocarcinoma
PD-L2	programmed cell death protein ligand 1
PDGF	platelet-derived growth factor
PDGFR	platelet-derived growth factor receptor
PDPN	podoplanin
Pi16	peptidase inhibitor 16
PlGF	placenta grwoth factor
Postn	periostin
POT1	protection of telomeres 1
RAF	rapidly accelerated fibrosarcoma
RAGE	receptor for advanced glycation endproducts
RAS	rat sarcoma
RCC	respiratory ciliated cell
ROCK	rho-associated protein kinase
RTK	receptor tyrosine kinase
S100A4	S100 Calcium Binding Protein A4

SAA3	serum amyloid A 3
sCAF	S100a4 CAF
SCC	squamous cell carcinoma
scRNA	single cell ribonucleic acid
Scgb	secretoglobin
Sec14l3	SEC14 like lipid binding 3
Sftpb/d	surfactant protein b/d
Slc34a2	solute carrier family 34 member 2
SMC	smooth muscle cell
TERT	telomerase reverse transcriptase
TGF-b	transforming growth factor beta
TLR2/4	toll-like receptor 2/4
TME	tumour microenvironment
Tmem100	transmembrane protein 100
t-NET	tumour-induced neutrophil derived extracellular trap
TNF	tumour necrosis factor
Tnxb	tenascin-X
UMAP	uniform manifold approximation and projection
UV	ultraviolet
vCAF	vascular CAF
VEGF	vascular endothelial growth factor
Vwf	von Willebrand factor
WNT	Wingless and Int-1
Wt1	Wilms' Tumour

9 Bibliography

References

R. S. Apte, D. S. Chen, and N. Ferrara. Vegf in signaling and disease: Beyond discovery and development. *Cell*, 176:1248, 3 2019. ISSN 10974172. doi: 10.1016/J.CELL.2019.01.021. URL https://www.ncbi.nlm.nih.gov/pmc/articles/PMC6410740/.

J. L. Astarita, S. E. Acton, S. J. Turley, and L. Onder. Podoplanin: emerging functions in development, the immune system, and cancer. 2012. doi: 10.3389/fimmu.2012.00283. URL www.frontiersin.org.

S. Baars, C. Bauer, S. Szabowski, B. Hartenstein, and P. Angel. Epithelial deletion of podoplanin is dispensable for re-epithelialization of skin wounds. *Experimental Dermatology*, 2015. doi: 10.1111/exd.12781. URL https://onlinelibrary.wiley.com/doi/10.1111/exd.12781.

F. R. Balkwill, M. Capasso, and T. Hagemann. The tumor microenvironment at a glance. *Journal of Cell Science*, 125:5591–5596, 12 2012. ISSN 00219533. doi: 10.1242/jcs.116392. URL https://jcs.biologists.org/content/125/23/5591.

M. Bartoschek, N. Oskolkov, M. Bocci, J. Lövrot, C. Larsson, M. Sommarin, C. D. Madsen, D. Lindgren, G. Pekar, G. Karlsson, M. Ringnér, J. Bergh, Åsa Björklund, and K. Pietras. Spatially and functionally distinct subclasses of breast cancer-associated fibroblasts revealed by single cell rna sequencing. *Nature Communications*, 9, 12 2018. ISSN 20411723. doi: 10.1038/s41467-018-07582-3. URL https://pubmed.ncbi.nlm.nih.gov/30514914/.

I. Bedrosian, M. B. Faries, R. Elenitsas, L. Schuchter, R. Mick, F. R. Spitz, L. P. Bucky, A. Alavi, D. E. Elder, D. L. Fraker, and B. J. Czerniecki. Incidence of Sentinel Node Metastasis in Patients With Thin Primary Melanoma (1 mm) With Vertical Growth Phase. Technical report, 2000.

S. Breiteneder-Geleff, A. Soleiman, H. Kowalski, R. Horvat, G. Amann, E. Kriehuber, K. Diem, W. Weninger, E. Tschachler, K. Alitalo, and D. Kerjaschki. Angiosarcomas express mixed endothelial phenotypes of

blood and lymphatic capillaries : Podoplanin as a specific marker for lymphatic endothelium. *The American Journal of Pathology*, 154:385, 1999. ISSN 00029440. doi: 10.1016/S0002-9440(10)65285-6. URL https://www.ncbi.nlm.nih.gov/pmc/articles/PMC1849992/.

M. B. Buechler, R. N. Pradhan, A. T. Krishnamurty, C. Cox, A. K. Calviello, A. W. Wang, Y. A. Yang, L. Tam, R. Caothien, M. Roose-Girma, Z. Modrusan, J. R. Arron, R. Bourgon, S. Müller, and S. J. Turley. Cross-tissue organization of the fibroblast lineage. *Nature*, 5 2021. ISSN 0028-0836. doi: 10.1038/s41586-021-03549-5. URL http://www.nature.com/articles/s41586-021-03549-5.

L. Chiriboga, S. Meehan, I. Osman, M. Glick, G. D. L. Cruz, B. S. Howell, G. Friedman-Jiménez, R. J. Schneider, and S. Jamal. Endothelin-1 in the tumor microenvironment correlates with melanoma invasion. *Melanoma Research*, 26: 236–244, 2016. ISSN 14735636. doi: 10.1097/CMR.0000000000000235. URL https://journals.lww.com/melanomaresearch/Fulltext/2016/06000.

M. Cives, F. Mannavola, L. Lospalluti, M. C. Sergi, G. Cazzato, E. Filoni, F. Cavallo, G. Giudice, L. S. Stucci, C. Porta, and M. Tucci. Non-Melanoma Skin Cancers: Biological and Clinical Features. *International Journal of Molecular Sciences*, 21(15):1–24, aug 2020. ISSN 14220067. doi: 10.3390/IJMS21155394. URL https://www.ncbi.nlm.nih.gov/pmc/articles/PMC7432795/.

W. H. J. Clark, D. E. Elder, D. Guerry, M. N. Epstein, M. H. Greene, and M. Van Horn. A study of tumor progression: The precursor lesions of superficial spreading and nodular melanoma. *Human Pathology*, 15(12):1147–1165, dec 1984. ISSN 0046-8177. doi: 10.1016/S0046-8177(84)80310-X.

A. M. Czarnecka, E. Bartnik, M. Fiedorowicz, and P. Rutkowski. Targeted therapy in melanoma and mechanisms of resistance, 7 2020. ISSN 14220067. URL www.mdpi.com/journal/ijms.

W. E. Damsky, N. Theodosakis, and M. Bosenberg. Melanoma metastasis: new concepts and evolving paradigms. *Oncogene*, 33(19):2413–2422, may 2014. ISSN 0950-9232. doi: 10.1038/onc.2013.194. URL http://www.nature.com/articles/onc2013194.

M. Daugaard, M. Jäättelä, and M. Rohde. Hsp70-2 is required for

tumor cell growth and survival, 2005. ISSN 15514005. URL https://www.tandfonline.com/action/journal.

M. G. Davey, N. Miller, and N. M. Mcinerney. A Review of Epidemiology and Cancer Biology of Malignant Melanoma. *Cureus*, 2021. doi: 10.7759/cureus.15087.

S. Davidson, M. Efremova, A. Riedel, B. Mahata, J. Pramanik, J. Huuhtanen, G. Kar, R. Vento-Tormo, T. Hagai, X. Chen, M. A. Haniffa, J. D. Shields, and S. A. Teichmann. Single-Cell RNA Sequencing Reveals a Dynamic Stromal Niche That Supports Tumor Growth. *Cell Reports*, 31(7): 107628, may 2020. ISSN 2211-1247. doi: 10.1016/J.CELREP.2020.107628. URL https://www.sciencedirect.com/science/article/pii/S2211124720305817.

M. Deyell, C. S. Garris, and A. M. Laughney. Cancer metastasis as a non-healing wound. *British Journal of Cancer*, page 124, 2021. doi: 10.1038/s41416-021-01309-w.

M. Djurec, O. Graña, A. Lee, K. Troulé, E. Espinet, L. Cabras, C. Navas, M. T. Blasco, L. Martín-Díaz, M. Burdiel, J. Li, Z. Liu, M. Vallespinós, F. Sanchez-Bueno, M. R. Sprick, A. Trumpp, B. Sainz, F. Al-Shahrour, R. Rabadan, C. Guerra, and M. Barbacid. Saa3 is a key mediator of the protumorigenic properties of cancer-associated fibroblasts in pancreatic tumors. *Proceedings of the National Academy of Sciences of the United States of America*, 115: E1147–E1156, 2 2018. ISSN 10916490. doi: 10.1073/pnas.1717802115. URL www.pnas.org/cgi/doi/10.1073/pnas.1717802115.

B. Domingues, J. M. Lopes, P. Soares, and H. Pópulo. Melanoma treatment in review. *ImmunoTargets and therapy*, 7:35–49, 2018. ISSN 2253-1556. doi: 10.2147/ITT.S134842. URL http://www.pubmedcentral.nih.gov/.

D. G. Duda, A. M. M. J. Duyverman, M. Kohno, M. Snuderl, E. J. A. Steller, D. Fukumura, and R. K. Jain. Malignant cells facilitate lung metastasis by bringing their own soil. *Proceedings of the National Academy of Sciences of the United States of America*, 107:21677–82, 12 2010. ISSN 1091-6490. doi: 10.1073/pnas.1016234107. URL http://www.ncbi.nlm.nih.gov/pubmed/21098274.

R. Dummer, P. A. Ascierto, H. J. Gogas, A. Arance, M. Mandala, G. Liszkay, C. Garbe, D. Schadendorf, I. Krajsova, R. Gutzmer, V. Chiarion-Sileni,

C. Dutriaux, J. W. B. de Groot, N. Yamazaki, C. Loquai, L. A. M. de Parseval, M. D. Pickard, V. Sandor, C. Robert, and K. T. Flaherty. Encorafenib plus binimetinib versus vemurafenib or encorafenib in patients with braf-mutant melanoma (columbus): a multicentre, open-label, randomised phase 3 trial. *The Lancet Oncology*, 19:603–615, 5 2018. ISSN 14745488. doi: 10.1016/S1470-2045(18)30142-6. URL http://www.thelancet.com/article/S1470204518301426/fulltext.

E. Elyada, M. Bolisetty, P. Laise, W. F. Flynn, E. T. Courtois, R. A. Burkhart, J. A. Teinor, P. Belleau, G. Biffi, M. S. Lucito, S. Sivajothi, T. D. Armstrong, D. D. Engle, K. H. Yu, Y. Hao, C. L. Wolfgang, Y. Park, J. Preall, E. M. Jaffee, A. Califano, P. Robson, and D. A. Tuveson. Cross-Species Single-Cell Analysis of Pancreatic Ductal Adenocarcinoma Reveals Antigen-Presenting Cancer-Associated Fibroblasts. *Cancer discovery*, 9(8):1102–1123, aug 2019. ISSN 2159-8290. doi: 10.1158/2159-8290.CD-19-0094. URL http://www.ncbi.nlm.nih.gov/pubmed/31197017.

L. Falzone, R. Salemi, S. Travali, A. Scalisi, J. A. McCubrey, S. Candido, and M. Libra. Mmp-9 overexpression is associated with intragenic hypermethylation of mmp9 gene in melanoma. *Aging*, 8:933–940, 4 2016. ISSN 1945-4589. doi: 10.18632/AGING.100951. URL https://www.aging-us.com/article/100951.

G. Friedman, O. Levi-Galibov, E. David, C. Bornstein, A. Giladi, M. Dadiani, A. Mayo, C. Halperin, M. Pevsner-Fischer, H. Lavon, S. Mayer, R. Nevo, Y. Stein, N. Balint-Lahat, I. Barshack, H. R. Ali, C. Caldas, E. Nili-Gal-Yam, U. Alon, I. Amit, and R. Scherz-Shouval. Cancer-associated fibroblast compositions change with breast cancer progression linking the ratio of S100A4+ and PDPN+ CAFs to clinical outcome. *Nature Cancer*, 1(7):692–708, jul 2020. doi: 10.1038/s43018-020-0082-y. URL https://doi.org/10.1038/s43018-020-0082-y.

K. Fukino, L. Shen, S. Matsumoto, C. D. Morrison, G. L. Mutter, and C. Eng. Combined total genome loss of heterozygosity scan of breast cancer stroma and epithelium reveals multiplicity of stromal targets. *Cancer Research*, 64:7231–7236, 10 2004. ISSN 0008-5472. doi: 10.1158/0008-5472.CAN-04-2866. URL https://aacrjournals.org/cancerres/article/64/20/7231/511949/.

C. Gaggioli, S. Hooper, C. Hidalgo-Carcedo, R. Grosse, J. F. Marshall, K. Harrington, and E. Sahai. Fibroblast-led collective invasion of carcinoma cells with differing roles for rhogtpases in leading and following cells. *Nature Cell Biology*, 9:1392–1400, 12 2007. ISSN 14657392. doi: 10.1038/ncb1658. URL `https://www.nature.com/articles/ncb1658`.

N. Gengenbacher, M. Singhal, and H. G. Augustin. Preclinical mouse solid tumour models: status quo, challenges and perspectives. *Nature Reviews Cancer*, 17:751–765, 12 2017. ISSN 1474-175X. doi: 10.1038/nrc.2017.92. URL `http://www.nature.com/articles/nrc.2017.92`.

N. Gengenbacher, M. Singhal, C. Mogler, L. Hai, L. Milde, A. A. A. Pari, E. Besemfelder, C. Fricke, D. Baumann, S. Gehrs, J. Utikal, M. Felcht, J. Hu, M. Schlesner, R. Offringa, S. Chintharlapalli, and H. G. Augustin. Timed ang2-targeted therapy identifies the angiopoietin-tie pathway as key regulator of fatal lymphogenous metastasis. *Cancer discovery*, 10 2020. ISSN 2159-8290. doi: 10.1158/2159-8290.CD-20-0122. URL `http://www.ncbi.nlm.nih.gov/pubmed/33106316`.

J. E. Gershenwald, R. A. Scolyer, K. R. Hess, V. K. Sondak, G. V. Long, M. I. Ross, A. J. Lazar, M. B. Faries, J. M. Kirkwood, G. A. McArthur, L. E. Haydu, A. M. M. Eggermont, K. T. Flaherty, C. M. Balch, and J. F. Thompson. Online continuing education activity article title: Melanoma staging: Evidence-based changes in the american joint committee on cancer (ajcc) eighth edition cancer staging manual continuing medical education accreditation and designation statement. *A Cancer Journal for Clinicians*, 67:472–492, 2017. doi: 10.3322/caac.21409.

C. F. Guerrero-Juarez, P. H. Dedhia, S. Jin, R. Ruiz-Vega, D. Ma, Y. Liu, K. Yamaga, O. Shestova, D. L. Gay, Z. Yang, K. Kessenbrock, Q. Nie, W. S. Pear, G. Cotsarelis, and M. V. Plikus. Single-cell analysis reveals fibroblast heterogeneity and myeloid-derived adipocyte progenitors in murine skin wounds. *Nature Communications*, 10:650, 12 2019. ISSN 2041-1723. doi: 10.1038/s41467-018-08247-x. URL `http://www.nature.com/articles/s41467-018-08247-x`.

D. Hanahan and L. M. Coussens. Accessories to the crime: Functions of cells recruited to the tumor microenvironment. *Cancer Cell*, 21:309–

322, 3 2012. ISSN 1535-6108. doi: 10.1016/J.CCR.2012.02.022. URL https://www.sciencedirect.com/science/article/pii/S1535610812000827.

D. Hanahan and R. A. Weinberg. Hallmarks of cancer: The next generation. *Cell*, 144:646–674, 3 2011. ISSN 00928674. doi: 10.1016/J.CELL.2011.02.013.

M. T. Hansen, B. Forst, N. Cremers, L. Quagliata, N. Ambartsumian, B. Grum-Schwensen, J. Klingelhöfer, A. Abdul-Al, P. Herrmann, M. Osterland, U. Stein, G. H. Nielsen, P. E. Scherer, E. Lukanidin, J. P. Sleeman, and M. Grigorian. A link between inflammation and metastasis: serum amyloid a1 and a3 induce metastasis, and are targets of metastasis-inducing s100a4. *Oncogene 2015 34:4*, 34:424–435, 1 2015. ISSN 1476-5594. doi: 10.1038/onc.2013.568. URL https://www.nature.com/articles/onc2013568.

E. Hirata, M. R. Girotti, A. Viros, S. Hooper, B. Spencer-Dene, M. Matsuda, J. Larkin, R. Marais, and E. Sahai. Intravital imaging reveals how braf inhibition generates drug-tolerant microenvironments with high integrin beta1/fak signaling. *Cancer cell*, 27:574–88, 4 2015. ISSN 1878-3686. doi: 10.1016/j.ccell.2015.03.008. URL http://www.ncbi.nlm.nih.gov/pubmed/25873177.

S. Hiratsuka, A. Watanabe, Y. Sakurai, S. Akashi-Takamura, S. Ishibashi, K. Miyake, M. Shibuya, S. Akira, H. Aburatani, and Y. Maru. The s100a8-serum amyloid a3-tlr4 paracrine cascade establishes a pre-metastatic phase. *Nature Cell Biology*, 10:1349–1355, 2008. ISSN 14657392. doi: 10.1038/ncb1794.

A. Hoshino, G. Ishii, T. Ito, K. Aoyagi, Y. Ohtaki, K. Nagai, H. Sasaki, and A. Ochiai. Podoplanin-positive fibroblasts enhance lung adenocarcinoma tumor formation: Podoplanin in fibroblast functions for tumor progression. *Cancer Research*, 71:4769–4779, 7 2011. ISSN 0008-5472. doi: 10.1158/0008-5472.CAN-10-3228. URL http://cancerres.aacrjournals.org/.

Y. Hu, Q. An, K. Sheu, B. Trejo, and F. S. Guo. Single cell multi-omics technology: Methodology and application. *Single Cell Multi-Omics Technology: Methodology and Application. Front. Cell Dev. Biol*, 6:28, 2018. doi: 10.3389/fcell.2018.00028. URL www.frontiersin.org.

P. Hurtado, I. Martínez-Pena, and R. Piñeiro. Dangerous liaisons: Circulating tumor cells (ctcs) and cancer-associated fibroblasts (cafs), 10 2020. ISSN 20726694. URL https://www.ncbi.nlm.nih.gov/pmc/articles/PMC7599894/.

T. Iwamoto, M. Takahashi, M. Ito, K. Hamatani, M. Ohbayashi, W. Wajjwalku, K. Isobe, and I. Nakashima. Aberrant melanogenesis and melanocytic tumour development in transgenic mice that carry a metallothionein/ret fusion gene. *The EMBO Journal*, 10:3167–3175, 11 1991. ISSN 02614189. doi: 10.1002/j.1460-2075.1991.tb04878.x. URL http://doi.wiley.com/10.1002/j.1460-2075.1991.tb04878.x.

R. W. Jenkins and D. E. Fisher. Treatment of advanced melanoma in 2020 and beyond. *Journal of Investigative Dermatology*, 141:23–31, 1 2021. ISSN 15231747. doi: 10.1016/j.jid.2020.03.943. URL http://www.jidonline.org/article/S0022202X20312574/fulltext.

D. Joyce and J. J. Skitzki. Surgical management of primary cutaneous melanoma. *Surgical Clinics of North America*, 100:61–70, 2 2020. ISSN 0039-6109. doi: 10.1016/J.SUC.2019.09.001.

M. R. Junttila and F. J. de Sauvage. Influence of tumour microenvironment heterogeneity on therapeutic response. *Nature*, 501:346–354, 9 2013. ISSN 0028-0836. doi: 10.1038/nature12626. URL http://www.nature.com/articles/nature12626.

R. Kalluri and R. A. Weinberg. The basics of epithelial-mesenchymal transition. *The Journal of Clinical Investigation*, 119, 2009. doi: 10.1172/JCI39104. URL http://www.jci.org.

S. Kan, E. Konishi, T. Arita, C. Ikemoto, H. Takenaka, A. Yanagisawa, N. Katho, and J. Asai. Podoplanin expression in cancer-associated fibroblasts predicts aggressive behavior in melanoma. *Journal of Cutaneous Pathology*, 41, 2014. doi: 10.1111/cup.12322. URL https://onlinelibrary.wiley.com/doi/10.1111/cup.12322.

R. Kanzaki and K. Pietras. Heterogeneity of cancer-associated fibroblasts: Opportunities for precision medicine. *Cancer Science*, 111(8): 2708–2717, aug 2020. ISSN 13497006. doi: 10.1111/cas.14537. URL https://onlinelibrary.wiley.com/doi/full/10.1111/cas.14537.

A. Labernadie, T. Kato, A. Brugués, X. Serra-Picamal, S. Derzsi, E. Arwert, A. Weston, V. González-Tarragó, A. Elosegui-Artola, L. Albertazzi, J. Alcaraz, P. Roca-Cusachs, E. Sahai, and X. Trepat. A mechanically active heterotypic e-cadherin/n-cadherin adhesion enables fibroblasts to drive cancer cell invasion. *Nature Cell Biology 2017 19:3*, 19:224–237, 2 2017. ISSN 1476-4679. doi: 10.1038/ncb3478. URL https://www.nature.com/articles/ncb3478.

M. A. Lakins, E. Ghorani, H. Munir, C. P. Martins, and J. D. Shields. Cancer-associated fibroblasts induce antigen-specific deletion of cd8 + t cells to protect tumour cells. *Nature Communications*, 9:948, 12 2018. ISSN 2041-1723. doi: 10.1038/s41467-018-03347-0. URL http://www.nature.com/articles/s41467-018-03347-0.

J. Larkin, P. A. Ascierto, B. Dréno, V. Atkinson, G. Liszkay, M. Maio, M. Mandalà, L. Demidov, D. Stroyakovskiy, L. Thomas, L. de la Cruz-Merino, C. Dutriaux, C. Garbe, M. A. Sovak, I. Chang, N. Choong, S. P. Hack, G. A. McArthur, and A. Ribas. Combined vemurafenib and cobimetinib in braf-mutated melanoma. *The New England journal of medicine*, 371:1867–1876, 11 2014. ISSN 1533-4406. doi: 10.1056/NEJMOA1408868. URL https://pubmed.ncbi.nlm.nih.gov/25265494/.

J. Larkin, V. Chiarion-Sileni, R. Gonzalez, J.-J. Grob, P. Rutkowski, C. D. Lao, C. L. Cowey, D. Schadendorf, J. Wagstaff, R. Dummer, P. F. Ferrucci, M. Smylie, D. Hogg, A. Hill, I. Márquez-Rodas, J. Haanen, M. Guidoboni, M. Maio, P. Schöffski, M. S. Carlino, C. Lebbé, G. McArthur, P. A. Ascierto, G. A. Daniels, G. V. Long, L. Bastholt, J. I. Rizzo, A. Balogh, A. Moshyk, F. S. Hodi, and J. D. Wolchok. Five-year survival with combined nivolumab and ipilimumab in advanced melanoma. *New England Journal of Medicine*, 381:1535–1546, 10 2019. ISSN 0028-4793. doi: 10.1056/nejmoa1910836.

J. Lee and G. L. Beatty. Serum amyloid a proteins and their impact on metastasis and immune biology in cancer. *Cancers*, 2021. URL https://doi.org/10.3390/cancers13133179.

Y.-T. N. M. Lee. Malignant melanoma: Pattern of metastasis. *CA: A Cancer Journal for Clinicians*, 30:137–142, 5 1980. ISSN 1542-4863. doi: 10.3322/CANJCLIN.30.3.137. URL https://onlinelibrary.wiley.com/doi/full/10.3322/canjclin.30.3.137.

J. Lopes, C. M. Rodrigues, M. M. Gaspar, and C. P. Reis. Melanoma management: From epidemiology to treatment and latest advances. *Cancers 2022, Vol. 14, Page 4652*, 14:4652, 9 2022. ISSN 2072-6694. doi: 10.3390/CANCERS14194652. URL https://www.mdpi.com/2072-6694/14/19/4652/htm.

S. Madar, I. Goldstein, and V. Rotter. 'cancer associated fibroblasts' – more than meets the eye. *Trends in Molecular Medicine*, 19:447–453, 8 2013. ISSN 1471-4914. doi: 10.1016/J.MOLMED.2013.05.004.

E. Martín-Villar, D. Megías, S. Castel, M. M. Yurrita, S. Vilaró, and M. Quintanilla. Podoplanin binds erm proteins to activate rhoa and promote epithelial-mesenchymal transition. *Journal of Cell Science*, 119: 4541–4553, 11 2006. ISSN 0021-9533. doi: 10.1242/JCS.03218. URL https://journals.biologists.com/jcs/article/119/21/4541/29341/.

A. J. Miller and M. C. Mihm. Melanoma. *The new england journal of medicine*, 2006. doi: 10.1056/NEJMra052166. URL www.nejm.org.

N. Moro, C. Mauch, and P. Zigrino. Metalloproteinases in melanoma. *European Journal of Cell Biology*, 93:23–29, 1 2014. ISSN 0171-9335. doi: 10.1016/J.EJCB.2014.01.002.

H. Munir, J. O. Jones, T. Janowitz, M. Hoffmann, M. Euler, C. P. Martins, S. J. Welsh, and J. D. Shields. Stromal-driven and amyloid beta-dependent induction of neutrophil extracellular traps modulates tumor growth. *Nature Communications*, 12, 12 2021. ISSN 20411723. doi: 10.1038/s41467-021-20982-2. URL https://pubmed.ncbi.nlm.nih.gov/33514748/.

M. D. Muzumdar, B. Tasic, K. Miyamichi, L. Li, and L. Luo. A global double-fluorescent cre reporter mouse. *genesis*, 45:593–605, 9 2007. ISSN 1526954X. doi: 10.1002/dvg.20335. URL http://doi.wiley.com/10.1002/dvg.20335.

A. V. Nguyen and A. M. Soulika. The Dynamics of the Skin's Immune System. *International Journal of Molecular Sciences*, 20(8), apr 2019. ISSN 14220067. doi: 10.3390/IJMS20081811. URL https://www.ncbi.nlm.nih.gov/pmc/articles/PMC6515324/.

V. Ntranos, L. Yi, P. Melsted, and L. Pachter. A discriminative learning approach to differential expression analysis for single-cell rna-seq. *Na-*

ture Methods, 16:163–166, 2019. doi: 10.1038/s41592-018-0303-9. URL https://doi.org/10.1038/s41592-018-0303-9.

C. H. O'Flanagan, K. R. Campbell, A. W. Zhang, F. Kabeer, J. L. P. Lim, J. Biele, P. Eirew, D. Lai, A. McPherson, E. Kong, C. Bates, K. Borkowski, M. Wiens, B. Hewitson, J. Hopkins, J. Pham, N. Ceglia, R. Moore, A. J. Mungall, J. N. McAlpine, S. P. Shah, and S. Aparicio. Dissociation of solid tumor tissues with cold active protease for single-cell rna-seq minimizes conserved collagenase-associated stress responses. *Genome Biology*, 20: 210, 12 2019. ISSN 1474-760X. doi: 10.1186/s13059-019-1830-0. URL https://genomebiology.biomedcentral.com/articles/10.1186/.

D. Öhlund, A. Handly-Santana, G. Biffi, E. Elyada, A. S. Almeida, M. Ponz-Sarvise, V. Corbo, T. E. Oni, S. A. Hearn, E. J. Lee, I. I. C. Chio, C. I. Hwang, H. Tiriac, L. A. Baker, D. D. Engle, C. Feig, A. Kultti, M. Egeblad, D. T. Fearon, J. M. Crawford, H. Clevers, Y. Park, and D. A. Tuveson. Distinct populations of inflammatory fibroblasts and myofibroblasts in pancreatic cancer. *The Journal of experimental medicine*, 214(3):579–596, mar 2017. ISSN 15409538. doi: 10.1084/JEM.20162024.

J. Patel, M. Didolkar, J. Pickren, and R. Moore. Metastatic pattern of malignant melanoma. *The American Journal of Surgery*, 135:807–810, 6 1978. ISSN 00029610. doi: 10.1016/0002-9610(78)90171-x. URL http://www.americanjournalofsurgery.com/article/000296107890171X/.

O. W. Petersen, H. L. Nielsen, T. Gudjonsson, R. Villadsen, F. Rank, E. Niebuhr, M. J. Bissell, and L. Rønnov-Jessen. Epithelial to mesenchymal transition in human breast cancer can provide a nonmalignant stroma. *The American Journal of Pathology*, 162:391–402, 2 2003. ISSN 0002-9440. doi: 10.1016/S0002-9440(10)63834-5. URL https://www.sciencedirect.com/science/article/pii/.

Q. Ping, R. Yan, X. Cheng, W. Wang, Y. Zhong, Z. Hou, Y. Shi, C. Wang, and R. Li. Cancer-associated fibroblasts: overview, progress, challenges, and directions. *Cancer Gene Therapy*, 28:984–999, 2021. doi: 10.1038/s41417-021-00318-4. URL https://doi.org/10.1038/s41417-021-00318-4.

M. Quante, S. P. Tu, H. Tomita, T. Gonda, S. S. Wang, S. Takashi, G. H.

Baik, W. Shibata, B. DiPrete, K. S. Betz, R. Friedman, A. Varro, B. Tycko, and T. C. Wang. Bone marrow-derived myofibroblasts contribute to the mesenchymal stem cell niche and promote tumor growth. *Cancer cell*, 19: 257–272, 2 2011. ISSN 1878-3686. doi: 10.1016/J.CCR.2011.01.020. URL `https://pubmed.ncbi.nlm.nih.gov/21316604/`.

K. Rajani, Y. Dai, S. A. Luebker, and S. A. Koepsell. Diverse mechanisms of braf inhibitor resistance in melanoma identified in clinical and preclinical studies. *Front. Oncol*, 9:268, 2019. doi: 10.3389/fonc.2019.00268. URL `www.frontiersin.org`.

K. J. Ransohoff, P. D. Jaju, J. Y. Tang, M. Carbone, S. Leachman, and K. Y. Sarin. Familial skin cancer syndromes: Increased melanoma risk. *Journal of the American Academy of Dermatology*, 74(3):423–434, mar 2016. ISSN 0190-9622. doi: 10.1016/J.JAAD.2015.09.070. URL `https://www.sciencedirect.com/science/article/pii/S0190962215023634`.

Y. Rinkevich, G. G. Walmsley, M. S. Hu, Z. N. Maan, A. M. Newman, M. Drukker, M. Januszyk, G. W. Krampitz, G. C. Gurtner, H. P. Lorenz, I. L. Weissman, and M. T. Longaker. Identification and isolation of a dermal lineage with intrinsic fibrogenic potential. *Science*, 348, 4 2015. ISSN 10959203. doi: 10.1126/science.aaa2151. URL `http://dx.doi.`

C. Robert, B. Karaszewska, J. Schachter, P. Rutkowski, A. Mackiewicz, D. Stroiakovski, M. Lichinitser, R. Dummer, F. Grange, L. Mortier, V. Chiarion-Sileni, K. Drucis, I. Krajsova, A. Hauschild, P. Lorigan, P. Wolter, G. V. Long, K. Flaherty, P. Nathan, A. Ribas, A.-M. Martin, P. Sun, W. Crist, J. Legos, S. D. Rubin, S. M. Little, and D. Schadendorf. Improved overall survival in melanoma with combined dabrafenib and trametinib. *New England Journal of Medicine*, 372:30–39, 1 2015. ISSN 0028-4793. doi: 10.1056/NEJMOA1412690. URL `https://www.nejm.org/doi/10.1056/NEJMoa1412690`.

E. Sahai, I. Astsaturov, E. Cukierman, D. G. DeNardo, M. Egeblad, R. M. Evans, D. Fearon, F. R. Greten, S. R. Hingorani, T. Hunter, R. O. Hynes, R. K. Jain, T. Janowitz, C. Jorgensen, A. C. Kimmelman, M. G. Kolonin, R. G. Maki, R. S. Powers, E. Puré, D. C. Ramirez, R. Scherz-Shouval, M. H. Sherman, S. Stewart, T. D. Tlsty, D. A. Tuveson, F. M. Watt, V. Weaver,

A. T. Weeraratna, and Z. Werb. A framework for advancing our understanding of cancer-associated fibroblasts. *Nature Reviews Cancer*, 20:174–186, 3 2020. ISSN 1474-175X. doi: 10.1038/s41568-019-0238-1. URL http://www.nature.com/articles/s41568-019-0238-1.

K. Sato, K. ichi Takayama, M. Hashimoto, and S. Inoue. Transcriptional and post-transcriptional regulations of amyloid-beta precursor protein (app) mrna. *Frontiers in Aging*, 2:34, 8 2021. ISSN 2673-6217. doi: 10.3389/FRAGI.2021.721579.

D. Schadendorf, D. E. Fisher, C. Garbe, J. E. Gershenwald, J.-J. Grob, A. Halpern, M. Herlyn, M. A. Marchetti, G. McArthur, A. Ribas, A. Roesch, and A. Hauschild. Melanoma. *Nature Reviews Disease Primers*, 1(1): 15003, dec 2015. ISSN 2056-676X. doi: 10.1038/nrdp.2015.3. URL http://www.nature.com/articles/nrdp20153.

J. Steininger, F. F. Gellrich, A. Schulz, D. Westphal, S. Beissert, and F. Meier. Systemic therapy of metastatic melanoma: On the road to cure. *Cancers 2021, Vol. 13, Page 1430*, 13:1430, 3 2021. ISSN 2072-6694. doi: 10.3390/CANCERS13061430. URL https://www.mdpi.com/2072-6694/13/6/1430/htm.

T. Stuart, A. Butler, P. Hoffman, C. Hafemeister, E. Papalexi, W. M. Mauck, Y. Hao, M. Stoeckius, P. Smibert, and R. Satija. Comprehensive integration of single-cell data. *Cell*, 177:1888–1902.e21, 6 2019. ISSN 10974172. doi: 10.1016/J.CELL.2019.05.031.

H. Suzuki, M. K. Kaneko, and Y. Kato. Roles of podoplanin in malignant progression of tumor. *Cells 2022, Vol. 11, Page 575*, 11:575, 2 2022. ISSN 2073-4409. doi: 10.3390/CELLS11030575. URL https://www.mdpi.com/2073-4409/11/3/575/htm https://www.mdpi.com/2073-4409/11/3/575.

F. Tang, C. Barbacioru, Y. Wang, E. Nordman, C. Lee, N. Xu, X. Wang, J. Bodeau, B. B. Tuch, A. Siddiqui, K. Lao, and M. A. Surani. mrna-seq whole-transcriptome analysis of a single cell. *Nature Methods 2009 6:5*, 6:377–382, 4 2009. ISSN 1548-7105. doi: 10.1038/nmeth.1315. URL https://www.nature.com/articles/nmeth.1315.

I. Tirosh, B. Izar, S. M. Prakadan, M. H. Wadsworth, D. Treacy, J. J. Trombetta, A. Rotem, C. Rodman, C. Lian, G. Murphy, M. Fallahi-Sichani, K. Dutton-

Regester, J.-R. Lin, O. Cohen, P. Shah, D. Lu, A. S. Genshaft, T. K. Hughes, C. G. K. Ziegler, S. W. Kazer, A. Gaillard, K. E. Kolb, A.-C. Villani, C. M. Johannessen, A. Y. Andreev, E. M. V. Allen, M. Bertagnolli, P. K. Sorger, R. J. Sullivan, K. T. Flaherty, D. T. Frederick, J. Jané-Valbuena, C. H. Yoon, O. Rozenblatt-Rosen, A. K. Shalek, A. Regev, and L. A. Garraway. Dissecting the multicellular ecosystem of metastatic melanoma by single-cell rna-seq. *Science (New York, N.Y.)*, 352:189–96, 4 2016. ISSN 1095-9203. doi: 10.1126/science.aad0501. URL `http://www.ncbi.nlm.nih.gov/pubmed/27124452`.

O. Urteaca and G. T. Pack. On the antiquity of melanoma. *Cancer*, 19, 1966. doi: 10.1002/1097-0142. URL `https://acsjournals.onlinelibrary.wiley.com/doi/10.1002/1097-0142`.

X. Wang, Y. He, Q. Zhang, X. Ren, and Z. Zhang. Direct comparative analyses of 10x genomics chromium and smart-seq2. *Genomics, Proteomics and Bioinformatics*, 19:253–266, 4 2021a. ISSN 22103244. doi: 10.1016/J.GPB.2020.02.005.

Z. Wang, Q. Yang, Y. Tan, Y. Tang, J. Ye, B. Yuan, and W. Yu. Cancer-associated fibroblasts suppress cancer development: The other side of the coin. 2021b. doi: 10.3389/fcell.2021.613534. URL `www.frontiersin.org`.

K. Watari, T. Shibata, H. Fujita, A. Shinoda, Y. Murakami, H. Abe, A. Kawahara, H. Ito, J. Akiba, S. Yoshida, M. Kuwano, and M. Ono. Ndrg1 activates vegf-a-induced angiogenesis through plcγ1/erk signaling in mouse vascular endothelial cells. *Communications Biology*, 3, 12 2020. ISSN 23993642. doi: 10.1038/s42003-020-0829-0. URL `https://www.ncbi.nlm.nih.gov/pmc/articles/PMC7060337/`.

F. M. Watt. Mammalian skin cell biology: At the interface between laboratory and clinic. *Science*, 346(6212):937–940, nov 2014. ISSN 10959203. doi: 10.1126/SCIENCE.1253734. URL `https://www.science.org/doi/10.1126/science.1253734`.

R. A. Weinberg. *The biology of cancer - Second edition*. Garland Science, Taylor and Francis Group, LLC, 711 Third AVenue, New York, NY 10017 and 3 Park Square, Milton Park, OX14 4RN, UK, 2014.

B. Wilm and R. Muñoz-Chapuli. Chapter 3 the role of wt1 in embryonic development and normal organ homeostasis. 2016. doi: 10.1007/978-1-4939-4023-3.

P. F. Wong, W. Wei, S. Gupta, J. W. Smithy, D. Zelterman, H. M. Kluger, and D. L. Rimm. Multiplex quantitative analysis of cancer-associated fibroblasts and immunotherapy outcome in metastatic melanoma. *Journal for ImmunoTherapy of Cancer*, 7:194, 7 2019. ISSN 20511426. doi: 10.1186/s40425-019-0675-0. URL `https://jitc.bmj.com/lookup/doi/10.1186/s40425-019-0675-0`.

J. Wutschka, B. Kast, M. Sator-Schmitt, S. Appak-Baskoy, J. Hess, H. P. Sinn, P. Angel, and M. Schorpp-Kistner. Junb suppresses distant metastasis by influencing the initial metastatic stage. *Clinical and Experimental Metastasis*, 38:411, 8 2021. ISSN 15737276. doi: 10.1007/S10585-021-10108-9. URL `https://www.ncbi.nlm.nih.gov/pmc/articles/PMC8318945/`.

B. Zbytek, J. A. Carlson, J. Granese, J. Ross, M. C. Mihm, A. Slominski, and A. Slominski. Current concepts of metastasis in melanoma. *Expert review of dermatology*, 3(5):569–585, oct 2008. ISSN 1746-9872. doi: 10.1586/17469872.3.5.569. URL `http://www.ncbi.nlm.nih.gov/pubmed/19649148`.

E. M. Zeisberg, S. Potenta, L. Xie, M. Zeisberg, and R. Kalluri. Discovery of endothelial to mesenchymal transition as a source for carcinoma-associated fibroblasts. *Cancer Research*, 67:10123–10128, 11 2007. ISSN 0008-5472. doi: 10.1158/0008-5472.CAN-07-3127. URL `http://cancerres.aacrjournals.org/cgi/doi/10.1158/`.

Q. Zhang, Y. Pan, J. Ji, Y. Xu, Q. Zhang, and L. Qin. Roles and action mechanisms of wnt4 in cell differentiation and human diseases: a review. 2021. doi: 10.1038/s41420-021-00668-w. URL `https://doi.org/10.1038/s41420-021-00668-w`.

B. Zheng, Z. Zhang, C. M. Black, B. D. Crombrugghe, and C. P. Denton. Ligand-dependent genetic recombination in fibroblasts: A potentially powerful technique for investigating gene function in fibrosis. *The American Journal of Pathology*, 160:1609–1617, 5 2002. ISSN 0002-9440. doi: 10.1016/S0002-9440(10)61108-X.

L. Zhou, K. Yang, T. Andl, R. R. Wickett, and Y. Zhang. Perspective of targeting cancer-associated fibroblasts in melanoma. *Journal of Can-*

cer, 6:717–26, 2015. ISSN 1837-9664. doi: 10.7150/jca.10865. URL http://www.ncbi.nlm.nih.gov/pubmed/26185533.

Y. Zhou, B. Zhou, L. Pache, M. Chang, A. H. Khodabakhshi, O. Tanaseichuk, C. Benner, and S. K. Chanda. Metascape provides a biologist-oriented resource for the analysis of systems-level datasets. 2019. doi: 10.1038/s41467-019-09234-6. URL https://doi.org/10.1038/s41467-019-09234-6.